A PARTICLE TRACKING SYSTEM FOR WAKE SURVEY

CARL JOHN JOSEPH HARRIS

ISBN 0-315-96044-2

A Particle Tracking System for Wake Survey

by

© Carl John Joseph Harris, B.Eng, P.Eng

A Thesis submitted to the School of Graduate Studies in partial fulfillment of the requirements for the degree of Master of Engineering

Faculty of Engineering and Applied Science
Memorial University of Newfoundland
St. John's, Newfoundland

September 1993

St. John's Newfoundland Canada

This Thesis is dedicated to the memory of my father
Captain Gordon Harris, Master Mariner
1912-1980

Abstract

This thesis presents the results of a study undertaken to evaluate the feasibility of a low-cost Particle Tracking Velocimetry system to measure two dimensional steady flow vectors. Emphasis was placed on the suitability of the technique for ship propulsion research.

Experiments were conducted in a cavitation tunnel. Flow illumination was provided by an air-cooled Argon-ion laser with a measured output of 30 mW. An oscillating mirror was used to redirect and spread the laser light into a sheet. The water was seeded with 40 μm Aluminium-Silicate micro-spheres and particle images recorded using a standard Charge Coupled Device (CCD) video camera. High frequency sweeping of the laser beam produced multiple exposures within a single video field. This allowed the system to be used with flow speeds beyond the limit normally imposed by the standard 30 Hz. video framing rate. A desktop computer with a frame-grabber board was used to digitize selected video fields. Particle tracks were analyzed individually using off-the-shelf image analysis software. Velocity was computed by dividing the measured length of the track by the shutter speed of the camera.

Experiments were carried out in four phases. Measurements were made in uniform flow and found to be accurate and repeatable to within a single pixel. This gave a resolution of 0.072 m/s for a flow speed of 1.656 m/s and a 140 mm x 110 mm field of view. Experiments were conducted to determine the flow field around a smooth

cylinder at a Reynolds number of 72,700. The results showed good agreement with potential theory in the region upstream of the separation point.

To demonstrate applicability of the work to ship propulsion research a set of experiments were done to measure the simulated nominal wake in the region behind a model ship skeg. The static thrust and torque of a four bladed B-screw propeller, both with and without the skeg, was measured in the cavitation tunnel. The effect of the skeg on propeller performance has been evaluated and discussed.

For the case of no skeg, a comparison is made between the experimental results and predictions of performance as given by lifting surface theory. The experimental values of thrust and torque were 22% and 12% higher respectively than what was predicted by lifting surface theory assuming a uniform wake.

For the case with the skeg the lifting surface theory, using as input the wake determined by the particle tracking experiments, showed qualitative agreement with experimental measurements in predicting increases in blade thrust and torque in the stalled flow behind the skeg.

Acknowledgements

The author thanks, first and foremost, the Institute for Marine Dynamics of the National Research Council Canada for their part in his study program. Without their financial support this thesis would not have been possible.

I am also indebted to Dr. Neil Bose, Associate Professor, Faculty of Engineering and Applied Science, and to Dr. Indranath Datta, Research Officer, IMD. Their support and guidance meant a great deal during the course of my research.

Thanks are due to Mr. Paul Hearn and Mr. Ernie Reimer of Canpolar East Inc. for providing me with the laser equipment and technical support throughout the study; Ms. Janice Keating for her assistance during the experiments; Mr. Shane Mckay and Mr. Bill Hammond for technical assistance with video equipment; and Mr. Dan Walker for assistance with the propeller tests;

Last but by no means least I would like to offer my deepest appreciation to my wife Susanne, my daughters Leah and Chloe, my mother and my brother Gordon. Without their support and encouragement this would not have been done.

Contents

List of Figures

List of Tables

Notation

CTA - Constant Temperature Anemmometry

CPU - Central Processing Unit

CW - Constant Wave (Mode of Laser Operation)

D - Propeller Diameter

d_p - Particle Diameter [microns]

DPTV - Digital Particle Tracking Velocimetry

EISA - Expanded Industry Standard Architecture

FOV - (Camera) Field of View

HIDPIV - High Image Density Particle Image Velocimetry

IMD - Institute for Marine Dynamics

ISA - Industry Standard Architecture

J - Propeller advance coefficient ($J = V \cdot n^{-1} \cdot D^{-1}$)

K_Q (KT) - Propeller torque coefficient ($KQ = Q \cdot \rho_w^{-1} \cdot n^{-2} \cdot D^{-5}$)

K_T (KQ) - Propeller thrust coefficient ($KT = T \cdot \rho_w^{-1} \cdot n^{-2} \cdot D^{-4}$)

LDV - Laser Doppler Velocimetry

n - Propeller Revolution Rate [rps]

NTSC - National Television Systems Committee

PIV - Particle Image Velocimetry

PLV - Pulsed Light Velocimetry

PTV - Particle Tracking Velocimetry

Q - Propeller Torque [N · m]

SBP - Space Bandwidth Product

T - Propeller Thrust [N]

TBC - Time Base Corrector

V - Water Speed [$m \cdot s^{-1}$]

α - Probe inflow angle [degrees]

β - Mirror Excursion Angle [degrees]

θ (THETA) - Propeller Blade Position [degrees] from Top Dead Center (TDC)

η_o (ETAO) - Propeller Open Water Efficiency ($\eta_o = K_T \cdot K_Q^{-1} \cdot J \cdot (2\pi)^{-1}$)

λ - Wavelength

ρ_p - Particle Density [grams/cubic cm.]

ρ_w - Density of Water [grams/cubic cm.]

Chapter 1

Introduction

This thesis presents the results of a study undertaken to determine the effectiveness of a low-cost, two dimensional Particle Tracking Velocimetry (PTV) system to measure steady flow vectors in water. The ability to make non-intrusive measurements of fluid flow is a powerful investigative tool. The capability to provide simultaneous measurements over relatively large areas within a flow field gives PTV an advantage over single point measurement techniques such as pitot tubes, Laser Doppler Velocimetry (LDV) or Constant Temperature Anemometry (CTA). However, in general, individual PTV measurements have a spatial and temporal resolution less than what is possible with the other techniques.

Particle Tracking Velocimetry can be seen as an extension of classical flow visualization. Modern techniques for qualitative visualization of flow phenomena date back to the work of Ernest Mach in the late 19th century. A collection of examples illustrating the different methods has been given by Van Dyke (1982). The primary obstacle to extracting quantitative information from these techniques has been the

daunting amount of information to be processed in order to gain any useable data from the experimental records. Another factor for consideration is the time delay inherent with photographic equipment which captures images on chemically processed film. This delay between capturing and processing an image can be costly in terms of time lost in repeating experiments in order to acquire suitable images. Aside from these technical difficulties, quantitative information on fluid flow has theoretically been available for many years. However, until recently the time constraints have restricted the widespread use of quantitative flow visualization, Gharib and Willert (1989).

Velocity vectors within a flow field can be computed by determining the movement of particulate markers within some suitable time frame, Lourenco et al. (1989). Utilizing this fundamental definition of velocity to derive quantitative data from images of a flow field is not a new concept. However recent advances in PTV have been aimed at increasing the accuracy of individual measurements and reducing the time and effort required to obtain such information. The ongoing development of solid-state digital video cameras and powerful desktop computers has contributed significantly to this effort. Using the video camera to capture and store images greatly simplifies qualitative flow visualization. Using commercially available software for image processing and image arithmetic, quantitative visualization has become economically feasible. A review of the current state-of-the-art in PTV is given by Adrian (1991).

1.1 Objectives and Scope of the Study

Particle Tracking systems utilizing multiple frames from a normal video camera are used only in the study of low speed flows, see e.g. Okuno (1990) and Hamilton et al. (1992). To ensure that the image of a particle is visible in two sequential frames, the particle displacement within the time step determined by the framing rate (30 Hz.) should not exceed, typically, one half of the field of view of the camera. The flow speeds for which such a system could be utilized are unrealistically slow for practical applications in naval architecture. The use of multiple exposures within a single video image avoids the limitations of the 30 Hz. framing rate, but requires the use of an expensive high-powered pulsed, or externally modulated constant wave (CW) laser for illumination, see e.g. Rimai et al. (1986).

Important criteria in the design of the present system was that it not be limited to low flow speeds, and that illumination be possible using a relatively low-power air-cooled laser. The flow speed consideration was necessary in order that the system be useful as a tool in practical propulsion research. The restriction on the illumination source was to keep cost as low as possible and avoid the complexities, such as special cooling arrangements and safety precautions, associated with large laser powers.

All experiments were conducted in the cavitation tunnel at the Institute for Marine Dynamics in St. John's, Newfoundland. The flow in the test section was illuminated

using an air-cooled Argon-ion laser with a measured output of 30mW. The laser beam was redirected and formed into a sheet using an oscillating mirror. Particle images formed by the laser light reflecting off particles in the flow were recorded using a digital Charge Coupled Device (CCD) video camera. Multiple 'sweeps' of the laser beam within the time frame defined by the shutter speed of the camera produced video fields containing multiple exposures of the particles' motion. Using this method the basic system satisfied both the speed and cost criteria. Digitization of the images and analysis of particle tracks were done using an IBM® compatible desktop computer. Individual fields from the videotape were digitized using a frame grabber board. Analysis of these images was performed manually using commercially available image analysis software. The length and attitude of the particle tracks were measured interactively using a screen cursor. The magnitude of the local flow velocity vector, as defined by particle displacement, was calculated by measuring the length of the particle track and dividing by the shutter speed of the camera. This experimental technique has been described as 'single frame/multiple pulse, low image density, Particle Image Velocimetry', Adrian (1991). More concisely, it is referred to in this thesis as Digital Particle Tracking Velocimetry(DPTV). This nomenclature refers both to the method of image acquisition (digital video camera) and the method of analysis (particle tracking).

The experimental study was divided into three levels, with each stage representing an increase in complexity of the flow being investigated. To evaluate the parameters of the system a uniform flow was selected for the initial investigation. Results indicated that

the method was accurate, and measurements repeatable, within single pixel resolution. For a flow speed of 1.6 m/s and a field of view of 140 mm x 110 mm, the image resolution was 0.29 mm/pixel. This represented an error of 0.072 m/s with a relative error on individual measurements of 4.3% for that combination of shutter speed, flow speed and field of view. Following this a series of experiments were conducted to investigate the flow around a 50 mm diameter smooth cylinder at a Reynolds number of 72,700. The flow speed at this Reynolds number was the same as that used for the measurements in a uniform flow, and was considered to be a 'practical' value for tests in the cavitation tunnel. Comparison of experimental vectors with the predictions of potential theory showed good agreement in the region upstream of the separation point where the theory is valid.

To demonstrate applicability of the DPTV system to ship propulsion research, a third set of experiments were undertaken to measure the nominal wake in a region behind a ship skeg. The afterbody of a typical 10 metre Newfoundland inshore fishing vessel was modelled in the tunnel test section by a simplified body with faired leading edges. The results were compared, qualitatively, to CTA measurements on a similar hull form in a towing tank. Experiments were also done to determine the static thrust and torque of a four bladed B-screw propeller, operating in the tunnel, both with and without the skeg present. Comparison of experimental results were made with predictions from an unsteady lifting surface theory, Kerwin and Lee (1978), using as input both a uniform flow field and the wake as determined by the DPTV experiments.

Chapter 2

Flow Measurement Techniques for Wake Survey

This chapter presents an overview of some of the methods used to determine the magnitude and direction of fluid velocity, particularly those techniques which have found application in hydrodynamic testing facilities such as towing tanks and cavitation tunnels. Emphasis is placed on Pulsed Light Velocimetry (PLV) as the method described in this thesis; Digital Particle Tracking Velocimetry (DPTV), is a form of PLV.

For the naval architect, an understanding of the fluid flow in the wake of a ship is essential to a properly engineered design of a ship's propulsion and steering systems. The characteristics of this flow will affect both the basic hull form as well as the selection and placement of propulsors and control surfaces, see e.g. van Manen and van Oossanen (1988) and Rawson and Tupper (1984). The nature of the wake will limit the hydrodynamic efficiency of a hull and determine the overall efficiency of the propulsion system. From this latter consideration then, it is necessary to consider in more detail both the exact (i.e. quantitative) nature of the wake as well as the gross structure of the flow. This is particularly important when selecting or designing a marine screw propeller which must operate in that wake field.

A significant effort has been expended in the past to quantify the characteristics of ship wake flows, see e.g. Harvald (1983). Considering the obvious difficulties of conducting full scale experiments, the vast majority of wake flow data has been produced from the results of model-scale measurements. However the amount of data available from measurements on full-sized ships is increasing, see e.g. Kux (1990), Kato and Ukon (1990), and Komura et al. (1991). For practical reasons full scale experiments are commonly limited in terms of measuring area and, as a design tool, the results are too scarce to allow for a true systematic analysis of the effect of hull form on wake flow.

Completely theoretical treatments of wake flows are not regularly pursued. The flow in the stern region of a ship is complex and three-dimensional. An exact analytical approach must incorporate the effect of viscosity in boundary layer generation and growth, and the solution of the complete Navier-Stokes equations of fluid motion in the wake region at high Reynolds numbers, see e.g. ITTC (1990). Figure 1 shows schematically the flow around a ship's hull and the theoretical formulations appropriate to each region. With the advent of super-computers using parallel processing architecture, such computational analyses could become feasible on a routine basis. However, from a practical perspective, data of increased accuracy from improved experimental techniques hold more immediate promise. A discussion of the numerical treatment of wake flows is beyond the scope of this thesis.

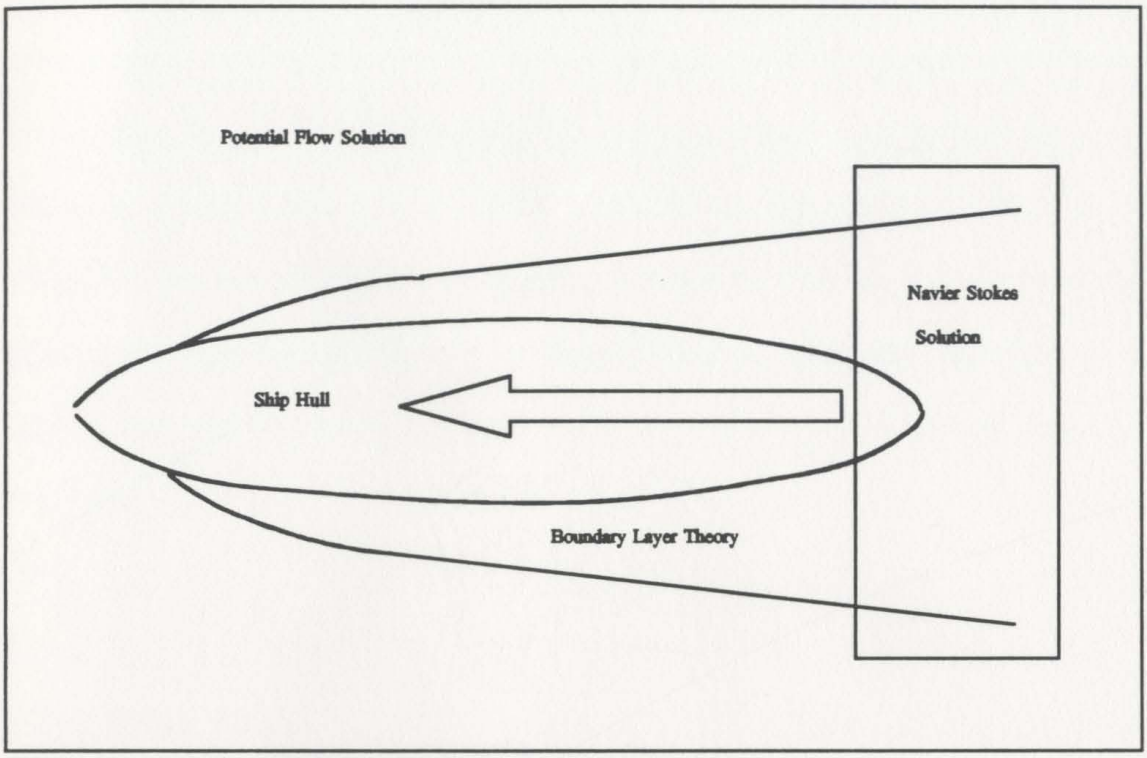

Figure 1 - Relevant Theories for Hull Flow Components.

2.1 Intrusive Techniques

The techniques for determining flow velocity vectors have traditionally been based on intrusive experimental methodologies. The flow is quantified using sensors which are placed in, and thus have some effect on, the flow being examined. This approach will inherently introduce some level of error into the final results. Even if such errors can be explicitly accounted for, and the results corrected accordingly, there remain practical limitations due to the finite size of the sensors. This consideration becomes more critical in situations where the physical size of the model itself is very small. Intrusive techniques can also be difficult to implement in situations where access to the test region is limited by the experimental facility.

Early methods, such as vane wheels and resistance rings, provided only global measurements, van Lammeren et al. (1948). These techniques were simple to implement, but the price for experimental simplicity was limited information on the flow field. Both techniques provided only a single mean axial flow velocity over the diameter of the transducer. Modern electronic transducers and recording technology could be used to improve the experimental efficiency of these procedures. However, regardless of the extent of any such improvements the simplicity of the data collected severely limits their usefulness.

2.1.1 Pitot Tubes

Pitot tubes have been used for many years to measure fluid flow. In its early form the pitot tube provided a quality of data comparable to that produced by vane wheels and resistance rings. Spatial resolution was higher due to the smaller size of the probes, van Lammeren (1948). Incorporating multiple pitot tubes within a single probe increases the amount of data to be collected, but directionally sensitive measurements are made possible, see e.g. Wickens and Williams (1985). Pressure measurements from pitot tubes were traditionally made using water manometers. Replacing the manometers with electronic transducers eliminated problems associated with dynamics of the water column which resulted in a 'lag' in the response to pressure changes at the probe. These transducers also decreased the experimental difficulty associated with multi-hole pitot tubes by removing the necessity to manually record the pressures for each test condition.

This was particularly important for experimental set-ups using multiple probes where each probe registered several pressures. Figure 2 shows, schematically, the setup for a wake survey 'rake' employing five, 5-hole, pitot tube probes. This rake is currently used in the Towing Tank at the Institute for Marine Dynamics (IMD).

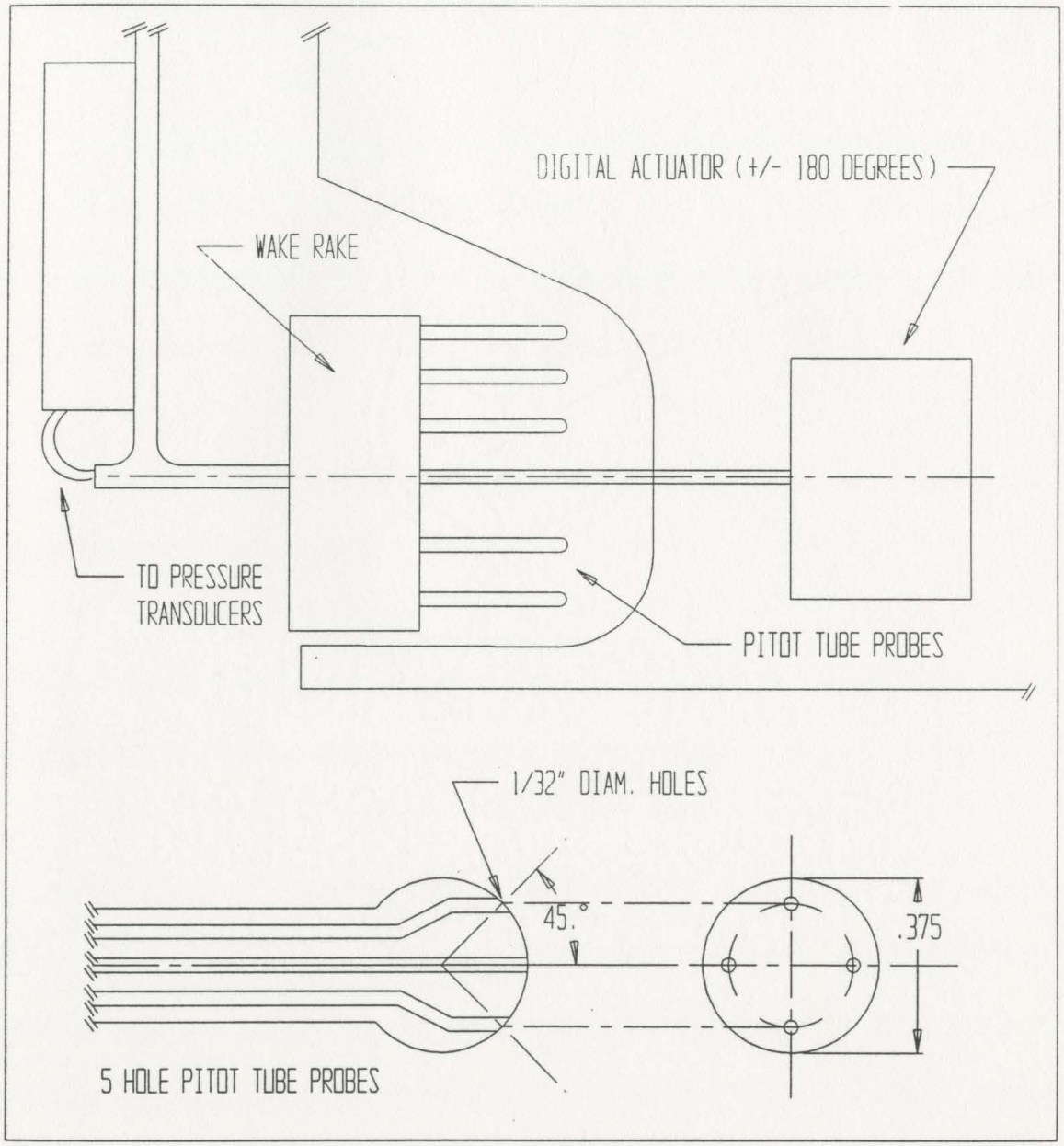

Figure 2 - Spherical Probes and 'Wake-Rake' Used at the Institute for Marine Dynamics.

Use of a computer to record, store and analyze experimental data has permitted the development of elaborate systems capable of obtaining multi-point, multi-directional data, Miles (1978). Further refinements to the design of probes, and data acquisition and analysis procedures, have produced very accurate systems utilizing very small probes, Brophy et al. (1987).

Pitot tube systems, being mechanically simple, relatively cheap and extremely robust, have been the preferred method for towing tank ship model wake surveys in steady flow. With appropriate pressure sensors, pitot tubes can be used over a wide range of flow velocities.

However, despite advances in experimental methodology, pitot tube systems retain certain restrictions and limitations:

i) The physical size of the probe prohibits their use in flows with a length scale which is comparable to the dimensions of the probe, Tritton (1988).

ii) A slow response time renders rapid velocity fluctuations transparent to the measuring system, and only a single mean velocity is obtainable in turbulent flows, Tritton (1988). Also, since the principle of operation for analysis is Bernoulli's equation for steady flow, pitot tube results are subject to an error which varies with the level of turbulence, Brophy et al. (1987)

iii) Calibration of the system is a two stage process: transducer output voltage against pressure, and probe tip geometry against inflow angle, Miles (1978). These are both time consuming tasks, both of which must be repeated, at least in part, prior to every set of experiments (from the authors experience in conducting ship model wake surveys in the towing tank at the IMD, 1986-1991).

iv) The range of inflow angle (α) that can be measured relative to the centerline of the probe is limited by probe-tip geometry. Figure 3 shows a spherical pitot tube head and the definition of (α) used here. Generally the maximum limits for 5-hole probes with spherical tips is taken to be about 30 degrees, although there are claims of reliable measurements up to about 40 degrees, Gunton (1978). Probes with conical tips are not normally calibrated beyond 30 degrees for use in water, Brophy et al. (1987), although similar probes used in wind tunnels have been calibrated up to 45 degrees. The geometry of the conical tip probes used by Wickens and Williams (1985) are shown in Figure 4. Probes with different tip geometries and sensing port distributions exhibit slightly different characteristics. The authors experience in tow tank' testing at the IMD, over the period 1986-1991, indicates that a practical upper limit on inflow angles for both spherical and conical tip pitot tubes can be taken to be about 35 degrees.

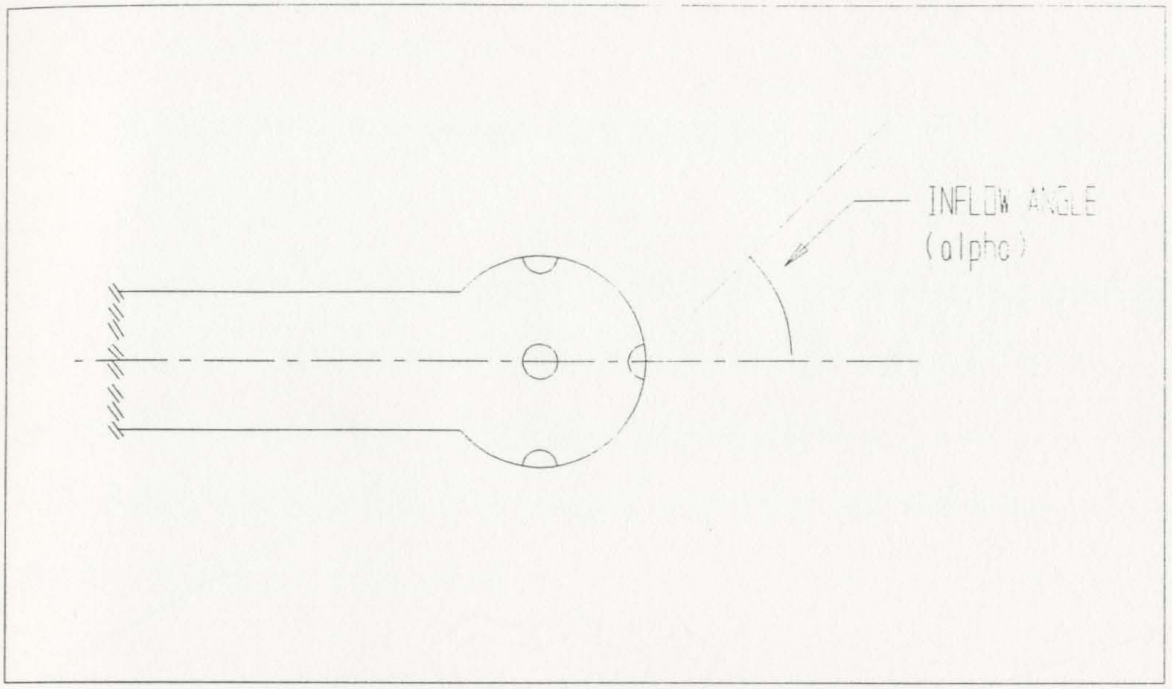

Figure 3 - Pitot Tube Probe Inflow Angle

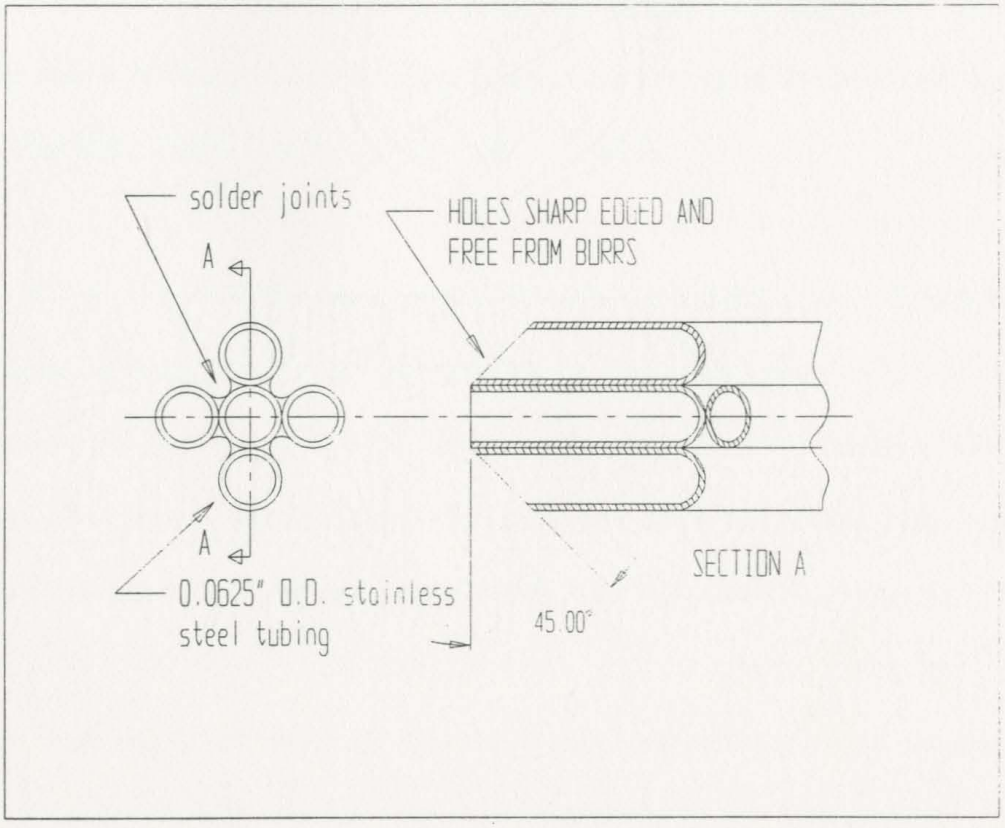

Figure 4 - Geometry of Conical Tip 5-Hole Pitot Tube Probe

2.1.2 Constant Temperature Anemometry

Constant Temperature Anemometry (CTA) is a technique wherein a feedback circuit maintains a sensing element in the flow at a constant resistance, and hence a constant temperature. The principle of hot-film annemometry for fluid flows is the same as for hot-wire anemometry used extensively in wind tunnel work, but the sensors are geometrically different, Tritton (1988).

The operating principle of CTA is implied in the name; an electrically heated element immersed in a flow is cooled at a rate which varies with the fluid velocity. The cooling rate is normally modelled using King's Law dealing with convective heat loss from a hot body placed in a fluid stream, Perry (1982).

Hot-wire anemometry was originally developed for use in gaseous flow fields and the delicacy of wire probes prohibited their use in harsh or conductive media, Durrani and Greated (1977). The development of new sensing elements has helped alleviate this problem. Film sensors heavily coated with quartz have been used successfully in towing tank applications, see e.g. Wu and Bose (1992a). The film sensors, and especially wedge shaped probes, are more robust than the wires, and the quartz coating protects the sensors from the conductivity of the water and contaminants in the towing tank. However in general CTA has not been used extensively in tow tank or water channel testing.

The limiting physical dimensions of the sensors are of the order of 1 - 5 microns; this dimension refers to element diameter in the case of hot wire and element thickness in the case of hot film sensors, (Dantec probe catalog). The size allows for the measurement of small scale flow structures. Output from the sensor is continuous with an extremely high response time which reveals information on the oscillatory characteristics of a flow, Tritton (1988). In this respect hot-wire anemometry is quite different from other (intrusive) techniques. It is possible to determine a mean flow component from the sensor output, but a measurement can also be obtained of the level and frequency of turbulence present in the flow, see e.g. Wu and Bose (1992b).

Despite superior performance in turbulent flows, as compared with pitot tubes, there are some fundamental criticisms of hot-wire anemometry. Those most relevant to applications in hydrodynamics are discussed below.

i) A system employing a single sensor is insensitive to flow direction. Simpson (1989) describes several experimental techniques used to overcome this limitation using different configurations of wire sensors. Hyun and Patel (1990) discuss problems associated with the use of directionally sensitive hot-wire probes in high turbulence level flows in a wind tunnel. Published accounts of directionally sensitive CTA experiments in water are rare.

ii) Flow velocity is not measured directly and thus the sensors must be calibrated, for mean flow, against some other device. For applications in a towing tank this is generally

the tow carriage. Wu and Bose (1992c) used this method and reported the accuracy of the probe velocity calibration as better than 1 mm/sec.

iii) The electrical output from the sensors is not linear with flow velocity. Data analysis must assume that the calibration curve is piece-wise linear, or adopt a more complex numerical model to account for the nonlinearities, see e.g. Wu and Bose (1992b)

iv) The output from the probe is sensitive to temperature variations in the fluid. Wu and Bose (1992c), who used CTA to conduct a nominal wake survey in a towing tank, have proposed several methods to account for this.

v) For the initial period of operation all sensors, whether hot-film or hot-wire, exhibit a change in metallurgical properties called aging, Perry (1982). Over this period, 20 hours or more for platinum and tungsten hot-wires in air, a stable calibration cannot be obtained. Wu and Bose (1992a) state that about 100 hours of continuous operation was required for new hot-film probes (in water) before the output became sufficiently stable to obtain repeatable calibrations. As this 'burn-in' time could represent a significant portion of useable lifetime, the replacement cost of probes would be a factor to consider before such a system was implemented for routine testing.

Hot-film anemometry has not been used extensively for measurements in water in a towing tank. This has been primarily due to problems with probe contamination and

the difficulties encountered with obtaining reliable calibrations. Recent efforts with more robust probes and modified numerical models for fitting calibration curves, Wu and Bose (1992b), show promise for future routine application of the technique to water flows. The probe arrangement used by Wu and Bose (1992b) is shown in Figure 5.

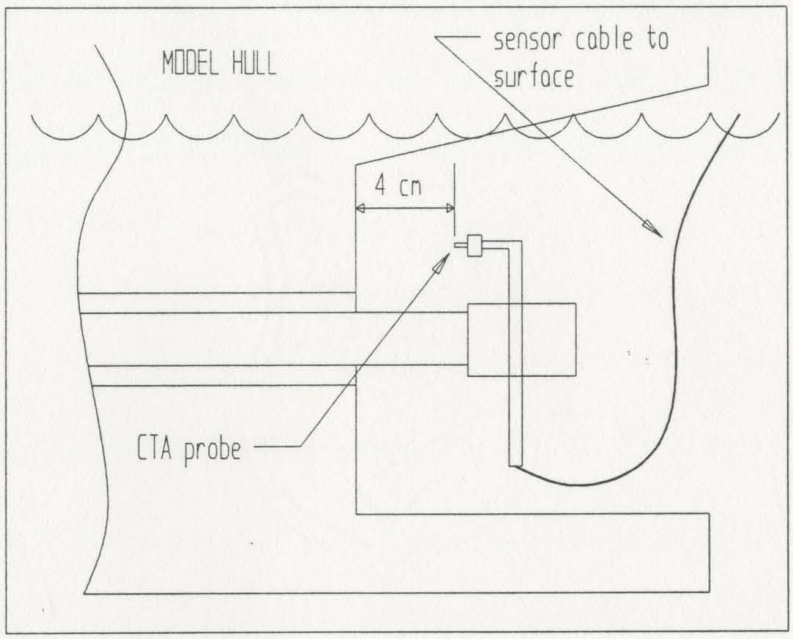

Figure 5 - CTA Probe Arrangement Used by Wu and Bose (1992c)

2.2 Non-Intrusive Techniques

The ability to make velocity measurements without the introduction of a transducer into the flow represents an obvious advantage over intrusive techniques. Nearly all such techniques are optically based, and although termed 'non-intrusive' some modification to the fluid is usually required in order for the techniques to function properly. This is usually the addition of (light) reflective particulate matter into the flow.

The presence of these 'seed particles' is assumed to have a negligible effect on flow properties, while the particles themselves are assumed to faithfully follow the fluid motion. Two methods are described in the following sections; Laser Doppler Velocimetry (LDV) and Pulsed Light Velocimetry (PLV). The introduction of the laser has been a key element in the development of both, but the function of the laser in each is considerably different. Rapid advances in computer and optical technologies have permitted the development of many possible variations of these basic methods, and therefore they are discussed only in terms of their fundamental properties.

2.2.1 Laser Doppler Velocimetry

The most commonly encountered non-intrusive technique is Laser Doppler Velocimetry (LDV). A Laser Doppler Velocimeter (sometimes called a Laser Doppler Anemometer (LDA)) measures velocity by measuring the Doppler shift in the frequency of (laser) light from incident and reflected light from microscopic particles within the flow, Tritton (1988). Since its introduction in 1964 the basic technique has been modified to take advantage of developments both in optical and in electronic processing technology, Durrani and Greated (1977). The majority of these modifications can be seen more as procedural refinements than significant new developments. Durrani and Greated (1977) present some of the possible experimental configurations and discuss their relative merits.

Laser Doppler Velocimeters, like Constant Temperature Anemometers, provide information on the turbulent nature of the flow which cannot be obtained with pitot tubes or other mechanical devices. Durrani and Greated (1977) show that a laser doppler system can have a spatial and temporal resolution comparable to CTA provided a large enough number of suitable light-scattering particles are present in the flow. The density of particle concentration is thus a critical factor for LDA operation and effectively determines the data sampling rate. In some instances the natural presence of dirt particles will be sufficient, while in other cases artificial seed particles are introduced to the flow. Another factor affecting operation is the size of the particles. Bachalo (1987) discussed the effect of seed particle size on system performance; particles which are too small will contribute to background noise levels, while too large a particle will be detected but may not be properly following the flow.

Aside from its non-intrusive nature, LDV has two fundamental advantages over CTA:

i) The system does not require calibration as fluid velocity is measured directly from the Doppler-shift in the frequency of coherent light reflected from microscopic particles.

ii) System output is a linear function of velocity and the velocity component is measured in a specified direction.

While in principle LDV measurements are non-intrusive except for the addition of seed particles to increase data rates to an acceptable level, implementation of an LDV system may become very intrusive depending on the test facility and arrangement of laser optics. For cavitation tunnels and small water channels the laser head and light collecting optics can be external to the flow, e.g Brophy et al. (1987). For towing tank applications, however, this equipment has either to be placed directly in the flow or, alternatively, the laser beam has to be routed through an optical train immersed in the flow. Pirrone and Lindenmuth (1992) comment on the interference effect of the LDV strut assembly commonly used in a towing tank. The relevance of the intrusion into the flow field is primarily a function of model and test conditions. Figure 6, taken from Pirrone and Lindenmuth (1992) is a schematic of a typical LDV installation in a towing tank using a strut-type arrangement.

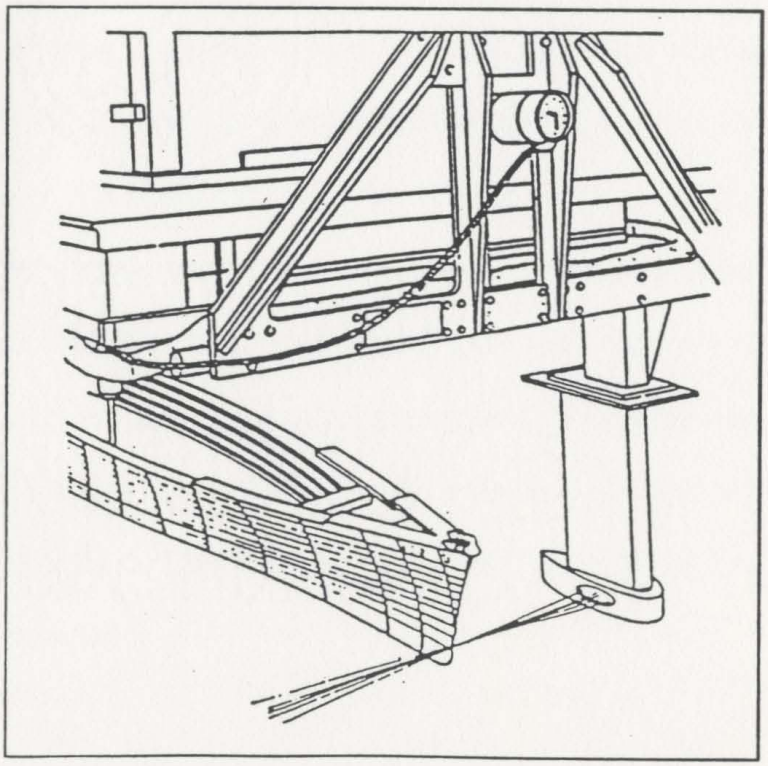

Figure 6 - Typical LDV Strut Arrangement in a Towing Tank Application

The application of fibre optic technology to LDV minimizes the size and hence the effect of the intrusive components, (Dantec sales brochure). However the optical conduit will absorb some of the laser light energy making less available to the interrogation beams.

The high cost of implementing an LDV system has traditionally limited use to government and/or military funded facilities capable of affording the very expensive sensors and equipment necessary to collect and analyze the data. Recent advances in both laser and computer technology and a corresponding decrease in cost has put LDV systems within reach of more researchers, however the capital outlay for a system capable of measuring a single velocity component (i.e. one axis only) can still be expected to be around $100,000.00 (CDN). The flow information provided by an LDV system is, like that available from pitot tubes and CTA sensors, Eulerian in nature; i.e. instantaneous or time dependant velocity measurements are made at a specified 'point' in the flow field. While it is technically possible to design an LDV system capable of recording simultaneous velocities at multiple points within a specified flow field, the cost and complexity would be prohibitive. Simpson (1989) reviews a number of single and multi-component laser doppler systems designed to measure sequential points in the flow by the use of moving optical components.

A practical restriction on the use of an LDV system is that optical access is required to the interrogation point. Selection of a suitable seed particle will also, to some

extent, determine system performance, Bachalo (1987). LDV has been used for model scale investigations, see e.g. Pirrone and Lindenmuth (1992) and has been adapted for full scale applications, see e.g. Tanibayashi (1990).

2.2.2 Pulsed Light Velocimetry

Pulsed Light Velocimetry (PLV) is a generic heading rather than a specific technique, Adrian (1991). Details and exact applications vary significantly, but all techniques within this category share at least one common feature: flow characteristics are deduced by noting the location of marked regions of fluid, within the flow field, at two or more known times. Such techniques then are fundamentally different from all others discussed so far. The results of PLV measurements are Lagrangian vectors describing the motion of the fluid in space and time.

Many variants of PLV have been developed based on novel methods of 'marking' the flow, different detection/recording equipment and improved analysis techniques. Hesselink (1988) and Adrian (1991) provide overviews of some of these factors. Of particular interest in the field of incompressible fluid flow is a subset of PLV called Particle Image Velocimetry (PIV). This technique deals explicitly with particulate markers and their images, Gharib and Willert (1989). If particle displacement is known within some suitable time scale, the fundamental definition of velocity will define a vector at the discrete locations defined by the particle images. Within this group a further

distinction is made between different techniques based on the relative concentration of particle images and the required method of analysis, Lourenco et al. (1989) and Adrian (1991). Figure 7 illustrates schematically the various modes of operation as a function of particle concentration. With very few exceptions, e.g. Agui and Jiminez (1987) and Wu et al. (1991), lasers are used for illumination of the flow.

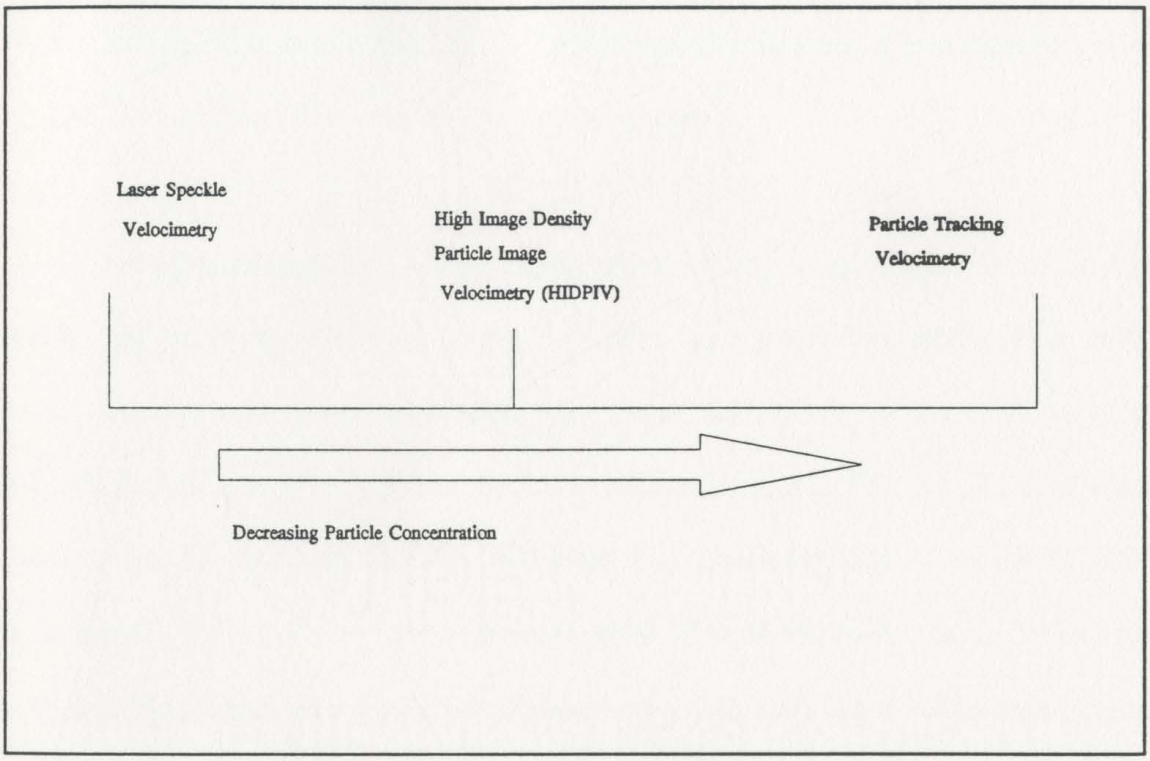

Figure 7 - Types of PLV Based on Particle Image Concentration

At one extreme, with a concentration of particles high enough so that the images of the particles overlap in the image plane, we have what is termed Laser Speckle Velocimetry (LSV), originally used in investigative solid mechanics, Erf (1978). This technique has been used infrequently with fluid flows due to the logistics and cost of

densely seeding large scale and/or high speed flows, Lourenco et al. (1989).

When particle concentration is reduced such that the images of discrete particles become discernible, and the inter-image spacing is of approximately the same order as the particle diameter, the method is referred to as High-Image-Density Particle Image Velocimetry (HIDPIV), Adrian (1991). Most recent studies, e.g. Lourenco et al. (1989), Okuno (1990), Katz and Huang (1990), Willert and Gharib (1991), and Hamilton et al. (1992), have adopted this level of particle concentration.

Photographic film has normally been used for recording images of seeded flow fields. The chemical developing process, using a high grade film produces an image possessing excellent spatial resolution, Adrian and Yao (1985). However the time lag between exposure and development can be a serious drawback. The use of digital video cameras has for some applications eliminated the processing step of earlier HIDPIV techniques, albeit at the expense of limiting application to low speed flows, Willert and Gharib (1991). The spatial resolution of video cameras is more limited than photographic film, but this has in large measure been offset by improvements in other areas. The initial cost of a video system is similar to that for a photographic one, and the storage media, videotape, is far cheaper than film. Connecting the video camera directly to a computer equipped with a frame grabber board can permit real-time display and processing of images, Marko and Rimai (1985). For measurements at low light levels, or with very small particles ($d_p < 20\mu m$) Silicon Intensified Target (SIT) video cameras

offer improved sensitivity over film, Rimai et al. (1986).

Analysis of HIDPIV images captured on film generally involves point-by-point interrogation of the negative. This simplifies reconstruction of the whole flow field as values of local velocity are thus calculated on a regular grid spacing, e.g. Willert and Gharib (1991) and Hamilton et al. (1992). Several different approaches have been used to deduce the velocity. Producing a Youngs' fringe pattern by illuminating the film negative with a low power laser is perhaps the simplest and hence the most widely used technique, e.g. Hesselink (1988). Katz and Huang (1990) describe an auto-correlation method of analysis used with double- and triple- exposed images of a complex flow inside a pump casing.

For HIDPIV using a video camera, analysis is somewhat simplified as the image is already in a digital format. A cross-correlation technique, using the intensity (gray level) distribution of sequential digital images has been presented by Okuno (1990) and Willert and Gharib (1991). Some HIDPIV systems merge photographic and video technologies by using a video camera to record the Youngs' fringes produced by spot illumination of a film negative, Katz and Huang (1990). A flow measurement system based on this technique is currently offered for sale by the University of Edinburgh, (personal communication with Mr. Peter Laurich, National Research Council of Canada).

A disadvantage of single-image techniques is the 180 degree ambiguity in

determining the direction of the velocity vector, Lourenco et al. (1988). This can be avoided by, for example, using suitable coding of the illumination time profile, see e.g. Marko and Rimai (1985) and Katz and Huang (1990). Adrian (1991) reviews some of the different techniques used to remove directional ambiguity .

At the opposite extreme (in terms of particle concentration) from Laser Speckle Velocimetry is Particle Tracking Velocimetry (PTV). With PTV the (particle) image density is sufficiently low so that individual particle images dominate. Multiple short-duration exposures, or a single long duration exposures leave 'tracks' which are relatively short compared with the inter-particle spacing.

In a general sense PTV can be seen as the logical extension of classical flow visualization techniques. A collection of examples of qualitative flow visualization can be found in van Dyke (1982). The data 'output' format has normally been photographic plates. The primary drawback in extracting quantitative information from such techniques has been the daunting amount of information to be processed in order to gain any useable information, Gharib and Willert (1989). Aside from this time restriction, quantitative information on fluid flow has theoretically been available for many years. Recent developments in PTV have been aimed at increasing the accuracy of individual measurements and reducing the time and effort required to obtain such information, e.g. Marko and Rimai (1985).

Determining flow characteristics from particle tracking is conceptually easier (calculating velocity by dividing a measured length by a known time) than the analysis required by particle imaging techniques. Manual analysis of recorded images by measuring individual particle tracks is the simplest, if most time consuming, method. Image recording for PTV systems is better suited to video than film technology. The relatively low number of particle images per 'picture' would make photographic techniques too expensive and time consuming. Analysis of PTV images has thus progressed along the lines of identifying and analyzing individual tracks rather than processing the entire image.

A single long duration exposure, e.g. Suzuki (1990), or the use of fluorescent or phosphorescent particles (with one or two exposures), e.g. Katz and Huang (1990), are the simplest form of PTV. The particle track is represented by a long narrow grouping of pixels whose intensity level is above that of the background. These methods are well suited to numerical edge-detection and edge-tracking routines based on image intensity or colour. Particle tracks are located based on the relative intensity of adjacent pixels. A user supplied threshold level is then utilized to define the outline of the particle track image, Hesselink (1988). From these outlines particle velocity, magnitude and direction can be computed.

For multi-pulse exposures more complex methods are required for an automation algorithim. Unless fluorescent particles are used the particle track is not a single region

of 'bright' pixels, but rather an unconnected set of pixel groups. Simple edge tracking is not adequate in such a case. Marko and Rimai (1985) refer to a technique using a contiguity criterion with a thresholded image, although details of the algorithm are not given. For both single and multiple exposure methods some manual intervention is normally required to initially identify the track, Rimai et al. (1986) or establish threshold levels, Gharib and Willert (1989). Work is ongoing in an attempt to eliminate the need for human intervention and to fully automate the analysis process.

The primary restriction on the use of PIV has been the high cost of lasers for illumination of the flow, and of the computers necessary to perform data analysis. This has been alleviated somewhat by using video technology and by taking advantage of the decreasing cost and increasing power of desktop computers. A primary restriction of video systems used with PTV has been the barrier on permissible flow speed, using sequential frame analysis techniques, imposed by the 30 Hz. framing rate, e.g Willert and Gharib (1991) and Okuno (1990). Rimai et al. (1986) describe a single frame video based system which had the possibility of measuring flow velocities of up to 30 m/sec in air. However their system was elaborate, using a high power (4 W) laser with a series of lenses and mirrors and an acousto-optic modulator system to control the illumination of the test section.

A limitation of Particle Tracking Velocimetry is that direct velocity measurements within the flow are only available at the discrete locations defined by the individual

particle images. For steady flows this is not a serious problem as sequential images can be superposed to produce the required data density. Alternatively, randomly spaced data values can be interpolated onto a regular grid. Gharib and Willert (1989) review some of the interpolation schemes which have been proposed to map irregularly spaced measurements to a regular mesh. Agui and Jimenez (1987) describe a method for estimating the errors in interpolated velocity measurements.

Particle tracking, like HIDPIV, is generally restricted to two dimensional regions. A single long illumination, i.e. streak photography, produces a track with a 180 degree ambiguity. This may be acceptable in some instances, but is not suited to situations were the possibility exists for flow reversal. A biased or time sequenced train of illuminations can correct this deficiency, e.g. Rimai et al. (1986). Suitably coded illumination profiles can also be used to determine out of plane particle motion as well as primary direction, Adrian (1991). Extensions of the basic technique to three-dimensional investigations are rare. However the development of full 3-D systems is limited more by financial and technical restrictions, (such as the cost of equipment and the ability to process data in an acceptable time) than by any fundamental considerations. The use of stereo-photography to obtain 3-D velocity vectors, in a laboratory setting, is described briefly by Okuno (1990). A more general discussion is provided by Hesselink (1988). Komura et al. (1991) present in some detail a method using multiple cameras for 3-D measurements in the wake of a full size ship.

The use of measurements made with, either, particle imaging or particle tracking is most often a tradeoff between image resolution and the field of view within the flow. Identifying gross flow structures often requires a larger field of view at the expense of resolution for individual particle measurements, e.g. Hamilton et al. (1992). Hesselink (1988) recommends a maximum relative error in velocity of 0.5% if measurements are to be used to determine vorticity in the flow. Depending on the image capture and analysis techniques this requirement may significantly reduce the field of view. The speed at which image data can be processed to produce quantitative information will almost certainly increase with the application of array processors, Willert and Gharib (1991). The ability to directly identify, and quantify, an instantaneous gross flow structures is a feature exclusive to PLV. Single-point measurement techniques such as Pitot tubes and CTA can not achieve this without using multiple sensors. Even then some *a priori* knowledge of the flow is often required in order to properly place the sensors.

Chapter 3

Design of a Particle Tracking System for the Cavitation Tunnel

In the design of a PTV system, considerations of the types of flows to be investigated and the type of equipment available, must be balanced with the accuracy of data which is desired as a final product. Experimental apparatus is expensive and procedural iterations can be time consuming. For the current study rigorous time and financial restrictions had been imposed. In order to complete the study within those constraints some compromise was necessary in the selection of system components. These concessions influenced the choice of variables for the initial validation process. Only steady, essentially two dimensional, flow was considered and the selection of flow speed was based primarily on considerations of available light sources, imaging equipment, and seed particle dynamics. Selection of seed particles was dictated by availability and cost. The choice of image processing and analysis systems was limited to those which would permit all data manipulation to be done on an IBM compatible desktop computer. Physical models were restricted to simplified bodies.

3.1 Cavitation Tunnel

All experiments for this study were carried out in the cavitation tunnel at the Institute for Marine Dynamics in St. John's, Newfoundland. This tunnel is of the closed circuit type with a 500 mm x 500 mm x 2200 mm test section. A description of the facility, along with operating instructions, is given by Doucet(1992a). The necessary visual access in order to permit system operation, in particular a 90° angular separation between light source and camera, was possible via transparent bottom and side viewports. Figure 8 is a schematic of the tunnel test section showing the general placement of system components and indicating the sign convention maintained throughout this thesis. The upstream viewports (windows), bottom and front side, were renewed prior to conducting experiments. The new windows were fabricated from cast Acrylic sheet, 19 mm thick for the bottom window and 38 mm for the side window. This improved clarity for image recording and minimized distortions of the laser light entering the test section. The small vertical dimension of the viewing area, 235 mm, restricted measurements significantly above or below the centre line of the test section. For these experiments this limitation was aggravated by the interference of the camera body and integral microphone with the locking mechanism for the viewports. Figure 9 shows the camera positioned at the test section viewport to obtain images of the calibration grid. The relative proportions of the camera and the viewport, and the potential problems with off centre-line measurements, are apparent. With unlimited funds miniature cameras, which would eliminate this problem, are available .

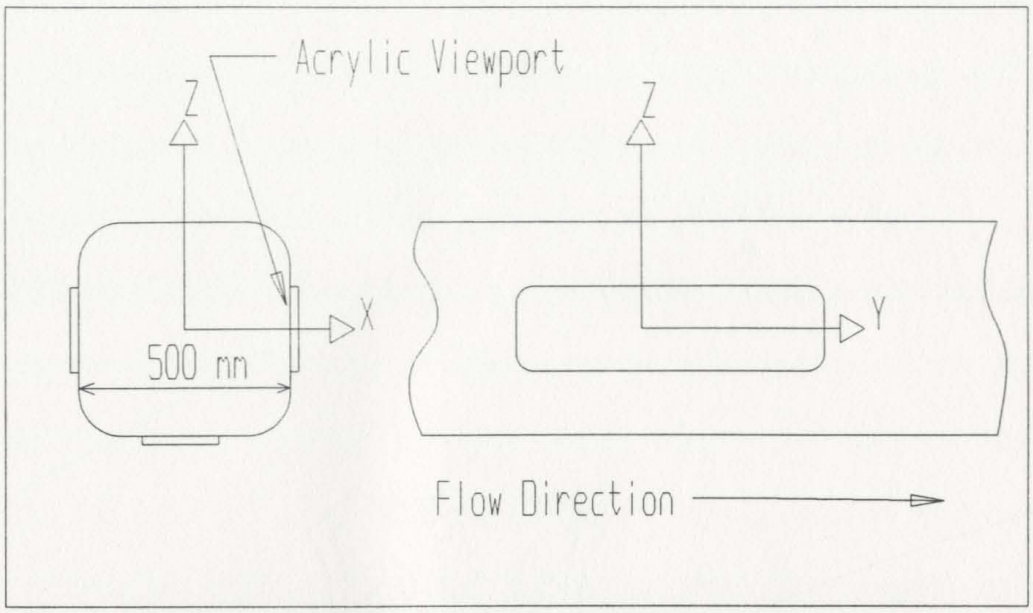

Figure 8 - Schematic of Cavitation Tunnel Test Section

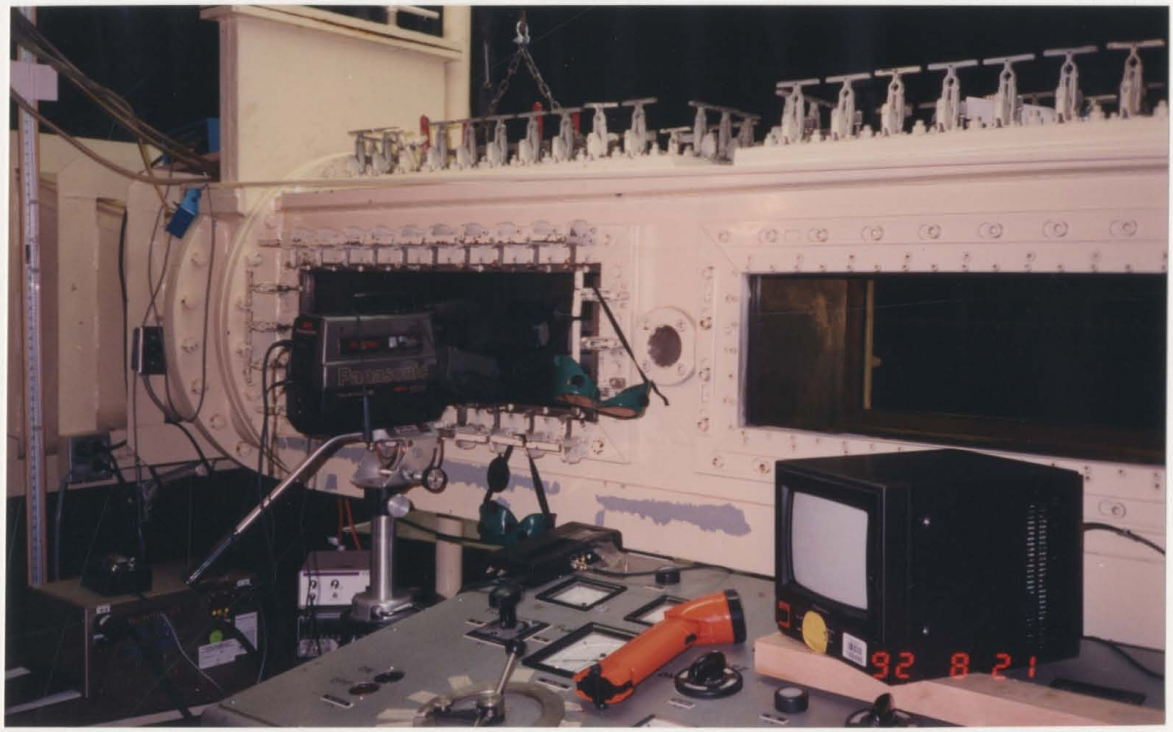

Figure 9 - Positioning of Video Camera at Test Section

Care was taken with the control and measurement of water flow speed within the test section. The design and manufacture of the tunnel impeller controls are 1950's vintage, and fluctuations in flow speed persisted well beyond the three minute settling time suggested by Doucet(1992b). This may have been due to a defective rheostat which controlled the impeller speed. (The electrical contact assembly for the rheostat failed and was replaced shortly after completing the experiments reported in this thesis.) The flow was allowed to stabilize for a minimum of fifteen minutes before conducting experiments. Water speed was measured using the water manometer system described by Doucet (1992b). Manometer readings were taken before and after each experiment, at approximately 2 minute intervals. The average of two readings bracketing an experiment was used to calculate mean flow speed in the test section. Equation 4.12 of Doucet (1992b) was used to convert manometer readings into flow speed. The offset in the zero speed readings on the water manometers, Doucet(1992b), was attributed to a pressure imbalance in the mercury manometers. An excess pressure was transmitted to the water manometers via a common manifold at the test section pressure taps. This offset was eliminated by isolating both sets of mercury manometers, velocity and pressure, from the test section for the duration of the experiments.

The tunnel test section area is enclosed in a heavy black canvas draping which kept out unwanted light during experiments and formed a 'laser control area'. A two-tone siren and flashing amber light were installed near the top of the tunnel enclosure. This alarm system was activated prior to commencing experiments using the laser, and provided an

audible and visual warning to personnel in the area. Details of the safety features and procedures, required for use with the laser, can be found in ANSI (1986). The relevant portions of those guidelines, adapted for these experiments, are reproduced in Appendix A.

3.2 Seed Particles

The primary requirements for a seeding material are that the particles produce images visible to the recording equipment when illuminated by the light source, and that they properly follow the flow, Adrian and Yao (1985). An important consideration for this study was the availability and price of the material in light of the unknown quantity required for seeding the water in the cavitation tunnel (about 20 cubic meters). The lack of a water quality control system for the cavitation tunnel required that the particles should ideally be inorganic so as not to lead to increased algae growth in the tunnel water. The development or purchase of custom designed particles, as suggested by Katz and Huang (1990), was not considered feasible for this study.

The use of Aluminium based particles for seeding water flows is well known, e.g. Adrian (1989). Other researchers, e.g. Rimai et al.(1986), have taken advantage of commercially produced micro-balloons as a cheap source of particles. The seed particles selected for this study were Aluminium-Silicate micro-spheres used in the fibreglass industry as a filler material for fairing compounds. They are manufactured and

distributed by Gougeon Brothers Incorporated under the registered trade name West System® 409 Microspheres. The cost of a nine ounce (255 gram) package was (US) $ 7.95. The Material Safety Data Sheet (MSDS) for this product is given in Appendix B.

These particles are inorganic with a nominal outside diameter of 75μm and a specific gravity is 0.18. Microscopic examination revealed that the particles were roughly equiaxed with a faceted surface. Particle diameter, measured from video images recorded during the examination, was found to be on average closer to 40μm than 75μm. Figure 10 shows a typical digitized image recorded using a video camera looking through the microscope, magnification is 200X. When introduced into water the particles exhibited a tendency to 'clump' and trap air at the junctures. Such 'clumps' of particles were very buoyant and thus did not contribute to the effective particle concentration. Air entrained in the tunnel water would also act as cavitation nuclei, and this had to be eliminated as it would adversely affect propeller cavitation tests being undertaken at about the same time as these experiments. To reduce the tendency of air entrainment and increase the ease of introduction into the tunnel water, particles were first wetted in a solution containing a surfactant. A solution of 50% water and 50% Kodak Photoflo 200, a photographic processing fluid, was used successfully for this purpose. A benchtop experiment, using a range of shutter speeds and ambient light levels, indicated that these particles were highly visible when illuminated with low levels of laser light.

These particles thus satisfied four of the five criteria: visibility, availability, cost and organic contamination. A possible violation of the fifth criterion, resulting from the discrepancy between the specific gravity of the particles (ρ_p=0.18) and that of water (ρ_w=1), was noted. Agui and Jiminez (1987), Gharib and Willert (1989) and Adrian (1991) all discuss the relationship between density mismatch, particle size and fluid viscosity for proper particle tracking in turbulent flow. However given the size of the particles chosen (d_p < 75 microns) and the fact that the study was to be limited to steady flow only, it was assumed that the viscosity of the water coupled with a relatively high flow speed would overcome the buoyant force exerted on the particle by the density mismatch. Observations made during early experiments outside of the cavitation tunnel tended to support this assumption. When properly wetted and introduced to a solution with some initial agitation (i.e. stirring) the particles took several hours to float to the surface. Uniform flow experiments, in the cavitation tunnel, using a 1/60 second shutter speed with a flow speed of 1.6 m/s resulted in a particle track approximately 25 mm long. This represents a particle displacement of about 350 diameters, and there was no measurably deviation of the particles motion from a straight line. Some displacement

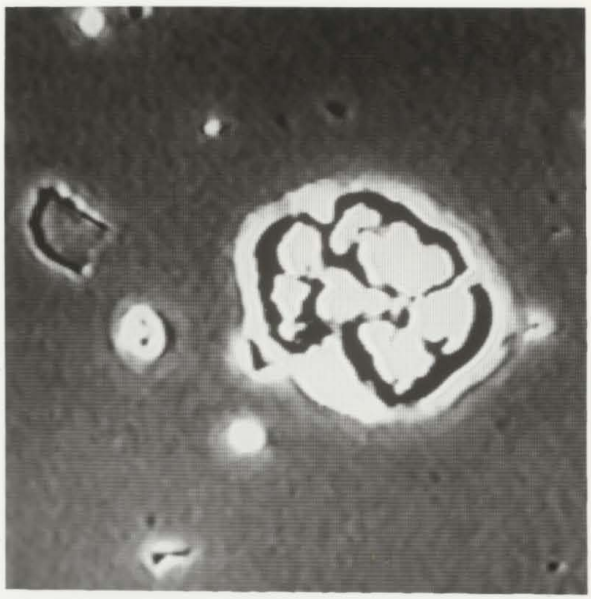

Figure 10 - Digitized Image of Seed Particle (200X Magnification).

vertically upward (+ve z) would have been expected had the density difference of the particles been a significant factor in particle motion within a steady flow field.

The optimum concentration of seed particles was not known *a priori*. Small quantities of particles, typically 5 grams at a time, were added at intervals during the course of the experiments for a total of about 30 grams. Water level in the tunnel was adjusted frequently during the course of the test program both to allow the introduction of more particles and to install models. Such adjustments are possible using a separate holding tank connected to the tunnel via a plumbing system, Doucet (1992a). Assuming negligible loss of particles during the transfer of water to and from the tunnel, this represents a final particle concentration in the cavitation tunnel of about 1.25 grams/m^3. The low concentration of particles, especially in the early stages of the test program, resulted in a low data sampling rate, that measure being defined here as the average number of complete particle tracks visible in each video frame. The rate varied from an initial value of about 0.25 up to a maximum of about 2 for the later experiments. With no practical means to selectively remove particles from the tunnel, the concentration was increased slowly to avoid a situation of too many particles visible in a single image. This would have resulted in overlapping tracks, making the analysis of individual tracks difficult. Had an excessive concentration occurred, the tunnel would have had to been completely drained and the process (of adding particles) would have to be begun again. It was considered wiser to accept a slowly increasing sampling rate and then use image superposition to define the flow field.

3.3 Laser and Laser Optics

The key criterion for selection of a suitable light source for any PTV system, is that the area of interest be sufficiently illuminated for the particle images to be recorded with the equipment available. This highlights the inter-relationships between the selection of a laser, a seeding material and a recording medium.

The purchase of a new laser was not possible within the budget allocated to this research, and had it been so it would still not have been the most practical solution. The laser power necessary for a given application depends on several different factors: size of the area to be illuminated; sensitivity of the (image) recording equipment; particle size, concentration and (light) reflective properties; and the speed of the flow being investigated. Adrian and Yao (1985) present a discussion on the interaction of some of these factors. In order to minimize expense, a laser having the minimum required power could have been purchased, but this minimum level could not be determined easily or accurately. The decision was thus made to rent a laser for the duration of the experiments and from there, to determine what level of laser power would be likely to be necessary for the application of the method to various different situations. The only criterion remaining, aside from price, was that the laser could not require special plumbing or wiring, neither of which would be possible to accommodate in the time available.

An air-cooled constant wave (CW) gas laser (American Laser Corporation Model 60B) with a rated output of 60 milliwatts was used for the experiments in this study. The lasing medium was Argon-ion gas emitting light at a wavelength of 514.5 nanometres. Beam diameter at the laser aperture was approximately 0.6 mm with a divergence of 0.7 millirads. More detailed specifications are given in Appendix C.

Prior to the experiments the output from the laser was measured (by the supplier, Canpolar East Inc.) at about 28 to 30 milliwatts using an Ophir Model 30-A portable power meter.

The light beam from the laser was not suitable for a particle tracking application until it had been formed into a sheet and directed into the flow. A common method used to achieve this is with the use of a cylindrical lens and a mirror. The placement of components varies depending on the testing facility, e.g. see Marko and Rimai (1985), Katz and Huang (1990), Okuno (1990), and Willert and Gharib (1991). With such a low power output (about 30 mW) available from the laser it was not practical to use a lens to expand the beam. The intensity of light energy within a sheet generated in such a manner would not have been sufficient for illumination of an area of practical size. For a given laser power the intensity of the light will vary inversely with the area being illuminated, Winburn (1987). If the 0.6 mm diameter beam were expanded to a sheet, of say 10 mm. in width, the intensity of the light would be only about 7% of that of the original beam. A 10 mm wide field of view would have little practical application in

defining flow structures in the wake of a ship model, even if the intensity could be accommodated by improved imaging and/or processing equipment. To maximize the effectiveness of the system it was necessary to obtain, in the light sheet, as much as possible of the intensity of the beam as emitted from the laser aperture. This was achieved by rapidly scanning or 'sweeping' the beam in order to generate a sheet of light. Okuno (1990) reported on work being carried out in Japan using a rotating (polygon) mirror for this purpose. An IDS 2512 optical scanner from General Scanning Incorporated was used for the work reported here.

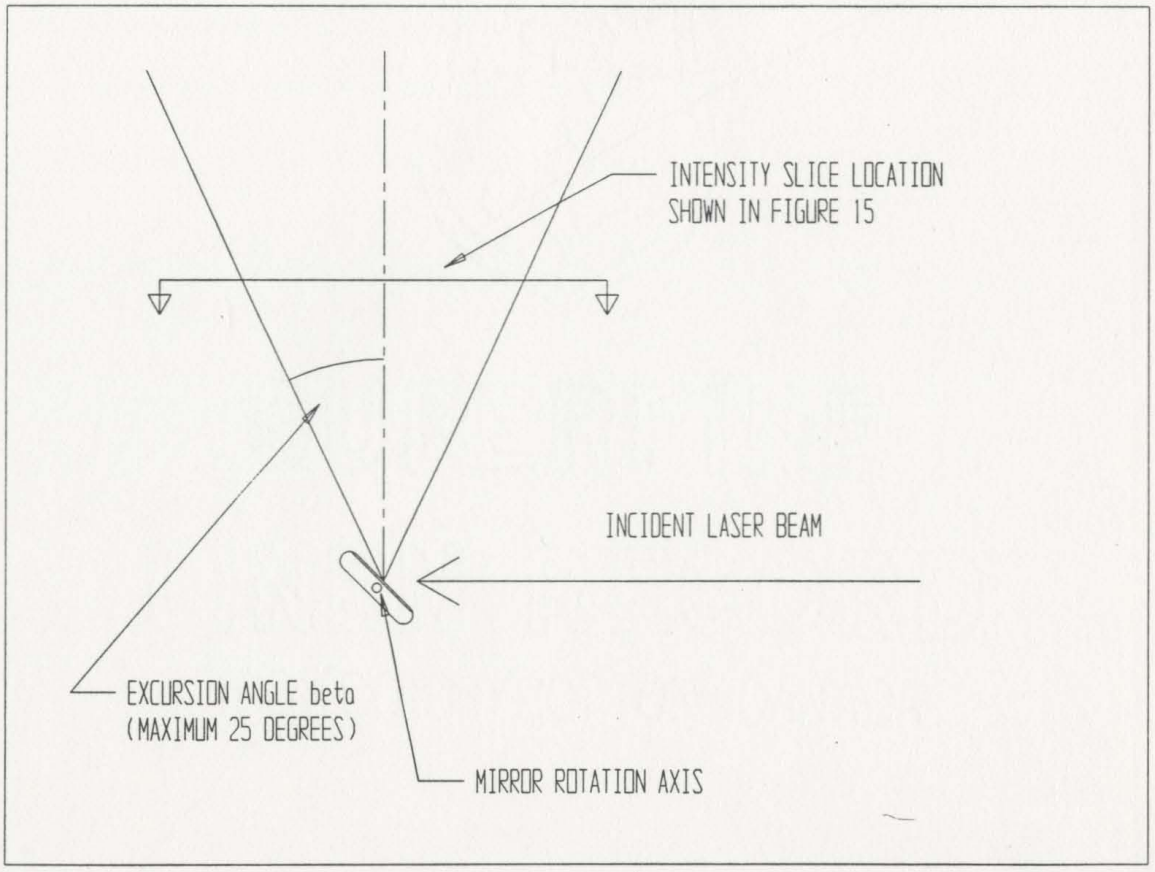

Figure 11 - Light Sheet Generation Using an Optical Scanner

This scanner is a galvanometer driven oscillating mirror with a maximum 25 degree excursion angle. Technical specifications are given in Appendix D. When placed in way of the laser beam the mirror redirected the beam, and its oscillatory motion formed the required sheet of light inside the tunnel test section. This arrangement is shown schematically in Figure 11. The thickness of the light sheet was calculated about 1.1 mm, determined using the beam divergence of 0.7 millirads and a path length of 750 mm as measured from the laser aperture to the vertical centerline of the tunnel test section. Distortions of the laser beam due to the mirror and the acrylic viewports in the tunnel were assumed to be negligible.

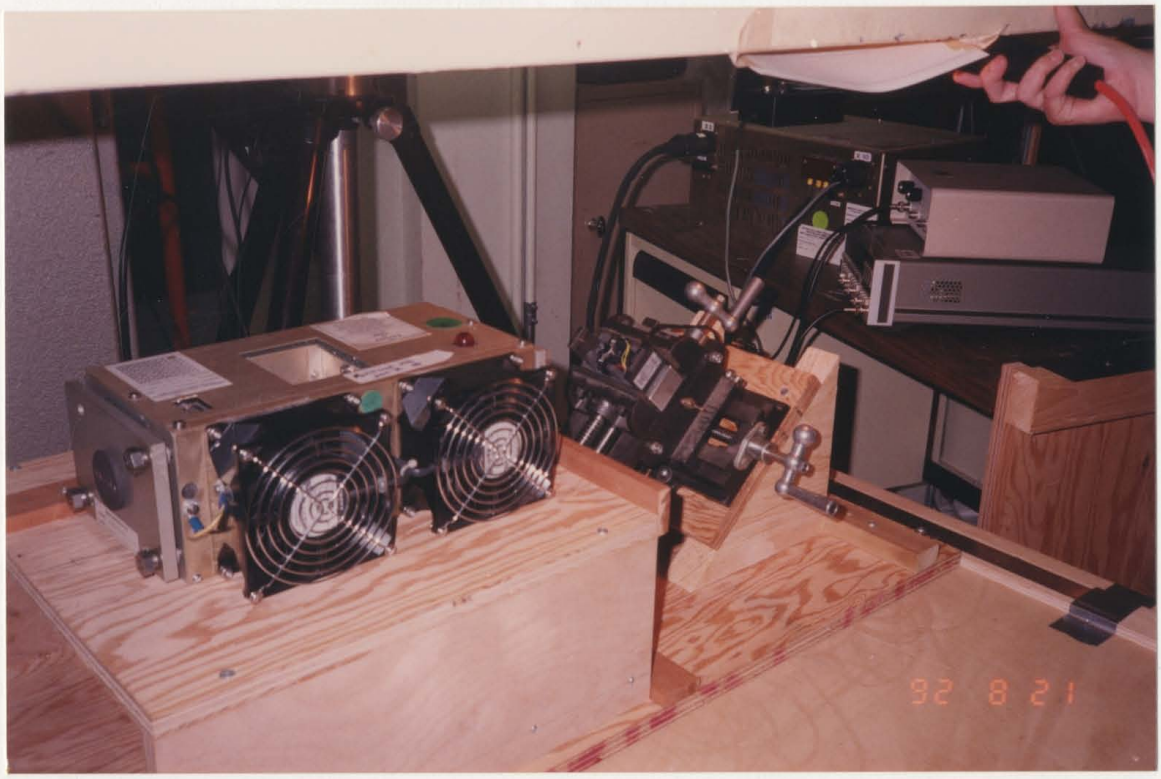

Figure 12 - Placement of Laser and Scanner Beneath Tunnel Test Section

The laser head was placed below the test section of the tunnel on a platform which rested on a plywood base, Figure 12. Alignment strips on the platform ensured that the laser head remained stationary during an experiment. The scanner was set in an X-Y traversing unit which was mounted at a 45 angle relative to the base of the laser head. The traversing mechanism, visible in Figure 12, simplified alignment of the scanner relative to the laser. The angular positioning ensured that with the mirror at rest the laser beam was reflected vertically into the test section, and when set in motion the light sheet was generated evenly about this centerline. Guide rails on the base allowed the laser and scanner to be moved as a unit in either the transverse(x) or longitudinal(y) direction, although not at the same time. This approach was effective; a minimum of time (about 15 minutes) was lost in changing the guide rails from one orientation to the other. Figure 13 shows the guide rail in position to permit adjustments in the transverse direction. The pointer and ruler visible in this Figure were used to determine movement of the unit.

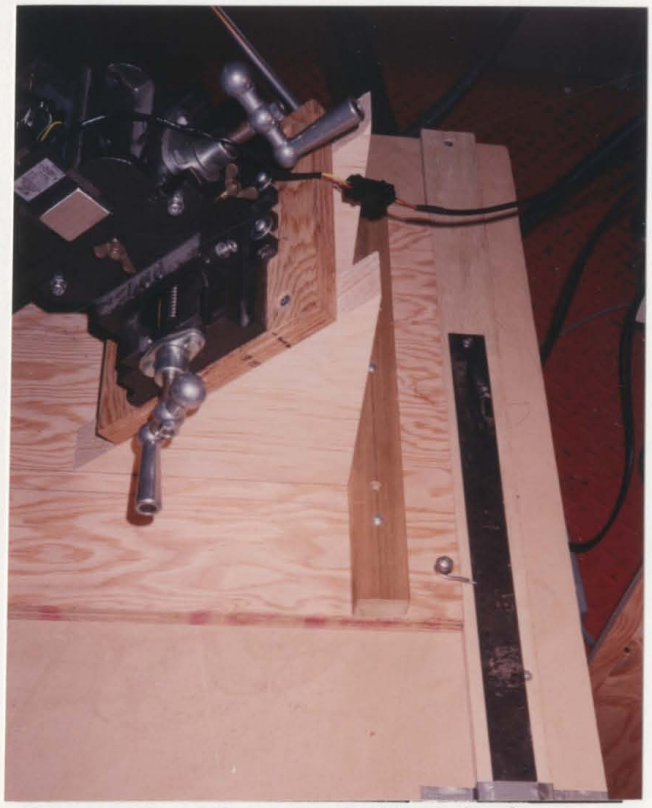

Figure 13 - Alignment Guide Rails for Laser Assembly.

A Hewlett-Packard 8116A function generator supplied a 1.19 kilohertz sine wave, 5 volts peak-to-peak, to the scanner driver. Oscillation amplitude of the mirror was then regulated by the driver's output gain control. System setup is shown schematically in Figure 14.

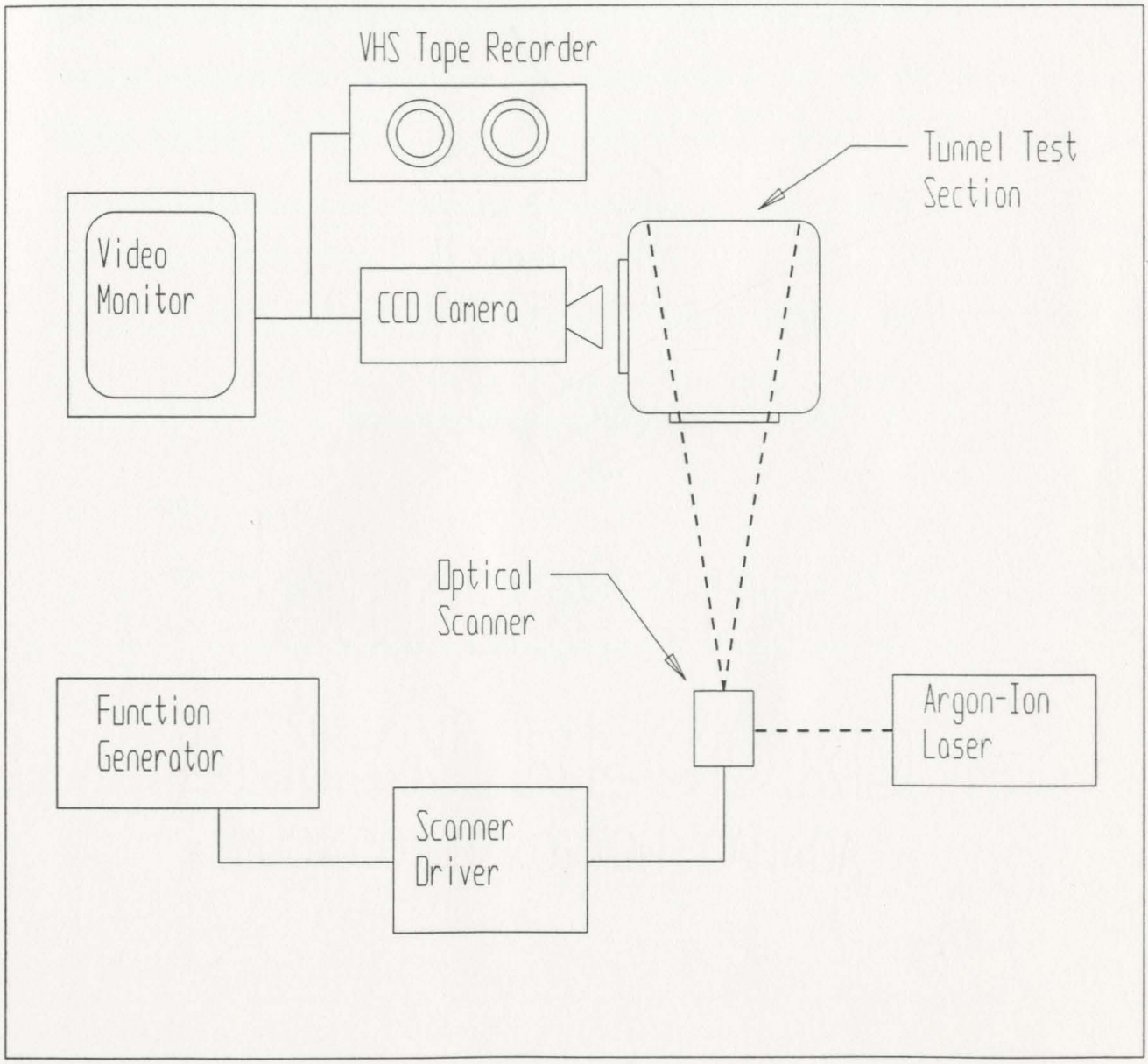

Figure 14 - System Assembly Schematic

Generation of the light sheet in this manner produced two significant results.

i) The energy intensity within the light sheet, at the instantaneous position of the beam, was maintained close to that of the original beam emitted by the laser. The small losses of energy due to imperfect reflection from the mirror surface and attenuation by the Acrylic viewport were unavoidable. Such effects would in any case be present in a system utilizing a cylindrical lens and a stationary mirror. Figure 15 shows a typical intensity distribution along a horizontal line within the light sheet. Intensity is represented

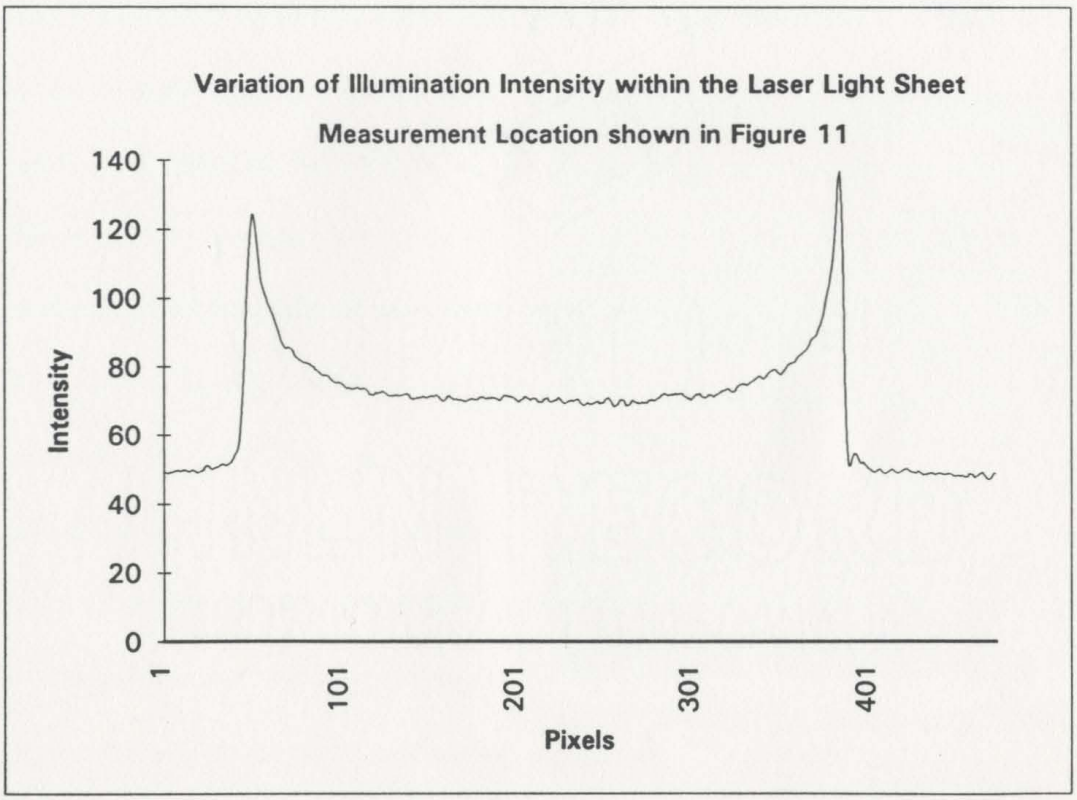

Figure 15 - Intensity Distribution in Laser Light Sheet

by non-dimensional grey-scale values in the digitized image and is plotted against pixel number. The increase in intensity at the edges of the sheet correspond to the reduction in angular velocity of the beam at the extremes of the mirror excursion. About 80% of the width of the sheet can be considered as having an approximately uniform intensity distribution.

ii) The movement of the beam resulted in a pulse-coded illumination of particles, Rimai et al. (1986). When particle motion and beam motion were in the same direction the particle image was elongated, when in opposite directions, the image was fore-shortened. Figure 16 shows a typical particle track produced using this method. However not all particle images had identical pulse codings. The ratio of the number of complete beam 'sweeps' to exposure time could not be set to an integer value using the shutter speed settings available on the video camera, and the beam was thus not in the same position at the beginning of each video field. This resulted in the illumination sequence for any given particle being a function of its position, within the camera's field of view, with respect to the position of the laser beam at the instant of shutter opening. The arbitrary nature of the code, and the

Figure 16 - Typical Particle Track Image.

possibility of slightly incomplete particle tracks, was considered acceptable for the initial investigation.

Generation of a pulse coded particle track using a C laser, without the aid of a separate modulation unit, reduced the cost of the system. An acousto-optic modulator, see e.g. Khalighi (1989), provides precise control over illumination sequence, but is a more expensive solution. Mechanical beam choppers (rotating slotted discs), while relatively cheap and flexible, do not provide perfect ON/OFF illumination, Agui and Jimenez (1987).

The maximum practical excursion angle of the mirror, shown in Figure 11, was found to be about 5°, giving a sheet of light about 70 mm wide at the vertical centerline of the tunnel test section. Beyond this point the beam was moving too rapidly to produce a sufficiently intense particle track image. This restriction was a result of both the low laser power available, and the combination of flow speed and camera shutter speed selected. Figure 17 is a 35 mm photograph showing the light sheet in the tunnel intersecting the leading edge of the cylinder.

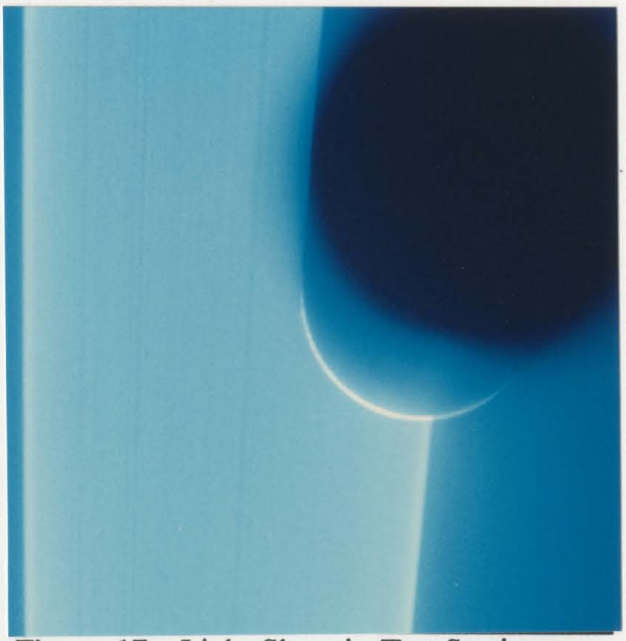

Figure 17 - Light Sheet in Test Section.

3.4 Image Recording

The low cost, availability, and ease of use of consumer video cameras were the deciding factors in the selection of a recording medium. Higher levels of sensitivity and improved resolution are available with the use of photographic film, Adrian and Yao (1985), but for this study the time and additional cost associated with a photographic approach was unacceptable. However, the method described in this thesis can be adapted for use with still photography. Figure 18 is an enlargement of a 35 mm photograph showing particle pathlines produced using this method. In this case the intensity of the light provided by the laser was insufficient to allow a shutter speed fast enough to record the particle pulse-code with the type of film used. (Photograph by J. Bourne, MUN University Relations). Figure 19 shows similar images, of flow around a cylinder, but have been printed from video records recorded using a 1/250 (nominal) shutter speed. Qualitative flow visualization can be easily achieved using the setup for these experiments.

The camera unit used for these experiments was a Panasonic Omni-Movie PVS350-K digital Charge Coupled Device (CCD) camera. Technical specifications are given in Appendix E. The camera was equipped with an 8.5-68 mm/f1:1.2, TV zoom lens, giving a field of view of about 140 mm x 110 mm at a range of 500 mm. The video signal output from the camera was in National Television Standards Committee (NTSC) format and written directly onto VHS videotape. The camera framing rate was the NTSC

standard of 30 full frames per second, each frame being composed of two interlaced fields sampled by the array at a rate of 60 Hz. (AT&T 1977)

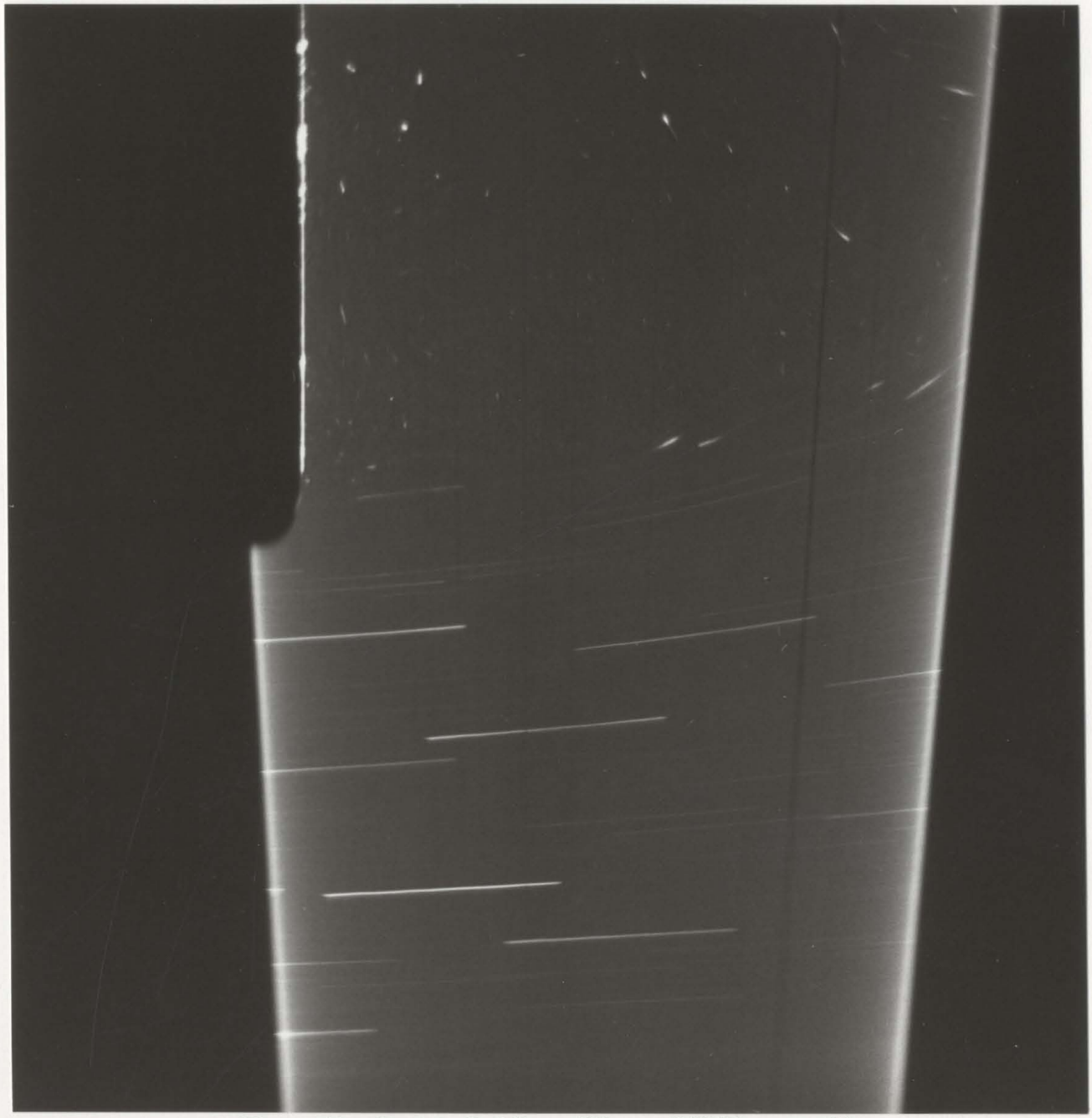

Figure 18 - Particle Pathlines (35 mm Still Photograph)

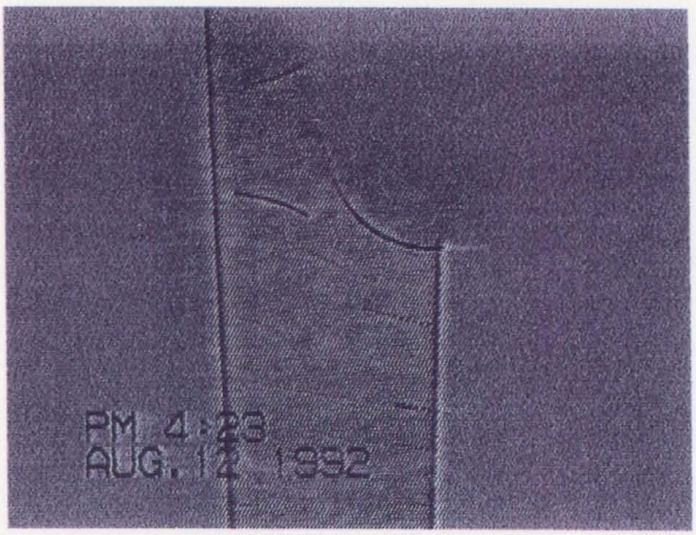

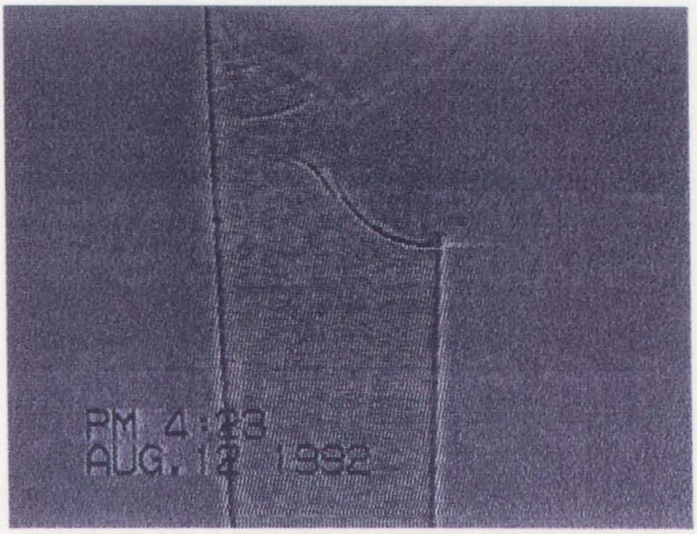

Figure 19 - Qualitative Flow Around a Cylinder.

For optimum system performance it was necessary to minimize spurious light reflections from entering the camera lens. Positioning the camera with the lens ring tight against the viewports in the tunnel test section accomplished this while at the same time providing a simple way to check camera alignment. The camera was mounted on a tripod and aligned with the illuminated region of flow by using a separate monitor to establish the field of view for the recorded image. Movement of the tripod due to vibrations transmitted through the tunnel work platform, or accidental contact with the operator during camera setting adjustments, was a major source of annoyance throughout the experiments. Fabrication of a more rigid mounting apparatus, perhaps fixed to the tunnel test section, was not possible in the time available. The camera was activated using a wired remote control switch in order to avoid unnecessary handling of the camera. During experiments movement of personnel on the platform was restricted as much as possible. A power-saving feature placed in the camera in standby mode after about 5 minutes of inactivity. However, when returned to READY mode via a switch on the camera housing, all settings including shutter speed were returned to their default status. This caused a loss of time in order to reselect the appropriate settings, and necessitated the repeat of several experiments.

The distance from the lens to the focal plane was outside the range over which the camera would focus automatically, and the camera was placed in MACRO mode and (re-)focused manually for each experiment involving a change in the distance from camera to light sheet.

For all experiments reported here the camera operated with a nominal shutter speed of 1/250 second. An exact shutter speed of 1/245.88 second can be calculated based on the charge time for the CCD array (Personal communication, Mr. Ed Butland, Audio System Ltd., 12 August 1992). The concept of 'electronic' shutter speeds in a video camera can be visualized using the simplified clock pulses shown in Figure 20.

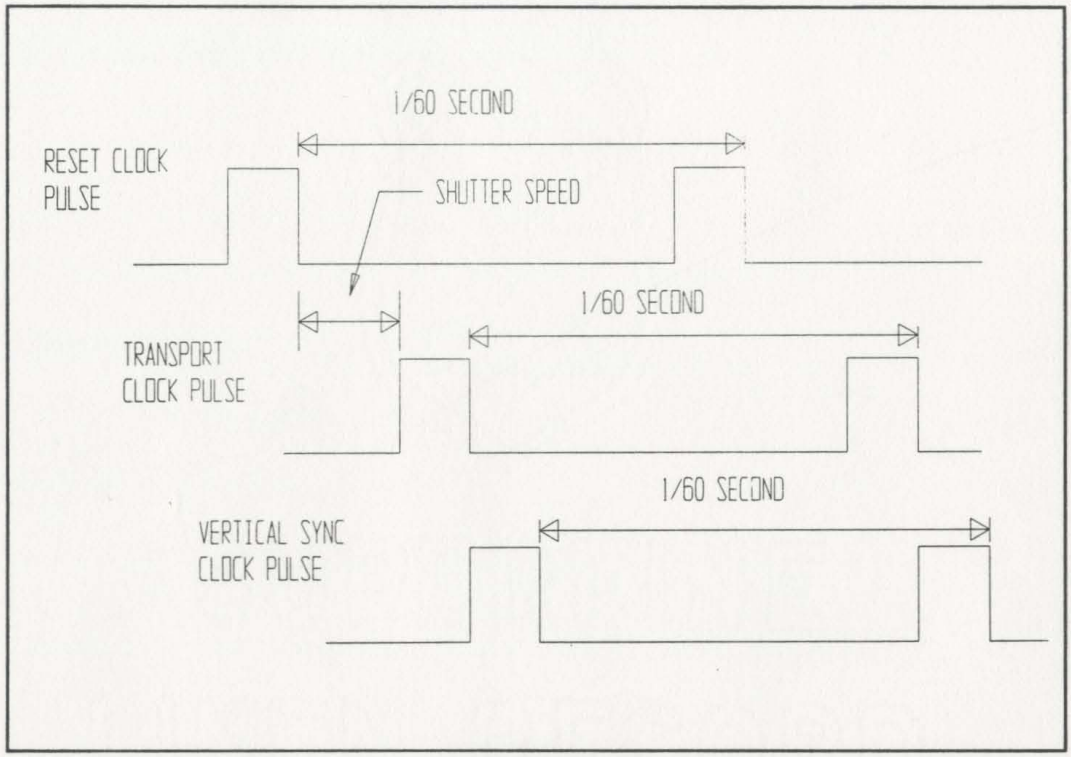

Figure 20 - Definition of 'Electronic' Shutter Speed.

With the first pulse of the RESET clock the CCD array is discharged and ready to receive the light energy entering through the lens. When the TRANSPORT clock pulse is encountered the intensity information in the primary array is shifted out in parallel, one line at a time, to a storage register. The time lag between the RESET and TRANSPORT clock pulses, when the CCD array is affected by the light entering through the camera's

lens, defines the shutter speed of the camera. From the storage register the information is output in a serial fashion, in the 1/60 second between pulses of the VERTICAL SYNC clock, and written to the video tape as an analog signal. This process produces a video field, and sequential fields, 1/60 second apart, can be interlaced to form a video frame, AT&T (1977). A simplified schematic of a CCD camera is given in Figure 21. (Personal communication Mr. J. Millan P.Eng, Electronic Services, IMD, National Research Council Canada, September 1992).

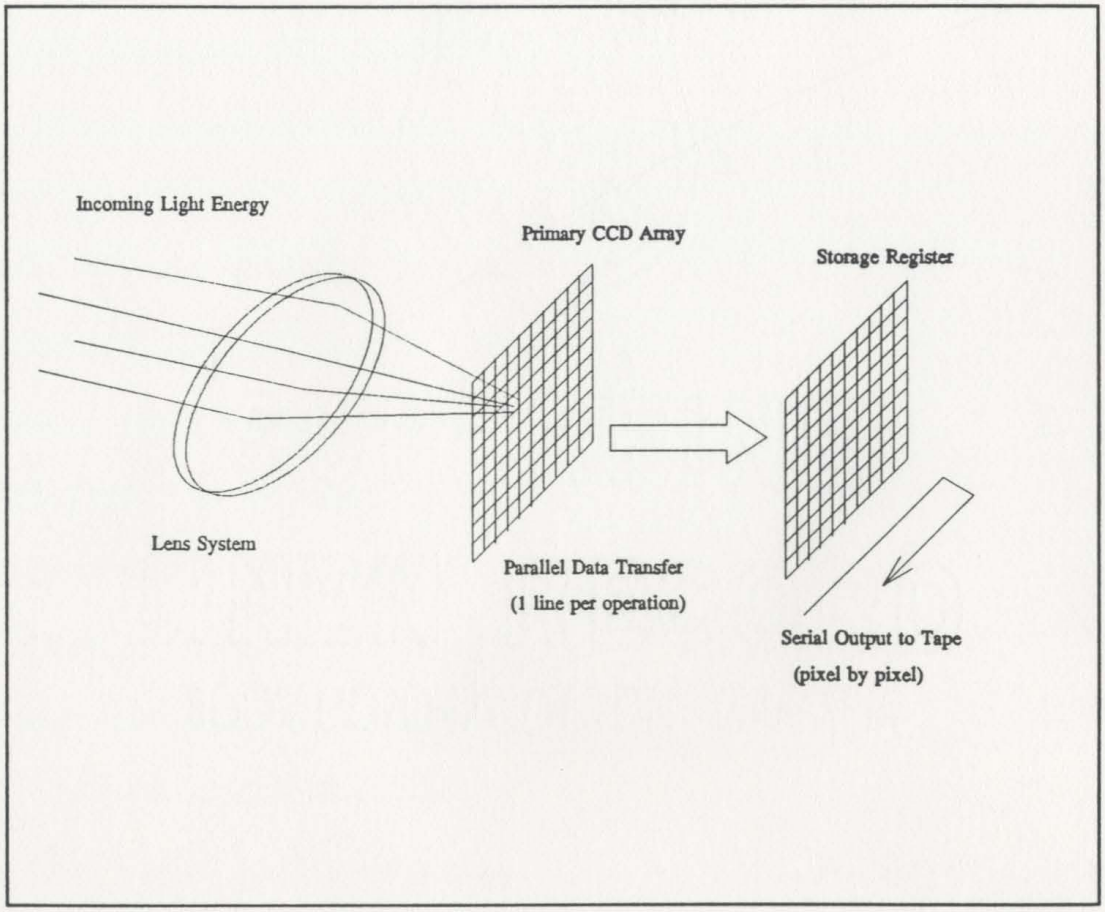

Figure 21 - Schematic of CCD Camera Operation

The camera itself was capable of shutter speeds from 1/60 seconds to 1/1000 seconds and selection of the most appropriate shutter speed was based on a qualitative evaluation of images recorded on the video tape. This was possible at the tunnel by using the built-in editing features on the camera and displaying the images on the separate monitor shown schematically in Figure 14. The primary considerations for selecting a shutter speed were image plane visibility and the ratio of particle track-length to the dimensions of the light sheet. The use of higher shutter speeds (i.e. 1/500 seconds and 1/1000 seconds) was not practical with the laser power available, and at the flow speed selected. The amount of light reflected by the particles in such a short time was insufficient to render the particle tracks visible in the recorded image. The lower shutter speed, (i.e. 1/60 seconds), while giving a brighter image, resulted in particle tracks which in length were equal to approximately half the width of the light sheet. In such a case the probability of having a complete particle track within the illuminated portion of the field of view was reduced. Longer exposure times in the case of flows which possess significant curvature in the time scale of the shutter speed produce curved particle tracks, Figure 22.

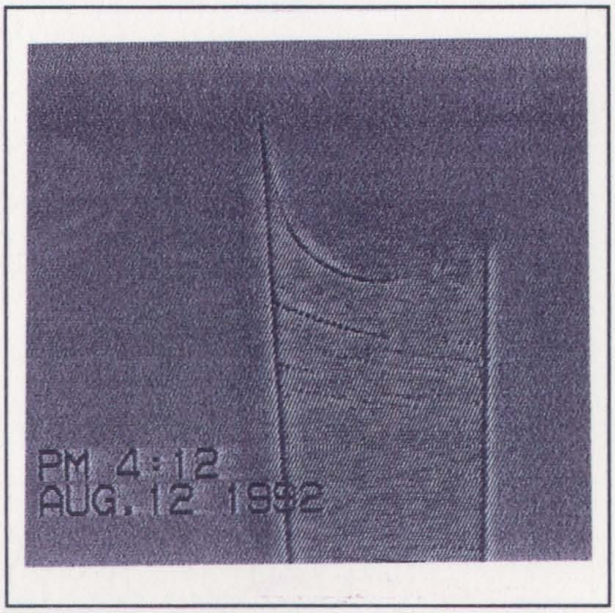

Figure 22 - Particle Tracks - Using 1/60 Second Shutter Speed.

This would be useful for qualitative visualization but the curvature of the tracks would complicate quantitative analysis of the images.

3.5 Data Reduction and Analysis

All data reduction and subsequent analysis was done using an IBM-compatible Hewitt-Rand microcomputer operating at a clock speed of 33 MHz. using an Intel 80486 CPU chip. This computer used an EISA (Expanded Industry Standard Architecture) bus configuration which reduced the burden on the main CPU during file manipulation. A similar system with an ISA (Industry Standard Architecture) bus was tried and found to be noticeably slower when reading/writing the image files from/to the hard disc.

The composite National Television Systems Committee (NTSC) signal from the recorded video tape was digitized using a Truevision® TARGA+® frame grabber board. This board had an output pixel resolution of 490 x 400 with the intensity of each pixel defined by one of 256 possible grey levels (8 bits). The space-bandwidth product (SBP) of the digitized image, as defined by Hesselink (1988) to express the quantitative information contained in an image, was thus constant at 2×10^5. To overcome the flow speed limitation imposed by the NTSC framing rate of 30 Hz., for analysis using sequential frames see e.g. Okuno (1990), the pulse coding generated by the laser scanning system was utilized to permit single-frame\multi-pulse analysis, Adrian (1991). A manual selection process prior to image digitization was essential as not every video

frame contained complete particle tracks due to the low particle concentration. In order to avoid blurring of the image, which would be present in the interlaced video frame due to the 1/60 second separation of the individual fields, it was necessary that only single fields be used for analysis. The frame-grabber board, when given the FREEZE command to digitize an image, would operate on whichever field was present in the video buffer at that instant and the result would be a complete and stable image. However, when the playback deck was put in PAUSE mode to display a suitable image containing complete particle tracks, synchronization between the playback deck and the frame-grabber board was lost. This was the result of the slightly different SYNC signal output by most video playback decks when put in PAUSE mode (personal communication Technical Support Services, Truevision Ltd., 27 August 1992). The result was a blurred image which was visually unstable. To overcome this problem a video playback deck (JVC model BR-S622U) with frame-by-frame advance and Time Base Correction (TBC) options was used. The frame advance feature allowed manual review, and selection, of individual fields containing appropriate images. The TBC stripped the original synchronization signal from the frozen composite image and inserted a new signal which was compatible with the frame grabber board. This allowed flicker-free digitization of the image represented by a single field. However it was not possible to view all of the recorded fields. The playback unit would only display a single field from each frame. If it were possible to examine all the fields then the effective sampling rate could theoretically be doubled.

The digitized field images were each approximately 198 kilobytes in size. The image files were written in a Tagged Image File (.TIF) format directly onto the computer hard-disc for intermediate storage. Data from different experimental sets were grouped and subsequently transferred to 3M® DC-2120 mini data cartridge tapes for longer term storage.

A commercially available video analysis package, JAVA®, by Jandel® Scientific Corporation, was used for analysis of the digitized images. This is menu-driven interactive software with basic image processing features such as contrast enhancement and image arithmetic, as well as geometric measurement capabilities for pixel co-ordinates, areas, lengths and angles. Details of the necessary hardware and software calibrations are given in Jandel (1990). The hardware calibration accounts for any pixel distortion introduced by the interaction of the camera and the frame-grabber board. The software calibration was necessary to relate the pixels in an image to physical 'real world' units. For these experiments a laminated section of graph paper placed between two plates of 3 mm acrylic and mounted vertically in a wooden

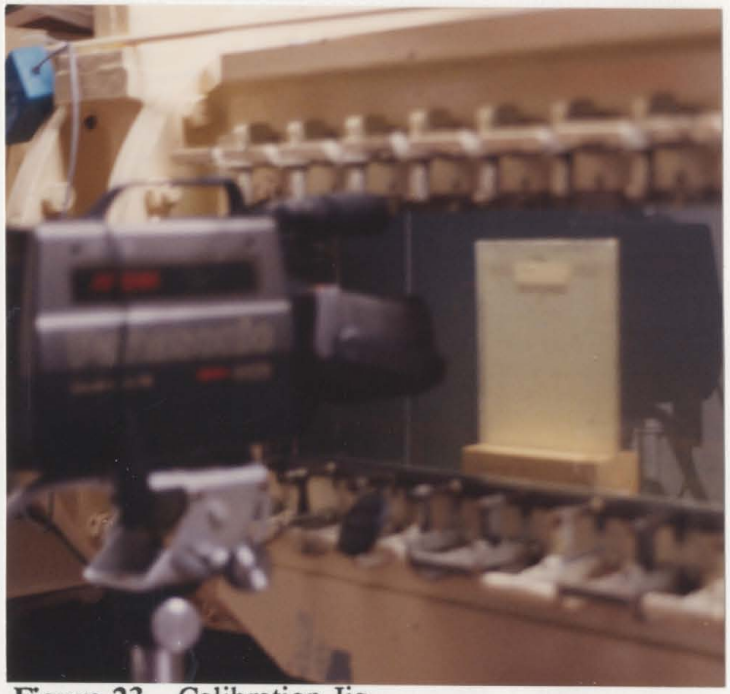

Figure 23 - Calibration Jig.

base was used for calibration purposes. Figure 23 shows the calibration jig in place in the tunnel test section. The jig was placed in the tunnel at each position for which measurements would be later be required and the image recorded on videotape. During the analysis process the physical dimension of an image, recorded at the different locations, could be computed by calibrating the software using the appropriate image of the graph paper. The calibration procedures used for these experiments, which are somewhat different from that described in the JAVA® user manual, are given in Appendix F. The procedures outlined in the manual, when followed exactly, produced erroneous results. This error was addressed by a set of product technical notes, Jandel (1991), but those notes are also incorrect.

Once the software was calibrated using the appropriate image of the calibration jig, a digitized image of the flow was displayed on a TV\video monitor (Sony KV-20EXR20) and the contrast enhanced as necessary to allow easy identification of the particle tracks. The linear contrast enhancement process assigns new gray levels (representing pixel intensity) to a new specified range of grays without altering the relationship between them, Jandel (1990). Figure 24 shows a typical image before and after contrast enhancement. The X,Y co-ordinates of the first and last pixels in the track image, the overall length of the track image, and its angle relative to the horizontal were identified using an interactive cursor. This information was placed automatically, by JAVA®, into a data worksheet, and at the end of an analysis session was output in a Data Interchange Format (.DIF) ASCII file. All data assembly, tabulation, and mapping of

velocity vectors into physical spatial co-ordinates, were achieved using the Microsoft® Excel® (Version 4.0) spreadsheet package.

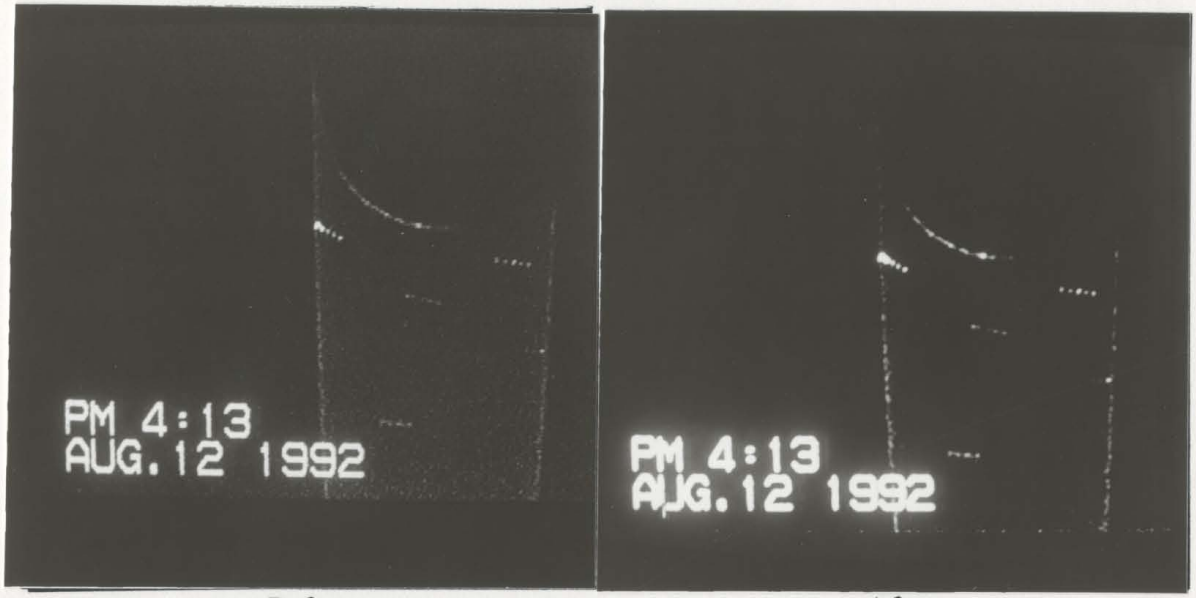

Before After

Figure 24 - Effect of Contrast Enhancement.

The first and last pixels in each track was usually easily identifiable following a single iteration of contrast enhancement. In some cases, with extremely bright particle images, no enhancement of any kind was required. Each digitized field was examined before applying any image processing.

For horizontal tracks the selection of the first and last pixels in a particle track was straightforward. The tracks were typically two pixels in width, and the uppermost row of pixels was used consistently to determine track length. An intensity distribution along a typical particle track is shown in Figure 25. Theoretically this information could

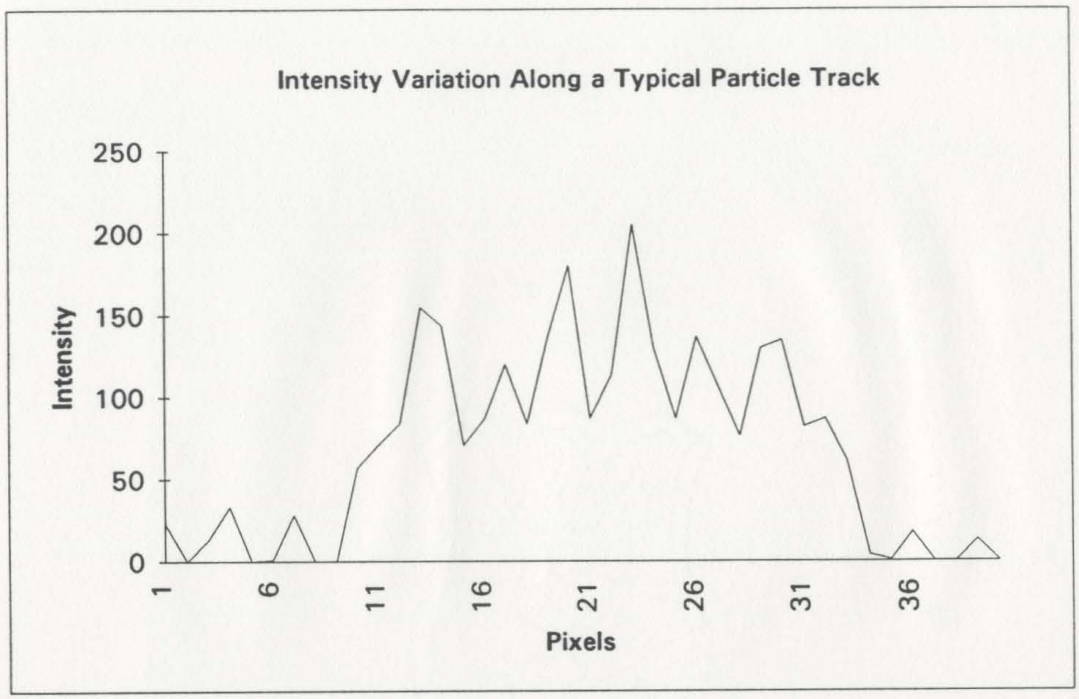

Figure 25 - Intensity Distribution Along a Particle Track

be used to determine track length by calculating the distance between the first and last intensity peaks. This is not easily done with the current software as it does not provide a means for relating linear intensity measurements to physical space. An indirect method was tried and abandoned due to the excessive time required to import and export the information required to make the necessary calculations. In the case of overlapping tracks, the mean length was determined by averaging the lengths of top and bottom rows of pixels. Figure 26 shows a typical overlapping particle track. For tracks inclined at some angle to the horizontal, a procedure was adopted whereby the length was determined by the extreme pixels on the 'inside' face of the tracks. Figure 27 shows

schematically the definition of 'inside' as used in this context. In all cases particle velocity was computed by dividing the measured particle length by the shutter speed of the camera.

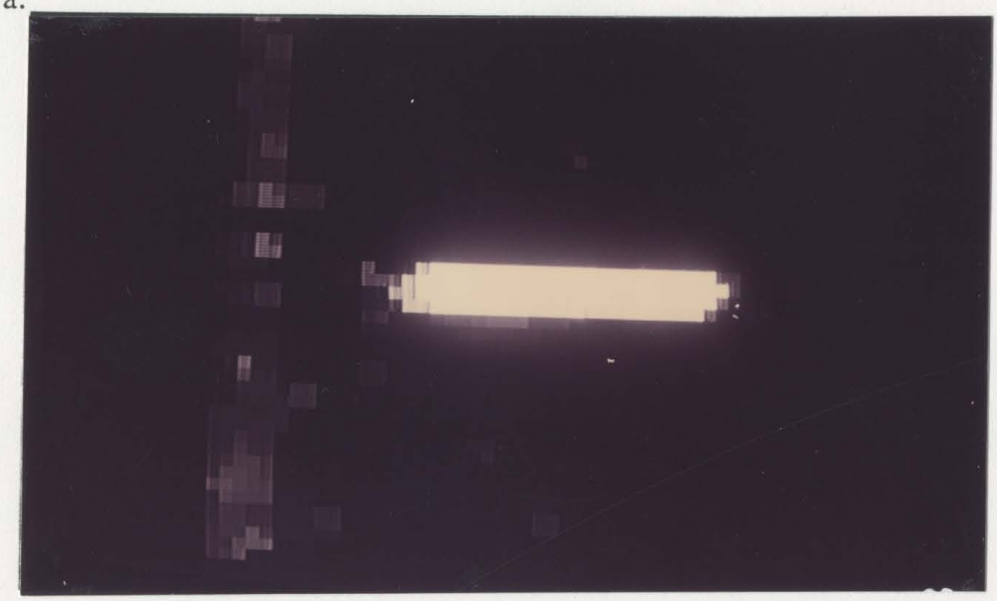

Figure 26 - Overlapping Particle Images

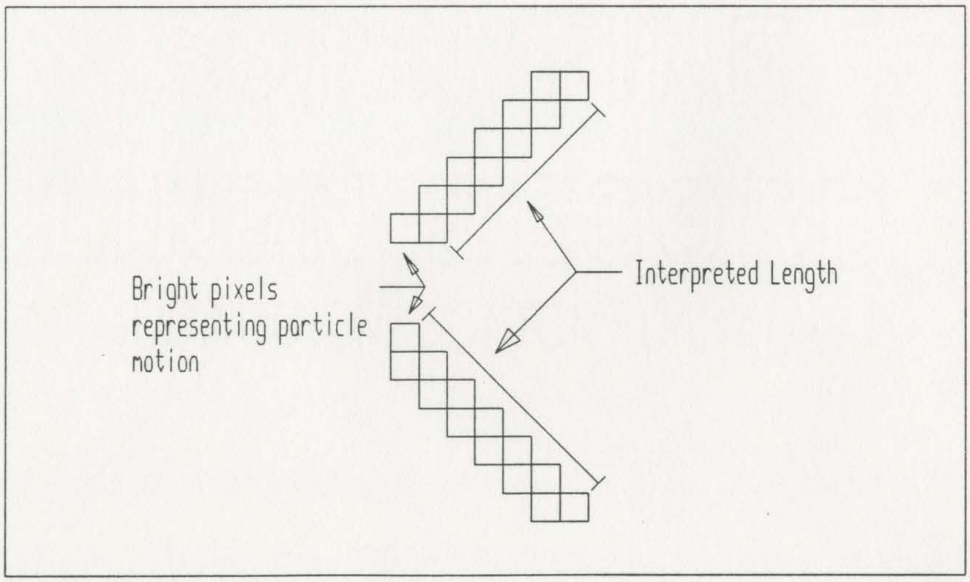

Figure 27 - 'Inside' Face of Particle Tracks.

Chapter 4

Experimental Results

This chapter presents the results of experiments conducted as part of this study. A discussion of the significance of these results is given in Chapter 5.

Section 4.1 presents the results of measurements made in a steady uniform flow using the Digital Particle Tracking Velocimetry(DPTV) system described in Chapter 3. Results are compared with the mean velocity in the test section as measured using a water manometer.

Section 4.2 presents results of measurements for a steady flow around a right circular cylinder, obtained using the same experimental setup. The values of velocity magnitude and direction from these experiments are compared with the same information as predicted by potential theory.

The final set of results using the DPTV system is for an investigation of the flow behind a model of a ship skeg. The model represents a portion of the afterbody of a typical 10 metre Newfoundland inshore fishing vessel. This type of vessel often have

wide, blunt sternposts with an associated uneven flow in the propeller region. The results of the current experiments are compared qualitatively with measurements on a similar type of hull obtained by Wu and Bose (1992c) using constant temperature anemometry in a towing tank.

The experimental setup for all of the DPTV experiments was as described in Sections 3 and 4 of Chapter 3. Schematic drawings are included to indicate the location and orientation of the illuminated (interogation) plane within the tunnel test section and the associated camera field of view. Basic analysis of the video images, to define velocity vectors was conducted using the methods described in Section 5 of Chapter 3.

Results of experiments to measure the static thrust and torque of a marine screw propeller, as obtained in the cavitation tunnel with and without the skeg, are presented and discussed in terms of the effect of the skeg on propeller performance. Predictions of propeller performance using lifting surface theory, assuming a uniform wake, are compared with the experimental results of the propeller with no skeg present. The data collected from the DPTV wake survey was used to calculate the nominal axial wake behind the skeg, and this information was used as an input to an unsteady lifting surface propeller program. The numerical predictions were compared with the experimental values of propeller performance behind the skeg.

4.1 Uniform Flow

Video images of steady uniform flow were recorded from the horizontal midplane of the tunnel test section. Velocity measurements were calculated from 57 particle track images extracted from 73 digitized video fields. Figure 28 is a digitized image of a typical video field collected during these experiments.

Figure 28 - Typical Image Recorded in Uniform Flow

Water speed in the test section was measured at 1.656 m/s using the water manometers. These manometers had previously been calibrated against a pitot/static tube placed in the test section of the tunnel, Doucet (1992b). Figure 29 shows the relationship of the DPTV data points to this mean value (x-y scatter plot). The average velocity as

computed from the mean of the PTV results was 1.643 m/s with a standard deviation of 0.04593.

The accuracy of measurements from a digitized image is determined by the pixel resolution of spatial dimensions. For the results presented in this section this was 0.294mm/pixel. This represented a 0.075m/s resolution for velocity values calculated from the lengths of the particle tracks.

From Figure 29 the majority of experimental velocity values are typically one of two values, the separation between those values being determined by the image resolution as defined above. In a few cases two particle tracks were close enough together to be considered a single image, see Figure 26. In such cases the measured lengths of the top and bottom of the track were averaged to yield a single value. These averaged values are seen in Figure 29 lying almost exactly on the line representing the velocity determined from manometer readings.

In Figure 29, a small number ($<10\%$) of the velocity measurements calculated from the particle track lengths are seen to be about 5% less than the population mean. The difference typically represented one pixel in the digitized image. This 'missing pixel' was attributed to the lack of synchronization between the scanning mirror and the electronic shutter on the video camera as discussed in Section 3.3. Although not

sufficient as a proof, it can be noted that no data points appear in a similar position above the mean value.

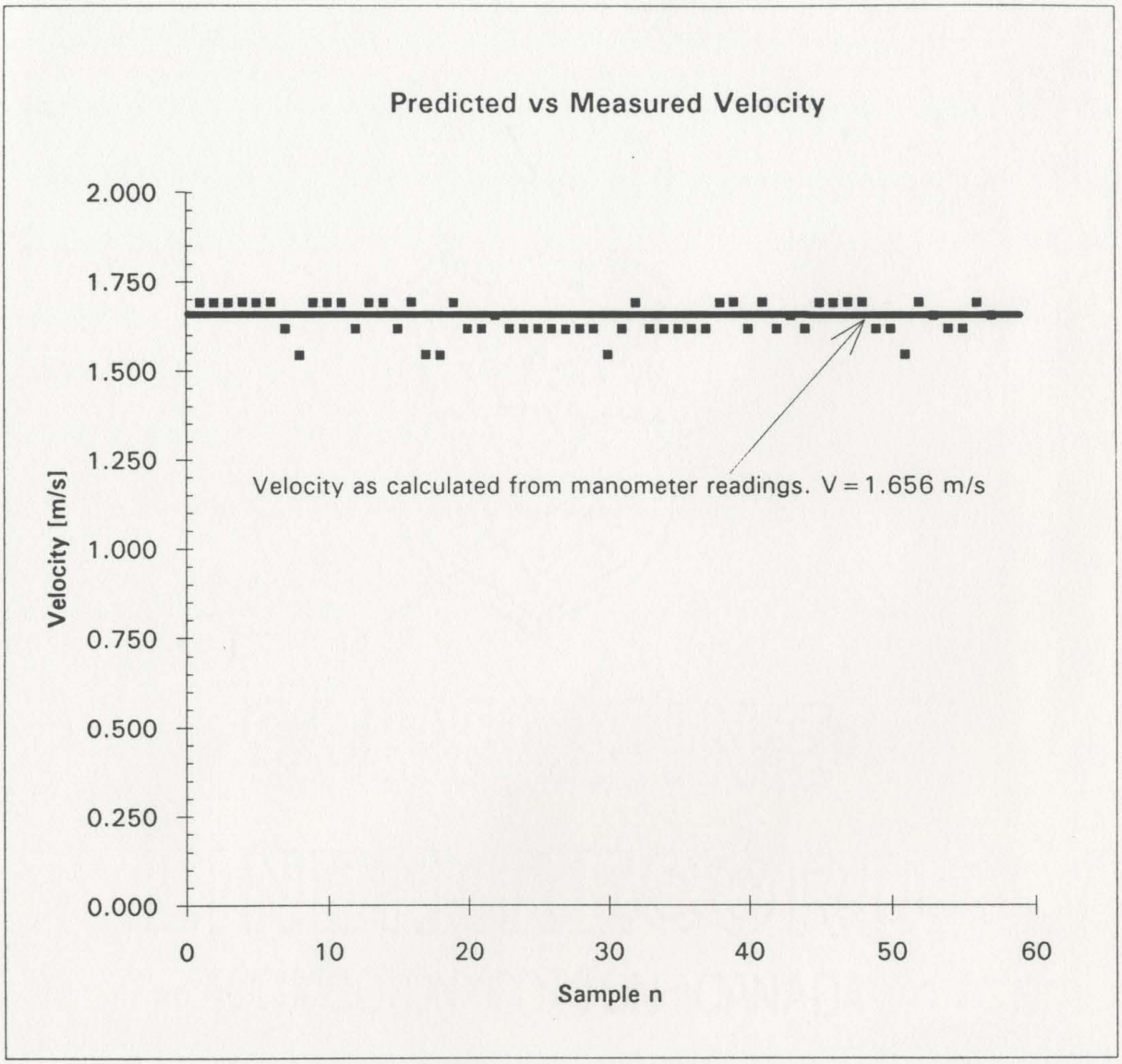

Figure 29 - DPTV Measurements in Uniform Flow (V=1.656 m/s)

4.2 Flow Around a Cylinder

The velocity magnitude and direction of a uniform flow streaming past a circular cylinder was determined using the DPTV system. The cylinder measured 50 mm in diameter and was machined from solid aluminium rod turned smooth on a lathe. The surface finish was matte black epoxy paint. One end of the cylinder was reduced to a nominal diameter of 25 mm and threaded to fit a mounting plate in the tunnel test section. Figures 30 shows the principal dimensions and the mounting arrangement of the cylinder.

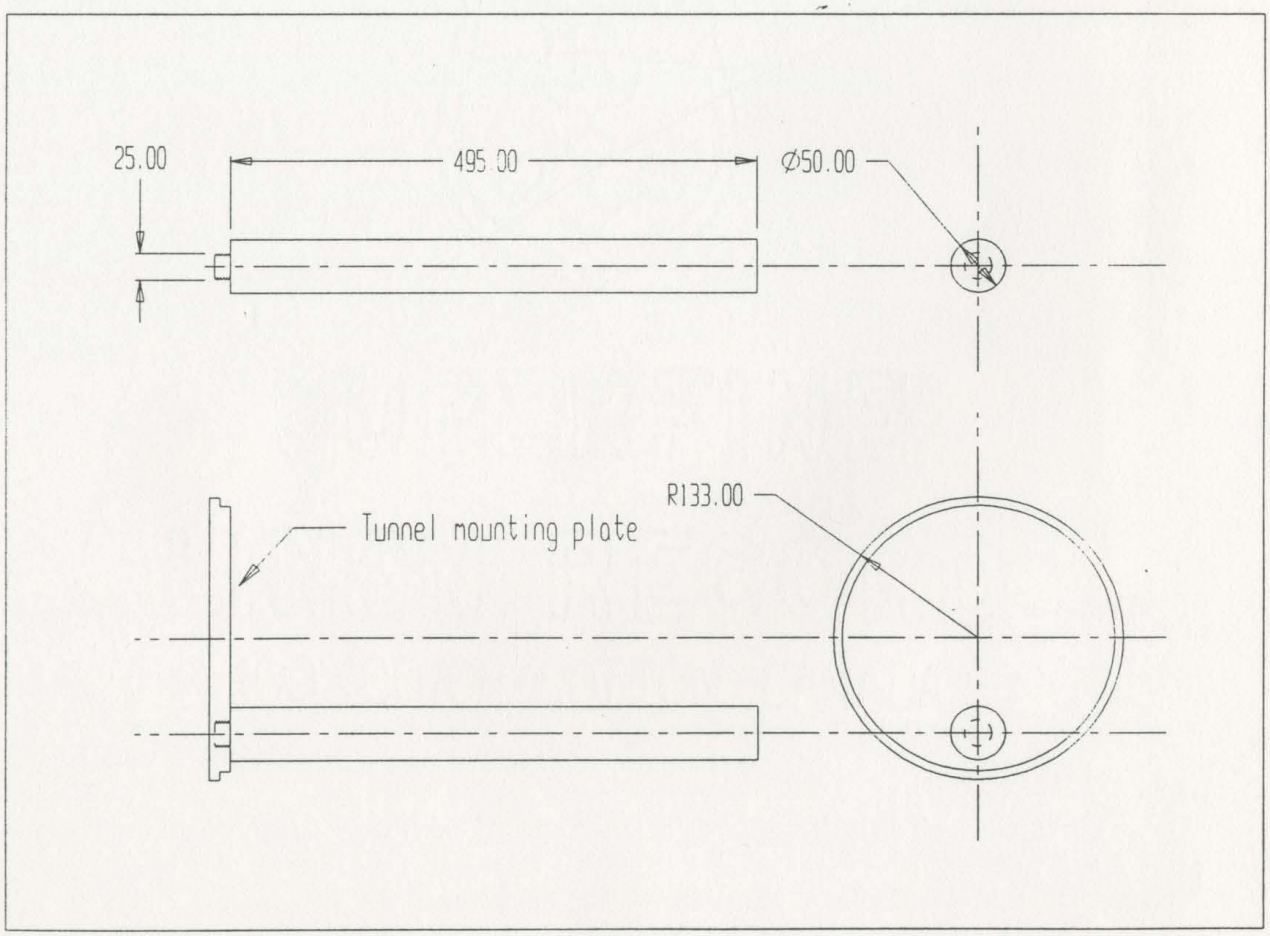

Figure 30 - Cylinder Dimensions and Mounting Details

The cylinder was placed transversely in the tunnel test section on the vertical centreline, with the free end approximately 5 mm from the inside face of the observation port opposite the mounting plate. Figure 31 shows the cylinder in place in the tunnel test section, the mounting plate is visible at the left hand end of the cylinder.

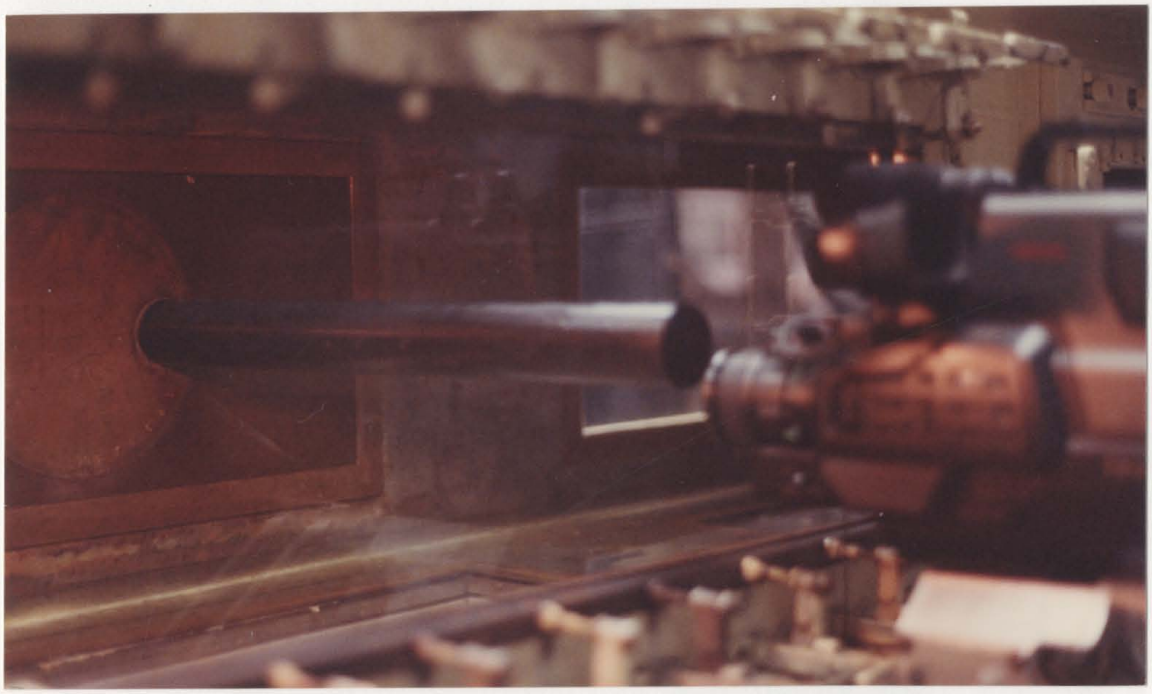

Figure 31 - Cylinder Mounted in Tunnel Test Section

Water flow speed in the test section was measured, using the water manometers, at 1.656m/s. This speed gave a Reynolds number of 72,700 based on cylinder diameter. All experiments were done on the tunnel centreline. The propeller shaft was removed from the cavitation tunnel for these experiments.

The width of the light sheet at the tunnel centerline was about 50 mm. In order to obtain images over a greater distance, normal to the cylinder axes, five separate

experiments were conducted using different laser positions. Figure 32 shows the overlap of the illuminated regions for the different laser positions.

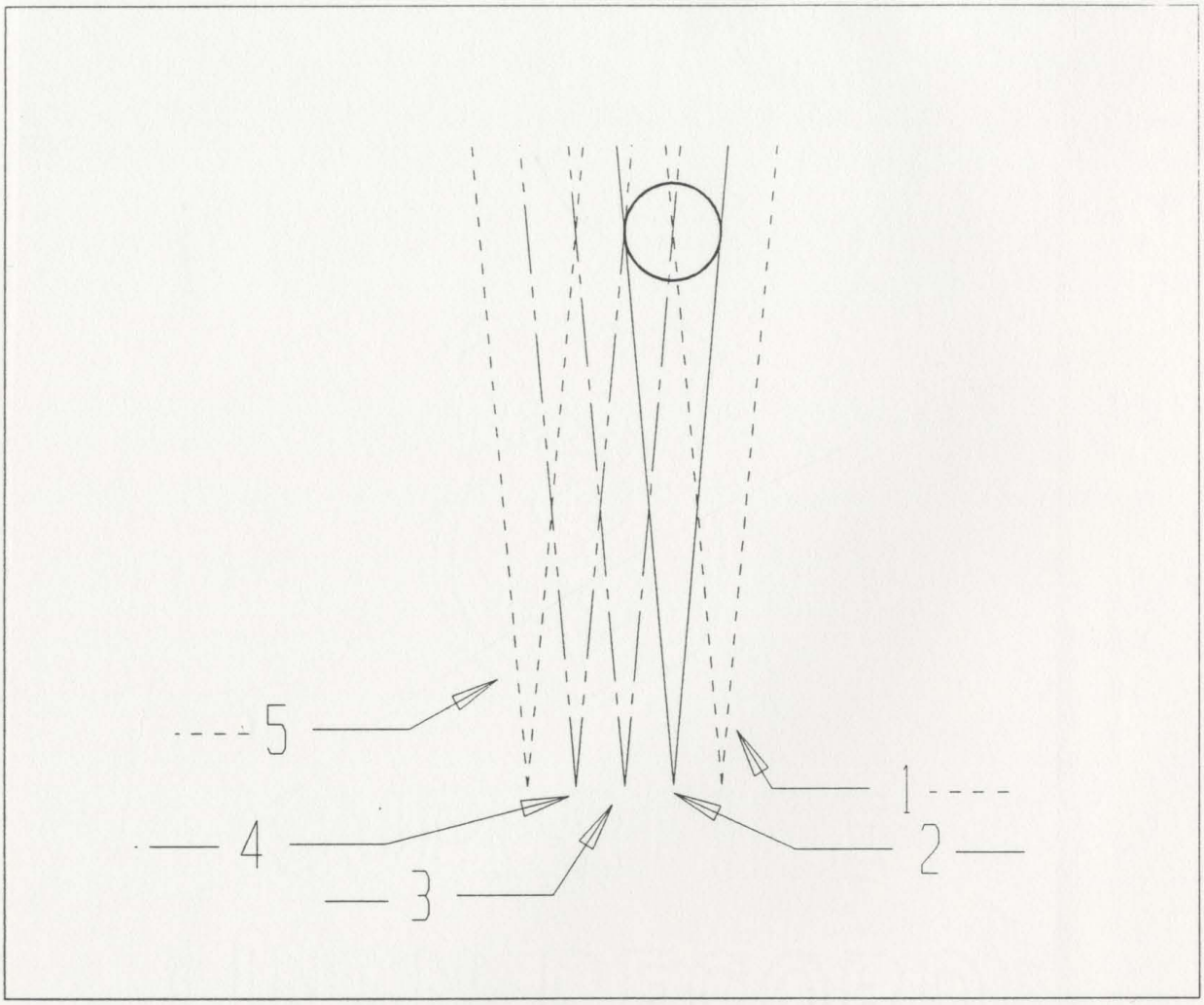

Figure 32 - Overlap of Illuminated Areas

A total of 79 experimental vectors were measured from 70 digitized images. These vectors were assembled and mapped, relative to the surface of the cylinder, as shown in Figure 33.

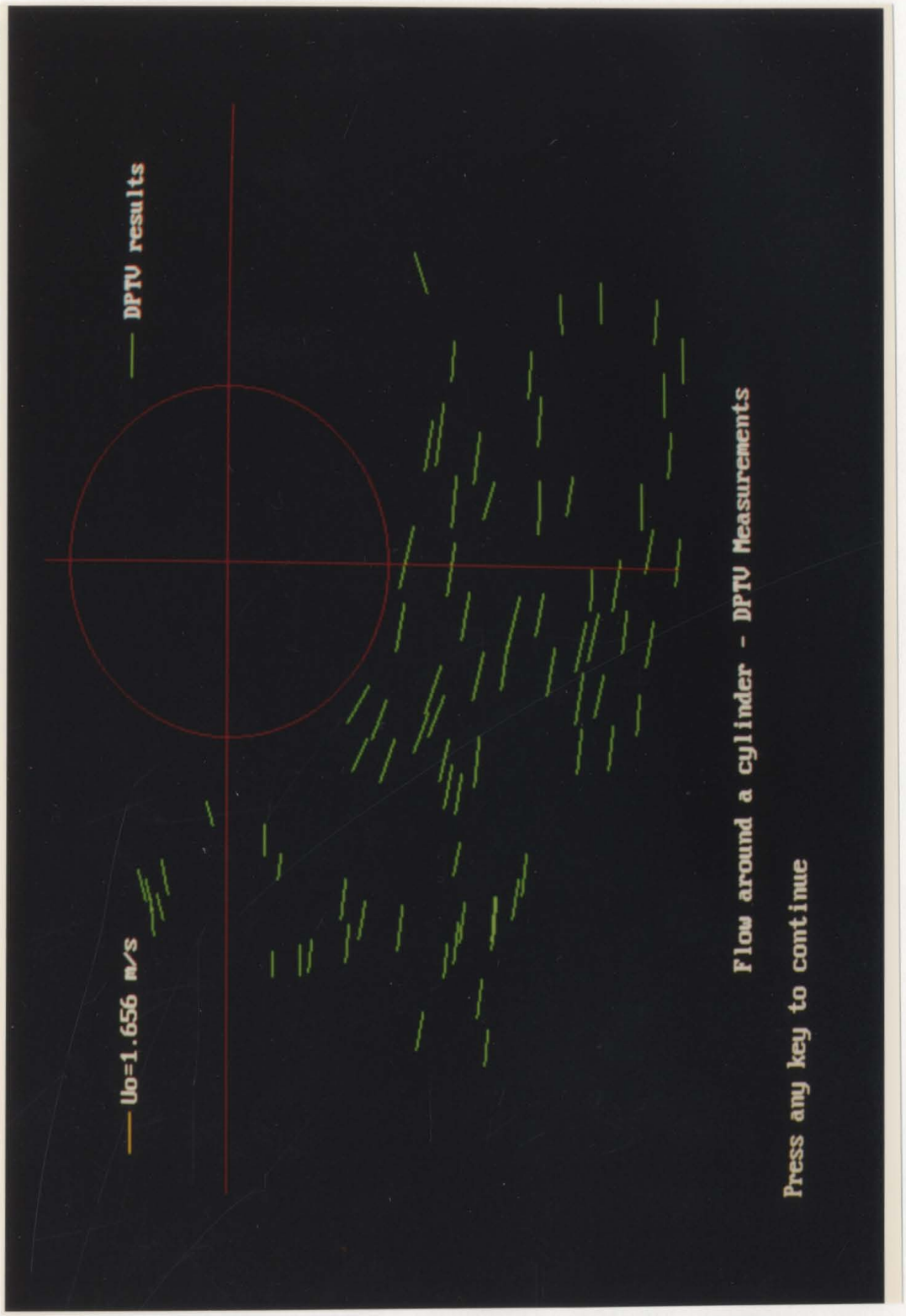

Figure 33 - DPTV Vectors for Flow Around a Cylinder (Rn=72,700).

(Flow is from Left to Right)

4.2.1 Comparison With Potential Theory

The flow described in Section 4.2 was modelled numerically using potential theory, O'Neil and Chorlton (1986). A computer program, Appendix G, written in Microsoft® QBasic®, was used to compute and plot the theoretical (ideal) flow field.

Blockage effects, from the tunnel walls. on mean velocity in the test section were not included in the numerical model. Boundary layer effects from the side walls of the tunnel were assumed to be negligible as all experiments were conducted on the midplane of the tunnel. End effects on the cylinder were ignored as the cylinder spanned the entire test section.

For an easier graphical comparison with experimental results, theoretical vectors were computed only at those locations for which experimental values were available. Calculations were made at the X-Y location corresponding to the upstream endpoint of each particle track. Figure 34 is a comparison between potential theory and the results of these experiments. Tabulated results are given in Appendix H.

The magnitude of the experimentally determined velocity vector, upstream of the flow separation point on the cylinder, was typically within 5% of that predicted by potential theory. Within the same region the measured velocity direction is typically within about $\pm 2°$ of that predicted by potential theory.

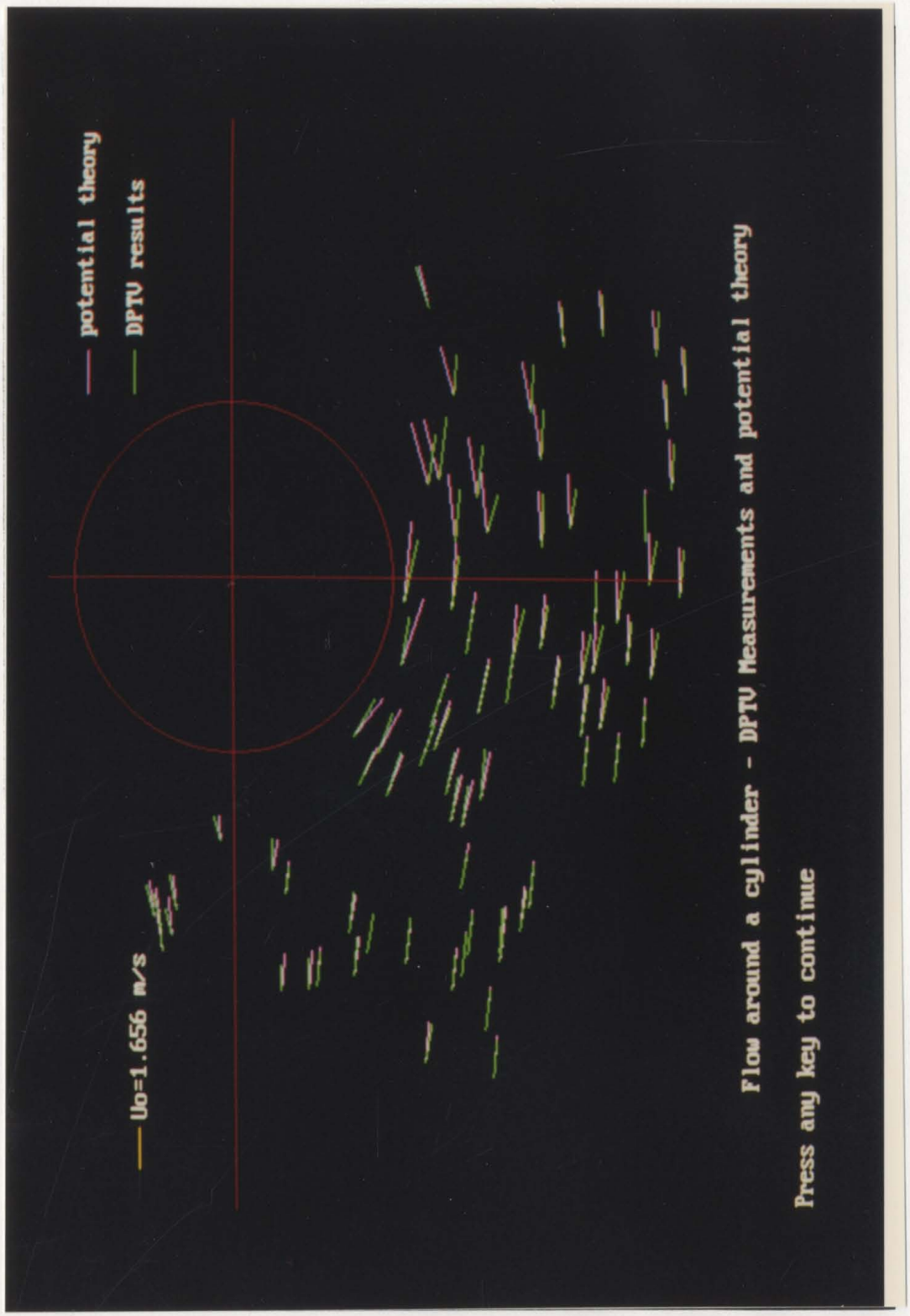

Figure 34 - Comparison of Measured and Theoretical Flow Vectors Around a Cylinder.

(Flow is from Left to Right)

4.3 Flow Behind a Ship Skeg

A simulated wake flow field was generated in the tunnel test section by installing a model representing a ship's stern. Principal dimensions of the model were selected to correspond to those found on a typical 10 metre Newfoundland inshore fishing vessel. These vessels commonly exhibit wide sternposts coupled with small propellers. The width of the sternpost can be 20% or more of the propeller diameter (personal experience of the author with the Fishing Vessel Fuel Efficiency Program, Federal Department of Fisheries and Oceans September-December 1985). This combination of small propellers and large sternposts results in very uneven flow into the propeller.

The model was made in two parts; a 'suppressor' plate situated above the shaft line in an attempt to simulate buttock flow, and a vertical portion surrounding the shaft to model the effect of a skeg and stern-post, Figure 35.

No attempt was made to generate a boundary layer on either the suppressor plate or the skeg which would have been more representative of the real ship. Surface mounted mesh screens can be used to stimulate boundary layer growth over this type of abbreviated (short) model, see e.g. Wilson (1989). This technique requires an iterative process to establish a desired wake pattern. As part of an initial investigation into the suitability of particle imaging for wake survey, accurate modelling of the boundary layer was considered unneccessary.

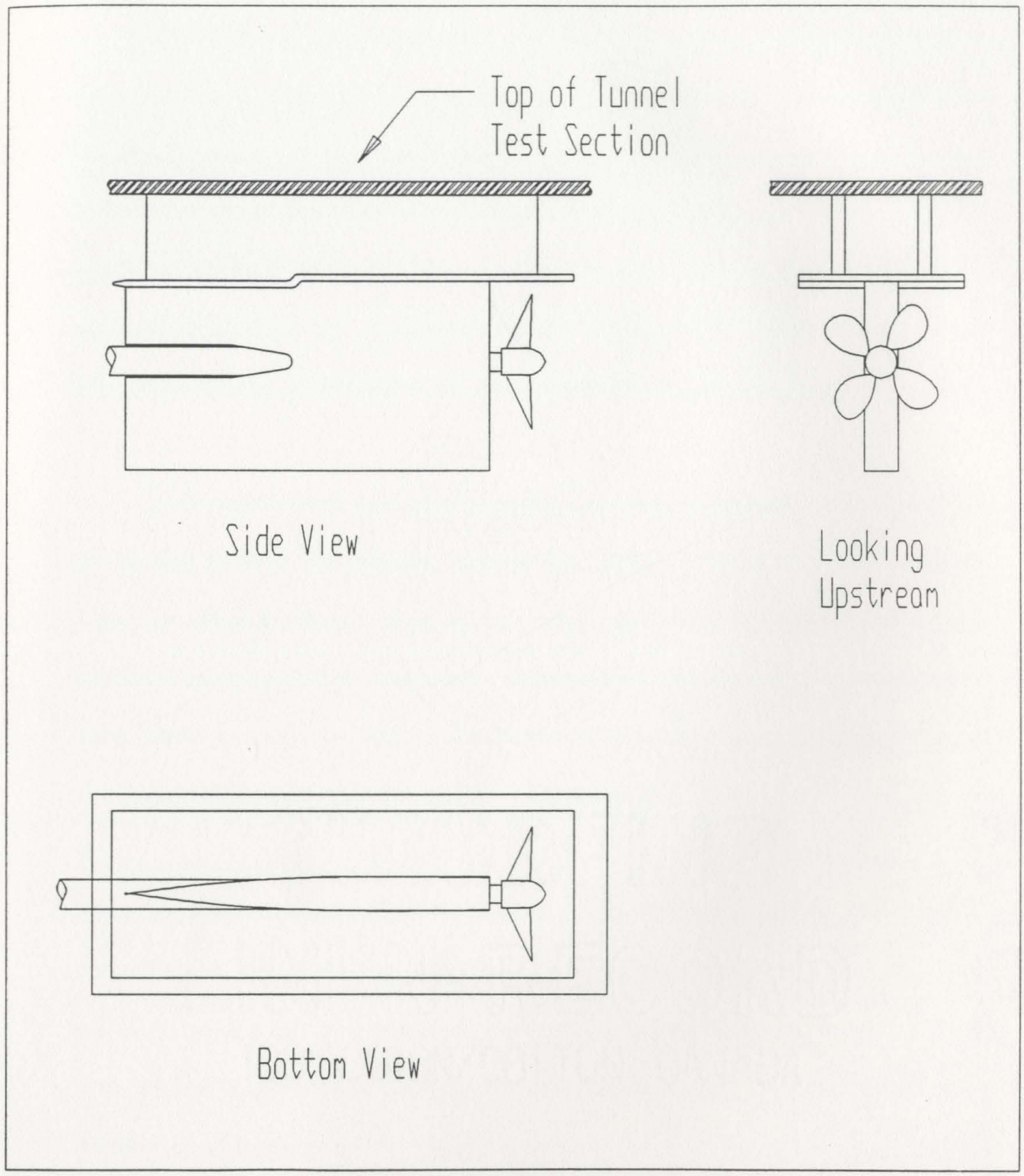

Figure 35 - Schematic of Skeg Model

The outline of the vertical portion of the model was, in plan view, a section of a circular arc of radius 1262.5 mm. This portion of the model was fabricated from aluminium using a 'frame-and-skin' method. Construction details are given in Appendix I. The upstream leading edges were rounded with a nominal radius of 5 mm on the skeg and 3 mm on the plate. The trailing edges of both plate and skeg were placed at right angles to the local surface. A solepiece was not included in the model as it would have interfered with the illumination of the area immediately behind the skeg.

A 48 mm diameter hole, centred on the long axes, was incorporated in the design of the skeg to allow the propeller shaft of the cavitation tunnel to pass through, see Figure 35. However, because of an earlier mechanical failure the propeller shaft was not available during the DPTV experiments. All measurements were made without the shaft being present and with both ends of the shaft opening covered by tape to avoid unrealistic flow patterns caused by flow through the body of the skeg.

Experiments were carried out to measure the velocity, magnitude and direction, of the flow in way of the propeller plane. A mean flow velocity of 1.721 m/s in the tunnel test section was measured using the water manometer. Experiments were done for four different (lateral) laser positions, or interrogation planes, and for each of three different camera positions. Table 1 shows the test matrix with the number of velocity vectors measured for each combination of camera and laser position.

Camera Position	Laser Position	0.28R	0.50R	0.7R	1.1R
Top	Tracks-->	11	14	15	25
Center	Tracks-->	15	12	17	25
Bottom	Tracks-->	12	11	16	12
	Total-->	38	37	48	62

Table 1 - Test Matrix for Wake Survey Behind Skeg.

The different laser positions represent vertical planes passing through the propeller disc at 0.28R, 0.50R, 0.70R and 1.10R where R is the propeller radius and in this case is equal to 100 mm, Figure 36. The three camera positions were necessary to allow measurements over the entire vertical area of the skeg. An overlap of about 25% was maintained between camera positions, Figure 37. As discussed earlier (Section 2.2.2) the camera field-of-view(FOV) and pixel resolution of the image are functions of distance to the focal plane. These were different for different interrogation planes. Dimensions of the FOV for different experiments, and the corresponding pixel resolutions, are given in Table 2.

Figures 38 through 41 show the axial component of the flow for each interrogation plane as a function of vertical position, assuming that all measurements are

valid at a single longitudinal location. The solid lines in these Figures represent second order curves which were fitted to the experimental data using a least squares routine. The decision not to use a straight line (first order) curve to describe the data was based on the authors previous experience in tow tank wake surveys (Institute for Marine Dynamics 1986-1991).

Location	0.28 R	0.50 R	0.70 R	1.1 R
FOV [mm]	132x102	128x96	117x89	107x82
[mm/pixel]	0.27	0.26	0.24	0.22

Table 2 - Dimensions of the FOV and Image Resolution for Wake Survey.

Quantitative measurements from the region immediately behind the skeg were not possible as the flow in this area was unsteady and strongly three-dimensional. However the results can be used qualitatively to obtain knowledge of the gross flow structure in this area. Viewing the recorded video-tape at very slow speeds revealed a significant flow reversal due to vortex shedding from the bottom trailing edge. Approximate measurements could be made from superposed images of sequential fields to determine the most appropriate location to make subsequent measurements using, say, a laser doppler anemometer.

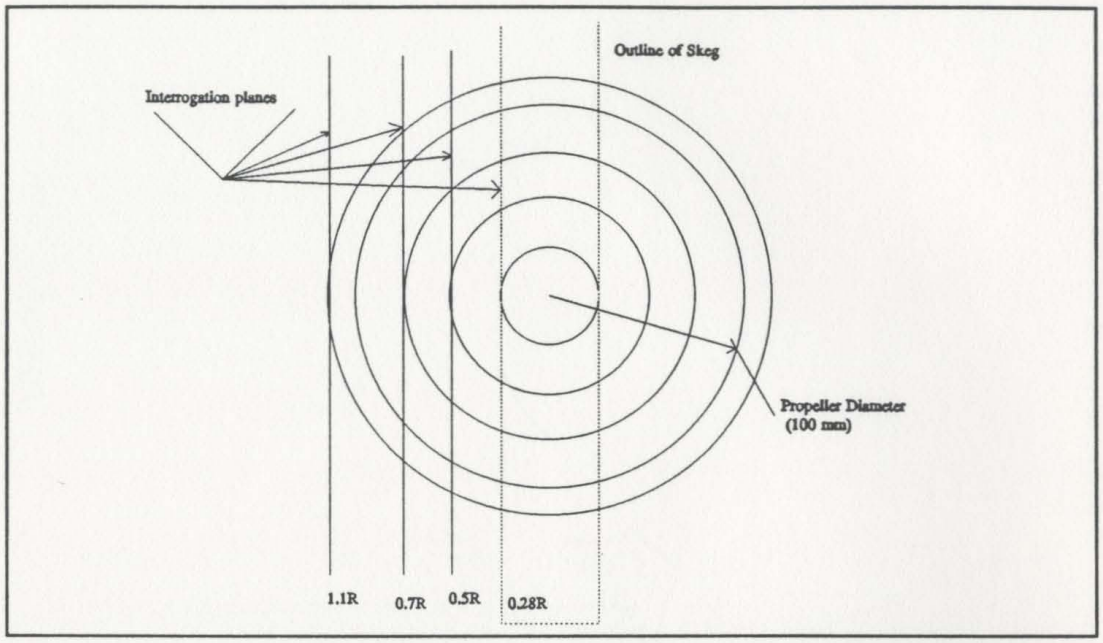

Figure 36 - Interrogation Planes for Ship Skeg.

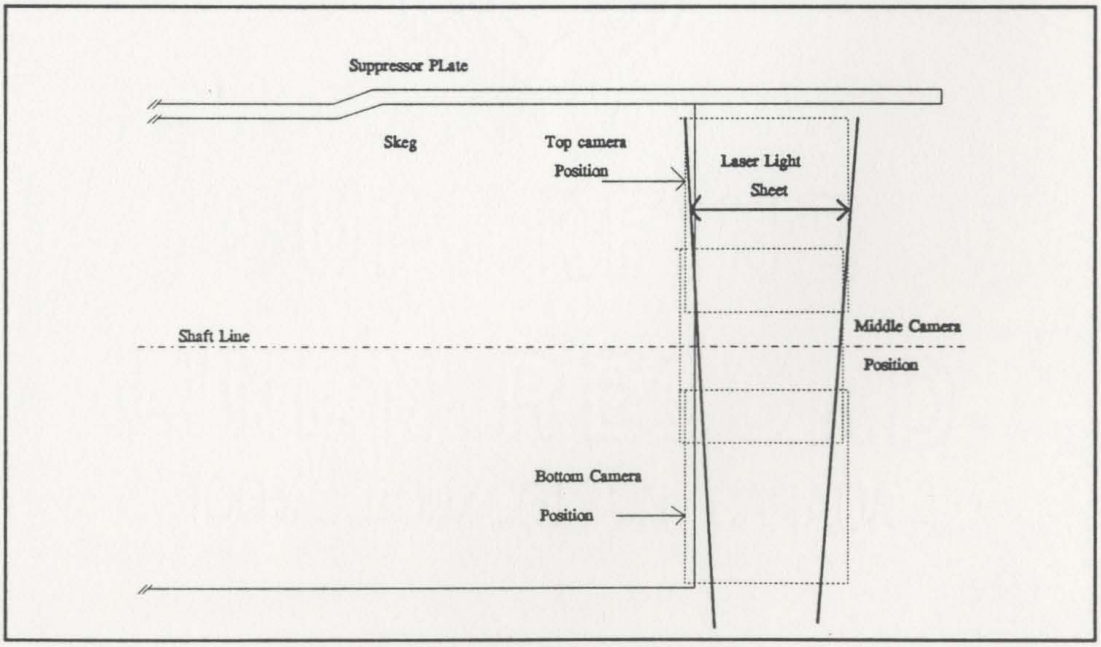

Figure 37 - Overlap of Camera Fields of View

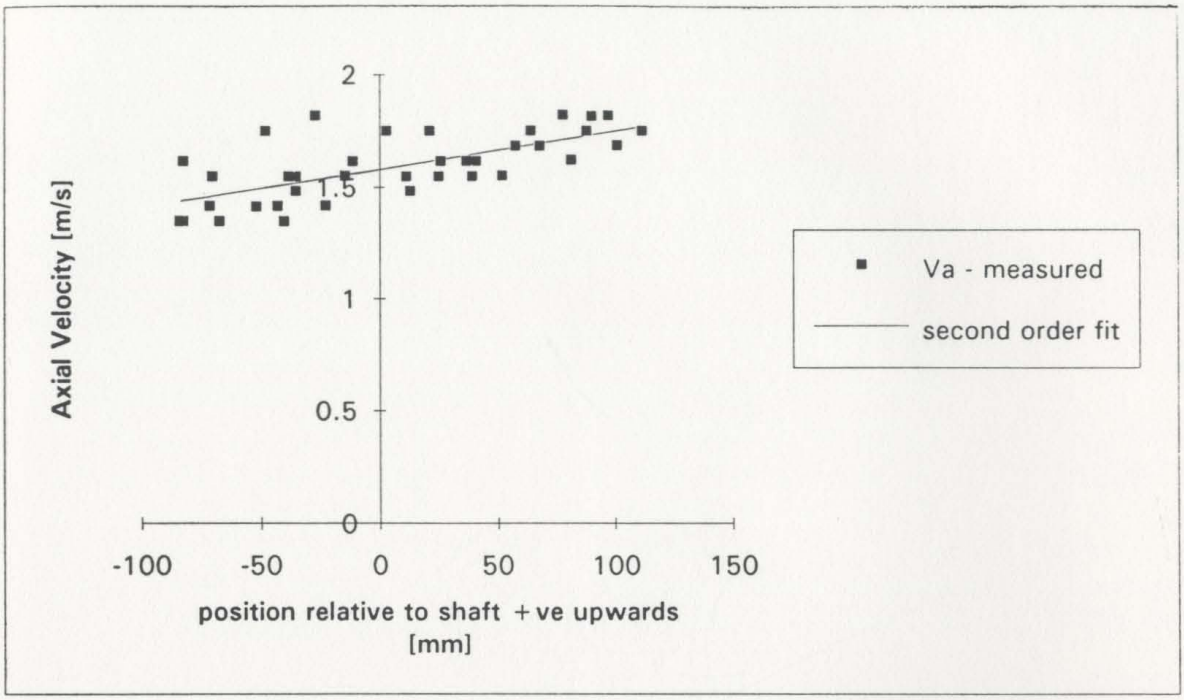

Figure 38 - Flow Velocity - 0.28R Interrogation Plane.

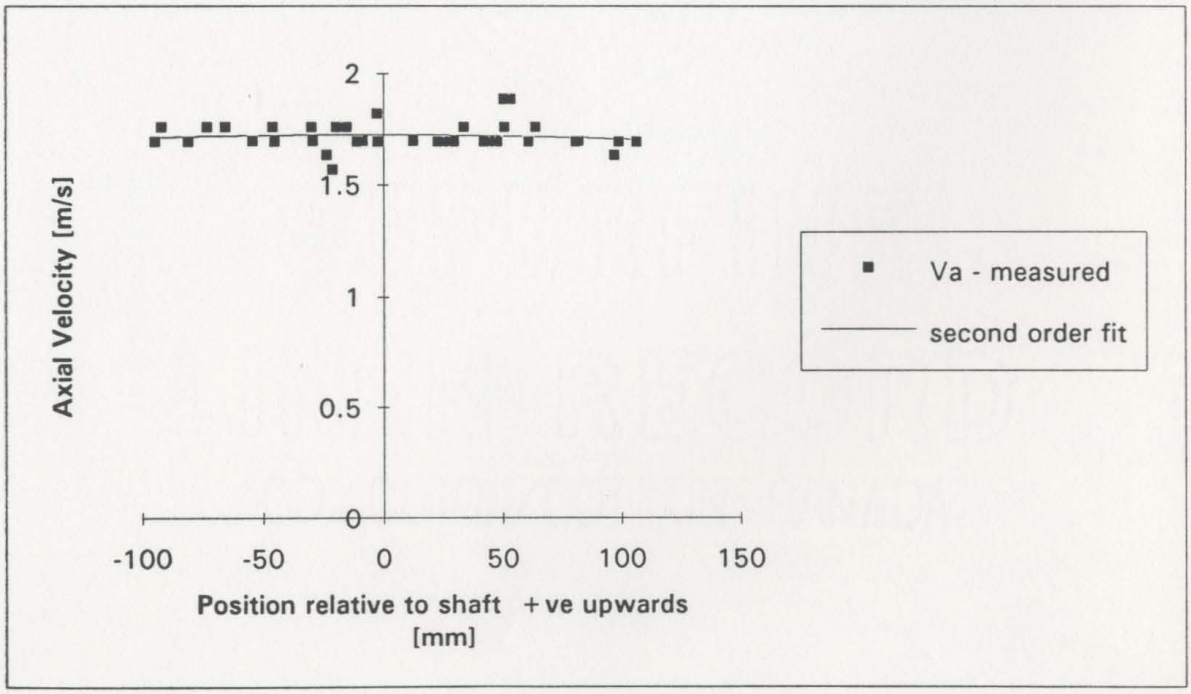

Figure 39 - Flow Velocity - 0.5R Interrogation Plane.

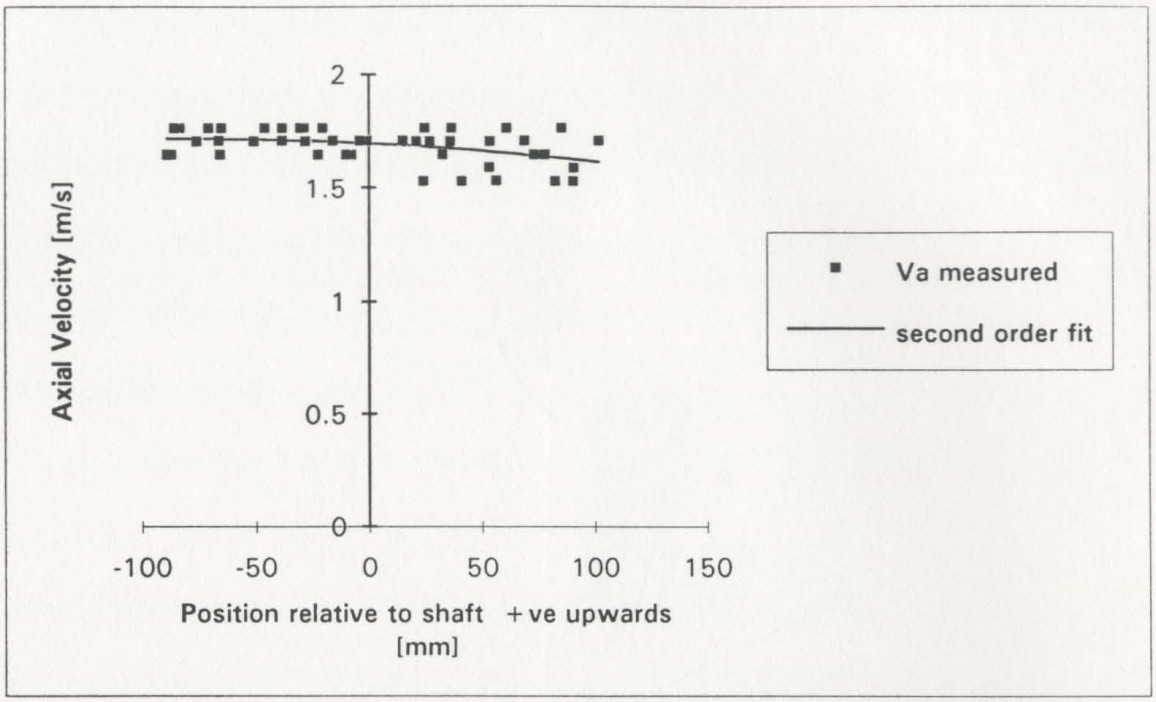

Figure 40 - Flow Velocity - 0.7R Interrogation Plane.

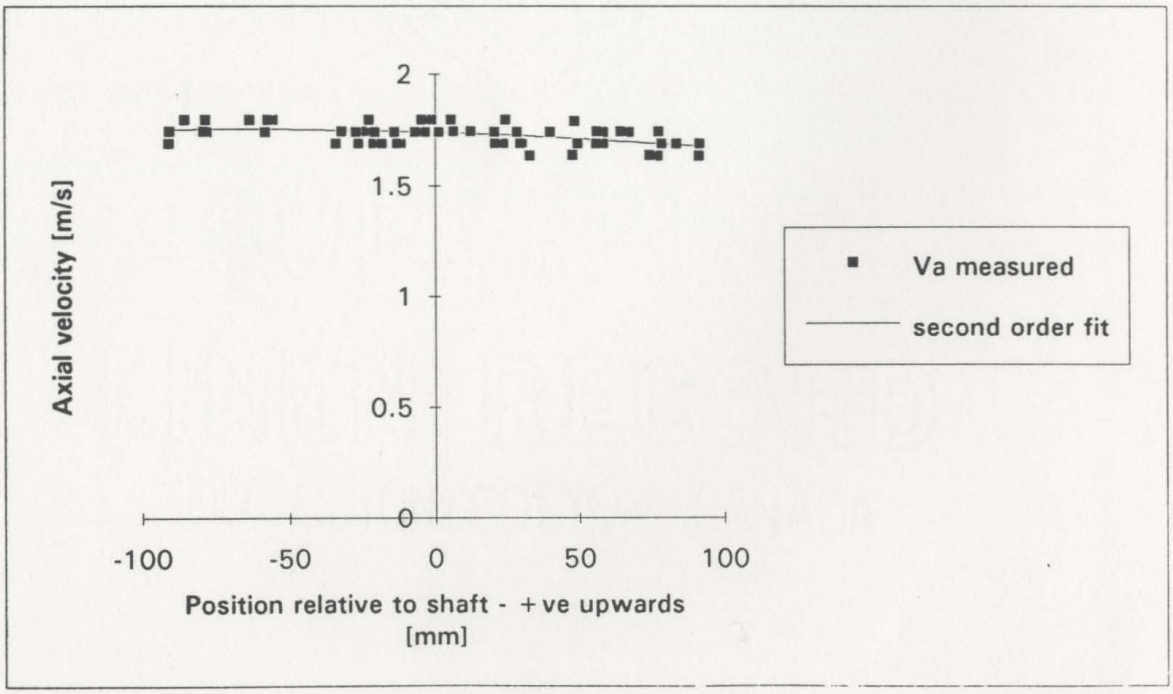

Figure 41 - Flow Velocity - 1.1 Interrogation Plane.

Measurements made at the 0.28R position, corresponding to the downstream vertical trailing edge of the skeg, revealed that the flow in this area had a velocity component in the transverse direction. This was readily apparent in the analysis process as out-of-plane motion of the particle was revealed by incomplete particle tracks, Figure 42. When the particle is moving at some angle to the light sheet only motion which takes place in the illuminated region, and within the time interval defined by the shutter speed, is recorded by the camera. This is shown schematically in Figure 43. However as described in Section 3.3 the pulse coding of individual particle tracks was not consistant, and thus no definite statement can be made as to whether the transverse component was in the positive or negative x direction.

Figure 42 - Partial Track Due to Out of Plane Motion.

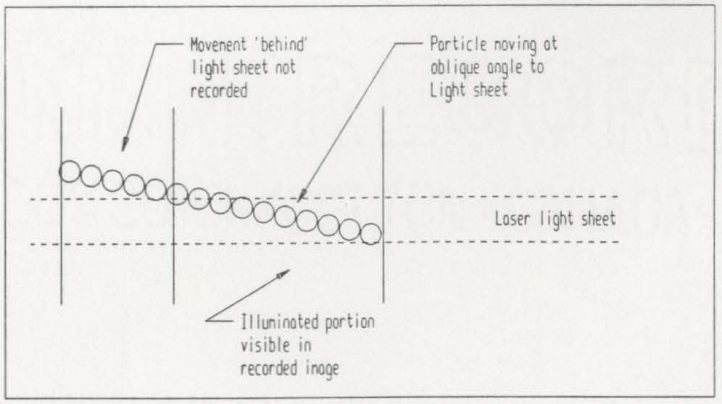

Figure 43 - Schematic of Out-of-Plane Particle Motion

The apparent reduction in axial flow velocity near to the bottom of the skeg, Figure 38, is attributed to a flow reversal due to the trailing edge vortex as discussed above. The flow at 0.5R, Figure 39, is essentially uniform and constant over the height of the interrogation plane. The flow at 0.7R and at 1.1R, Figures 40 and 41 respectively, show a slight reduction near the top of the interrogation plane. This was attributed to a boundary layer effect from the top plate.

For the interrogation plane at the edge of the skeg (0.28R) the standard deviation, of the experimental data from the fitted curve, was 0.333 (19%). For those planes away from the skeg (0.5R, 0.7R and 1.1R) the standard deviation of the experimental data, from the fitted curve was 0.248(14%), 0.257(15%) and 0.203(12%) respectively.

4.3.1 Effect of Skeg on Propeller Performance

The mean static thrust and torque of a four-bladed screw propeller was measured in the cavitation tunnel at atmospheric pressure. Experiments were conducted using a mean flow speed in the test section of 2.0 m/s and varying propeller rotation rate in order to cover a range of advance coefficient (J) from J=0.3 to J=1.3. The propeller was cast and finished by Avalon Propulsion Services Limited of St. John's. The mould pattern for the propeller was produced by the Institute for Marine Dynamics. The pattern was of a 4-bladed Wageningen B-series propeller with a 250 mm diameter, a blade area

ratio(BAR) of 0.7 and a pitch/diameter ratio of 1.0. The propeller as cast was not suitable for use at this diameter and blade area. The blades were cropped and the blade surface drilled to produce a propeller with a 200 mm diameter and a BAR of 0.40. The finished product thus corresponded to a B4.40 propeller. Principal particulars, calculated from the nondimensional coefficients given by Oosterveld and van Oossanen (1972), are given in Appendix J. Measured data for the propeller as tested were not available.

Tests were conducted both with and without the skeg. Experimental results, corrected for tunnel wall effects using the procedure described by Lindgren (1963), are given in Table 3. Figure 44 shows the propeller in place behind the skeg in the test section.

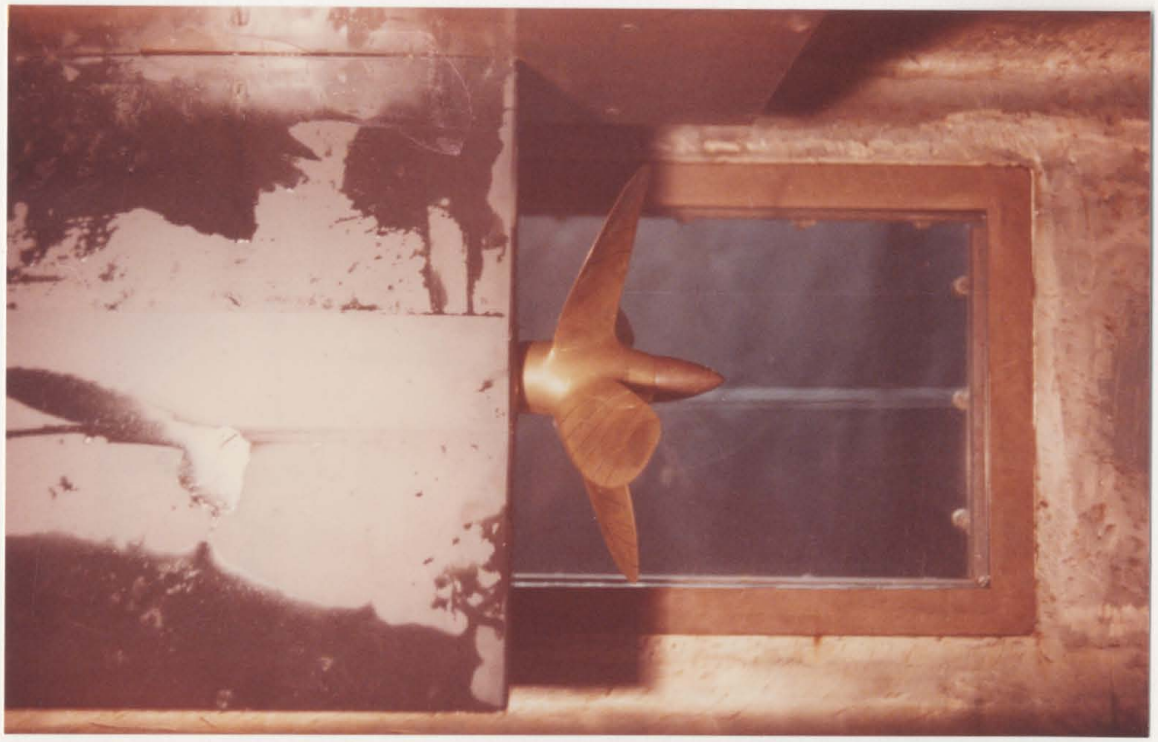

Figure 44 - Propeller in Place Behind Skeg.

Measurements From Tests with Propeller in Uniform Flow

Advance Coefficient J -	N (rpm) -	Thrust [N] -	Torque [Nm] -	Thrust Coefficient KT	Torque Coefficient 10*KQ	Open Water Efficiency ETAO
0.308	1947	781.38	30.37	0.4638	0.9013	0.2524
0.354	1697	590.86	23.08	0.4616	0.9017	0.2881
0.405	1483	424.81	16.07	0.4346	0.8218	0.3405
0.455	1319	318.05	11.93	0.4113	0.7715	0.3860
0.504	1190	249.10	9.02	0.3958	0.7163	0.4434
0.559	1074	187.94	7.02	0.3666	0.6843	0.4763
0.656	914	124.55	4.51	0.3355	0.6071	0.5773
0.756	794	85.63	3.12	0.3056	0.5565	0.6605
0.856	701	58.94	2.20	0.2699	0.5044	0.7288
0.958	626	41.15	1.56	0.2362	0.4476	0.8051
1.064	564	28.91	1.08	0.2045	0.3836	0.9027
1.156	519	20.02	0.81	0.1672	0.3398	0.9055
1.261	476	11.12	0.51	0.1104	0.2524	0.8776

Measurements From Tests with Propeller Behind Skeg

Advance Coefficient J -	N (rpm) -	Thrust [N] -	Torque [Nm] -	Thrust Coefficient KT	Torque Coefficient 10*KQ	Open Water Efficiency ETAO
0.328	1830	680.47	26.57	0.4572	0.8927	0.2672
0.380	1578	502.65	18.85	0.4542	0.8514	0.3228
0.431	1393	366.98	13.69	0.4255	0.7939	0.3674
0.476	1260	293.58	10.71	0.4161	0.7590	0.4155
0.538	1115	217.96	7.66	0.3945	0.6932	0.4874
0.581	1032	182.38	6.24	0.3853	0.6588	0.5412
0.632	950	142.34	5.02	0.3549	0.6253	0.5704
0.732	820	100.08	3.39	0.3349	0.5671	0.6877
0.833	720	73.40	2.51	0.3186	0.5443	0.7762
0.930	645	55.60	1.90	0.3007	0.5133	0.8674
1.031	582	42.26	1.42	0.2807	0.4728	0.9741
1.128	532	33.36	1.08	0.2652	0.4311	1.1042
1.232	487	24.47	0.81	0.2321	0.3859	1.1794
1.333	450	17.79	0.68	0.1977	0.3766	1.1139

Table 3 - Results of Thrust and Torque Measurements on Model Test Propeller.

The results of tests without the skeg are given in Figure 45. Nondimensional thrust(KT), torque(KQ) and open water efficiency (ETAO), are plotted against advance coefficient(J). The solid lines in Figure 45 represent predictions of performance as given by Oosteveld and van Oossanen (1972) for this type of propeller. The torque coefficient has been multiplied by a factor of ten in order to permit plotting on the same axes as the thrust coefficient. At J=0.9 the experimental results are 17% and 9% higher than the results of Oosterveld and van Oossanen (1972) for thrust and torque respectively. Open water efficiency based on the experimental results is 9% greater than that indicated by the polynomials of Oosterveld and Oossanen. The upturn in the experimental torque curve at low values of J was attributed to the flow being accelerated by the propeller which made true low-J values impossible.

Figure 46 shows a comparison of experimental results, with and without the skeg, for nondimensional thrust(KT) and torque(KQ) coefficients along with open water efficiency (ETAO) plotted against advance coefficient(J).

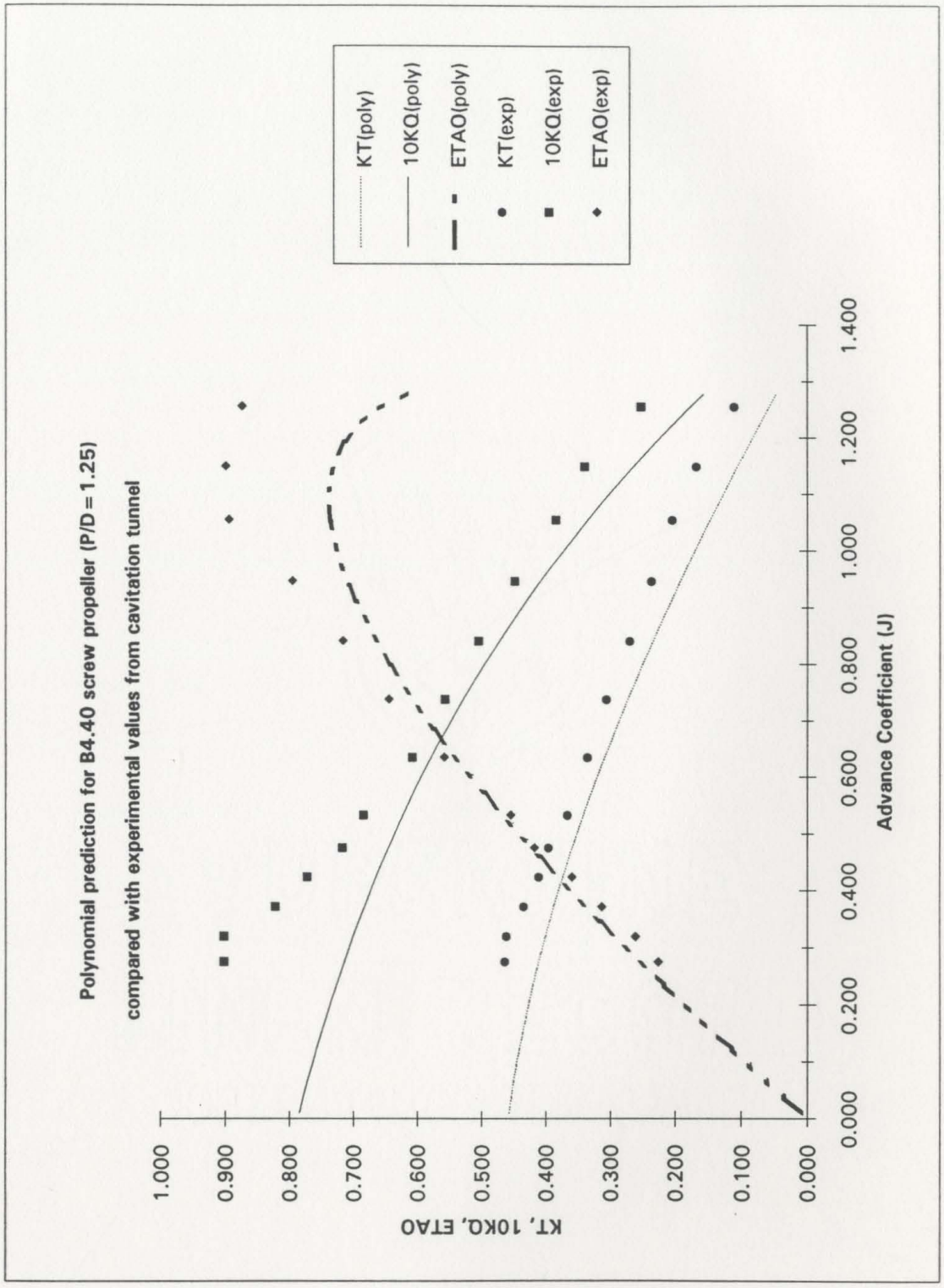

Figure 45 -Nondimensional Thrust and Torque in Uniform Flow.

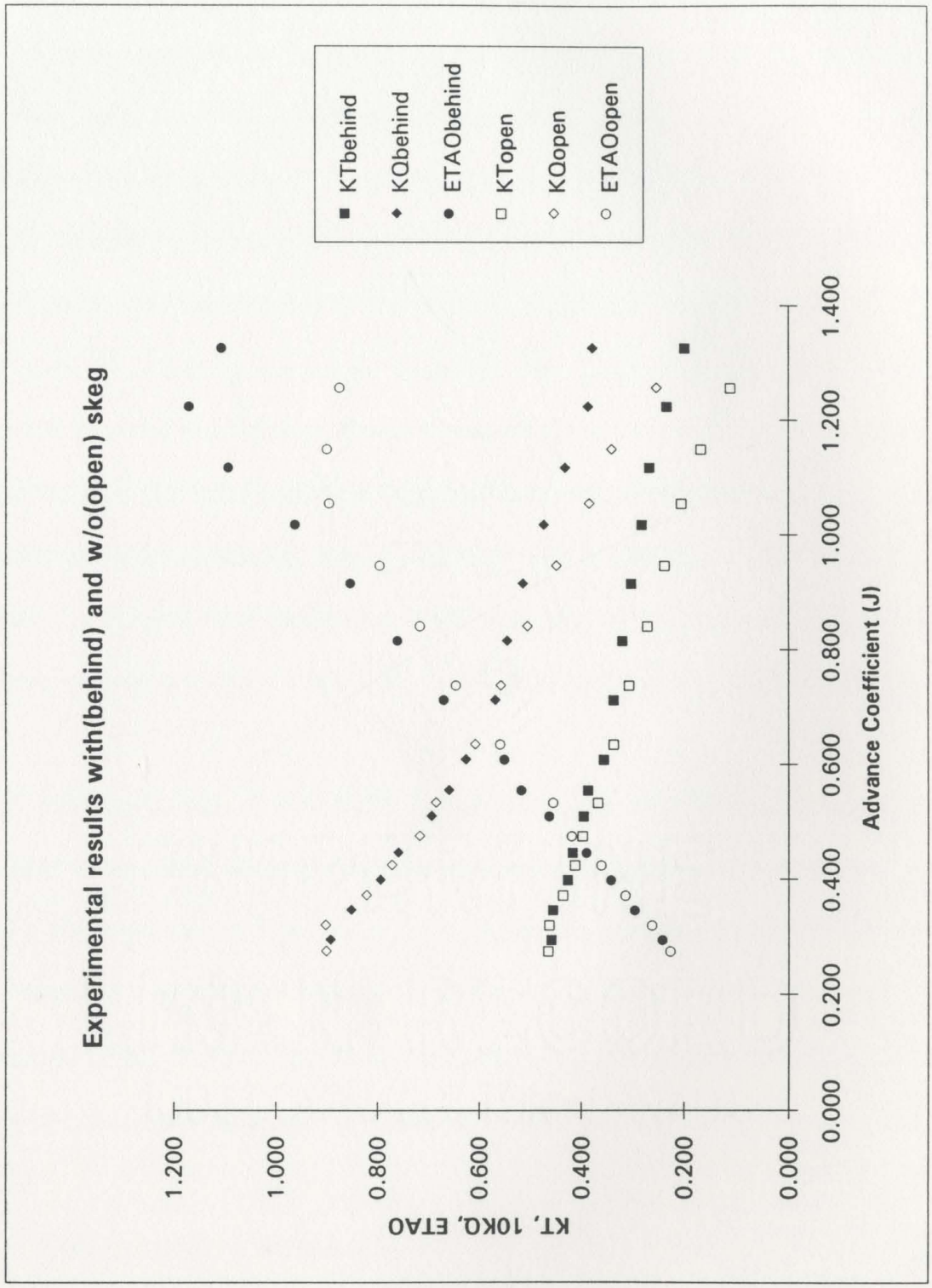

Figure 46 - Nondimensional Thrust and Torque With and Without Skeg.

4.3.2 Comparison with Lifting Surface Theory

Experimental data obtained with the test propeller in the cavitation tunnel, from tests both with and without the skeg model being present, were compared with predictions from an unsteady lifting surface theory for screw propellers, Kerwin and Lee (1978). To accommodate complex propeller geometry the procedure employs a discrete vortex/source line representation of the propeller blades, with elements located on the exact camber surface of the blade. Unsteady blade loading is realized within the procedure by permitting the axial, tangential and radial components of the inflow velocity to vary in both the radial and circumferential directions. Within such a flow-field the propeller is "rotated" through several revolutions, in a sequence of discrete angular intervals, until steady-state oscillations of the blade loading are achieved. This process has been automated within the MIT-PUF-2(PUF2) computer program, Kerwin (1985).

Predictions obtained from PUF2 for propeller performance in a uniform wake are compared in Figure 46 with the experimental data for the propeller tested in the tunnel without the skeg. For $J=0.9$ the theory underpredicts thrust and torque by 19% and 15% respectively. The experimental results for torque, for values of J below about 0.5, are considered unrealistically high. This was attributed to the problem of achieving low values of J in a cavitation tunnel, as discussed in Section 4.3.1.

The data presented in Section 4.3 was used to define the nominal wake behind the skeg. The equations of the fitted second order curves described in Section 4.3 were used

to calculate the axial velocity in the wake at points where selected radii intersected with the interrogation planes, see Figure 36. Making the assumption that the axial velocity immediately behind the sternpost could be taken to be zero, curves were fitted to the data using the interactive curve-fitting routine developed by Miles (1982). Figures 48 through 51 show the calculated values of axial velocity, normalized with respect to the mean flow velocity, and plotted against angular position in the propeller disc. On the ordinate axes 0 and 180 correspond to Top Dead Centre(TDC) and Bottom Dead Centre(BDC) respectively. The wake was assumed to be symmetric about the vertical centreline of the sternpost. In the same figure can be seen the spline curves which were fitted to the data points, these faired curves are similar to those found by Wu and Bose (1992c) from towing tank tests on a Newfoundland fishing boat hull-form.

Harmonic analysis, of the faired curves, produced a set of Fourier coefficients for a numerical description of the curves shown in Figures 48 through 51. Figures 52 through 55 show the original curves fitted to the data along with those represented by the Fourier series expansion. The oscillation seen in the Fourier representation of the curve corresponding to 1.1R was attributed to the sharp 'bend' in the faired curve at about 10 degrees and 170 degrees. This feature results from the rapid increase in velocity which occurs at the edge of the skeg where the flow is making the transition from essentially zero velocity behind the skeg to 95% or more of the free stream value outside the skeg boundary layer.

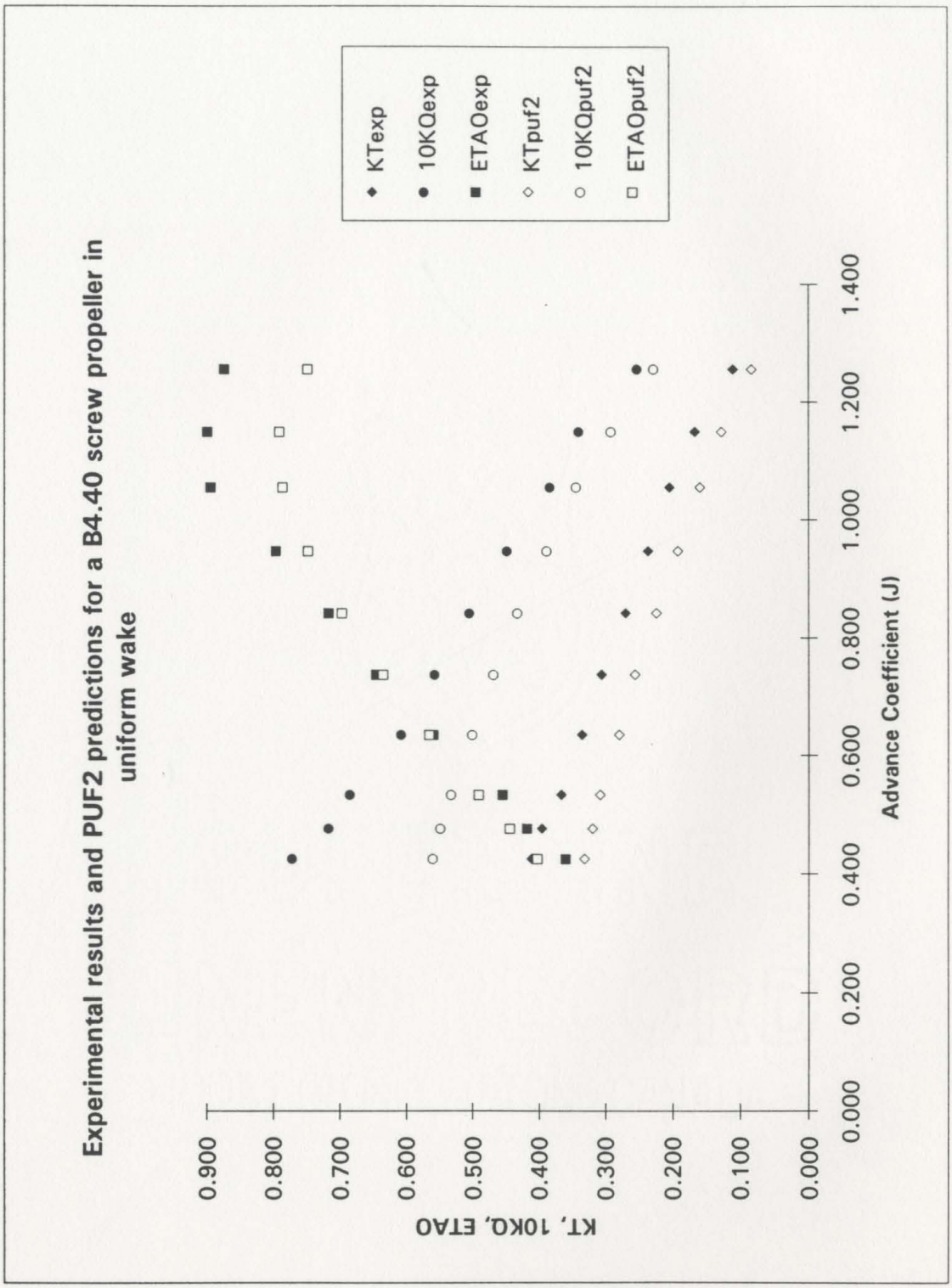

Figure 47 - Comparison of Experimental Results and PUF2 Predictions in Uniform Flow

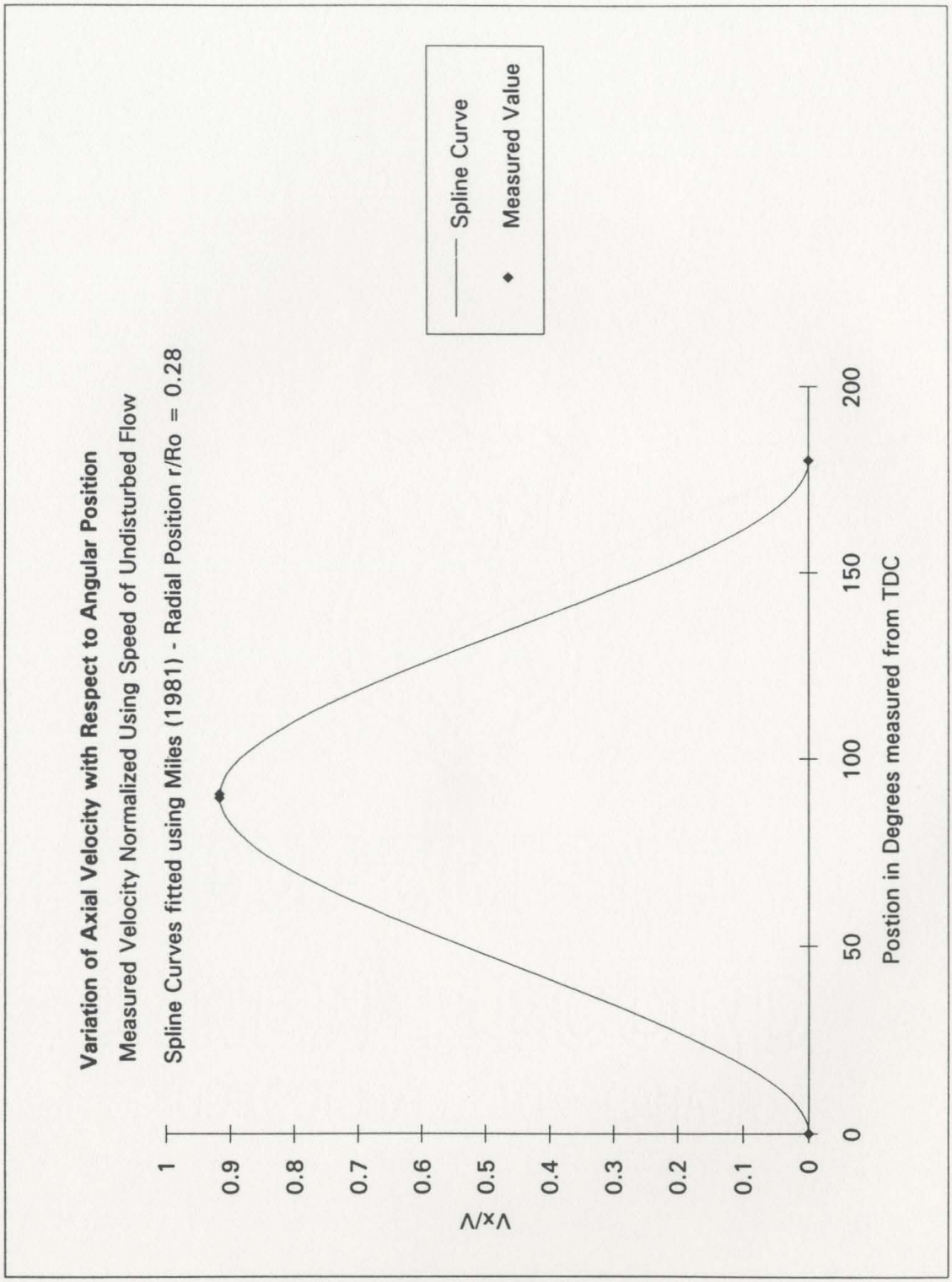

Figure 48 - Axial Flow Component - 0.28R Interrogation Plane.

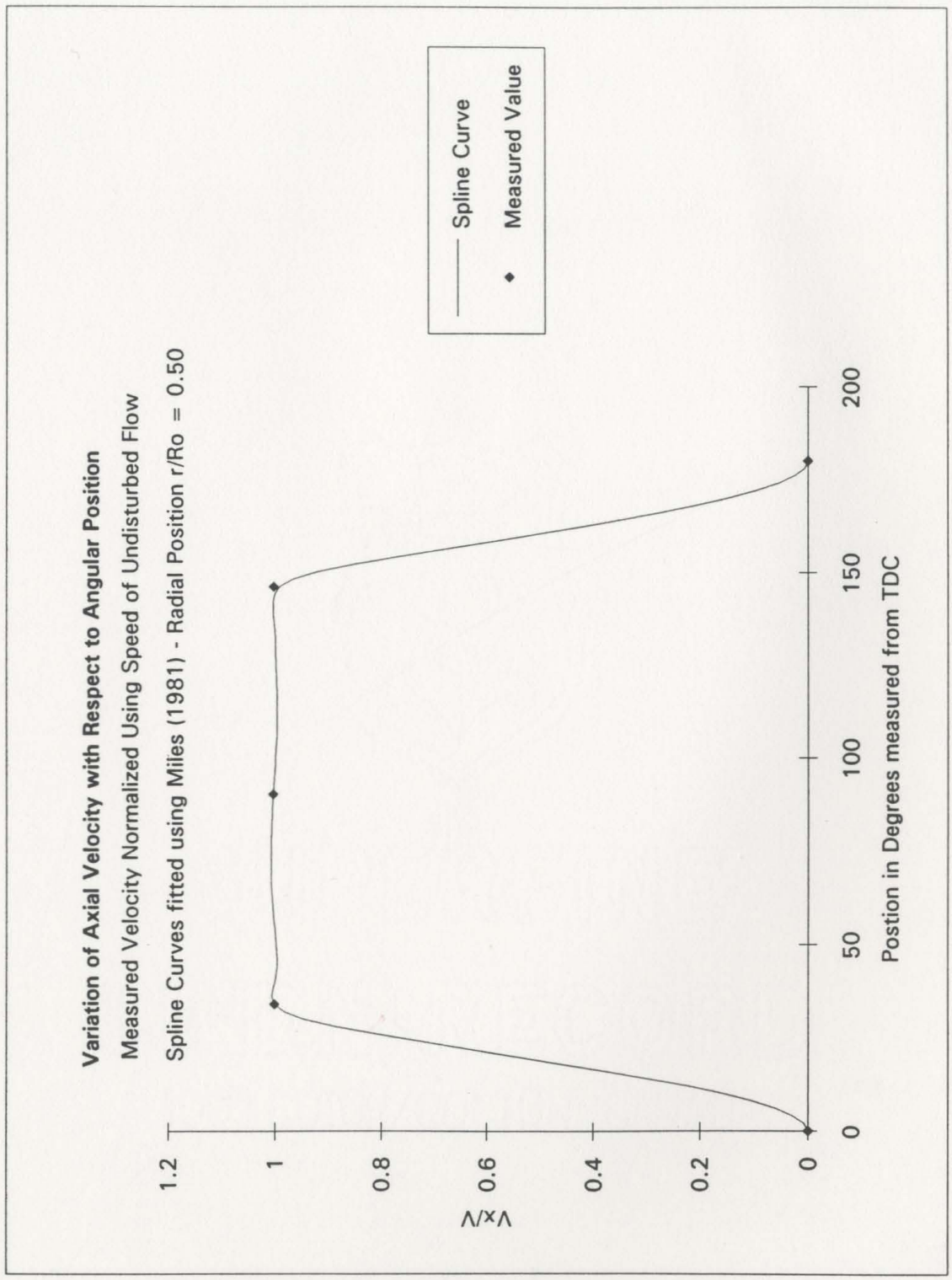

Figure 49 - Axial Flow Component - 0.5R Interrogation Plane.

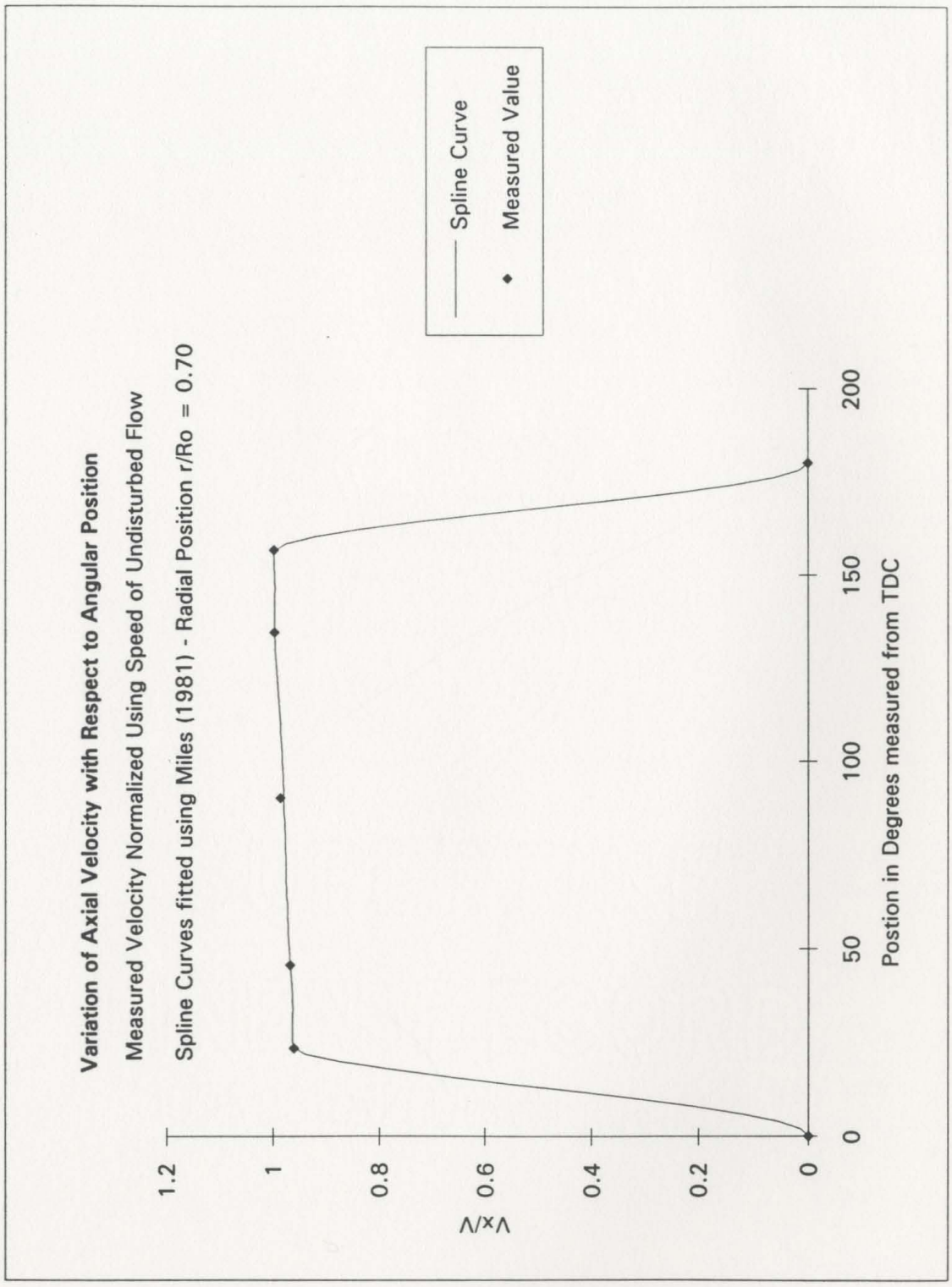

Figure 50 - Axial Flow Component - 0.7R Interrogation Plane.

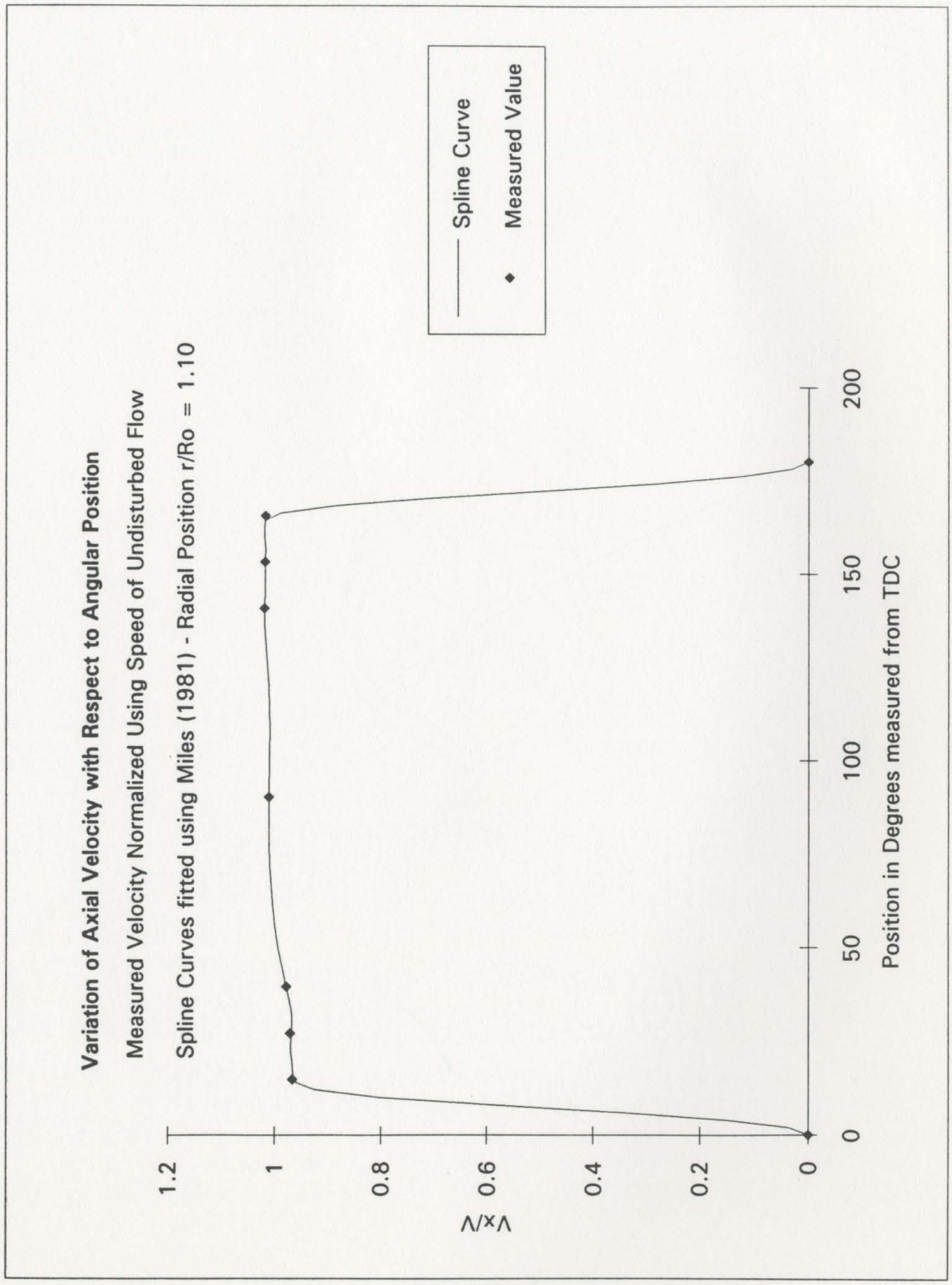

Figure 51 - Axial Flow Component - 1.1R Interrogation Plane.

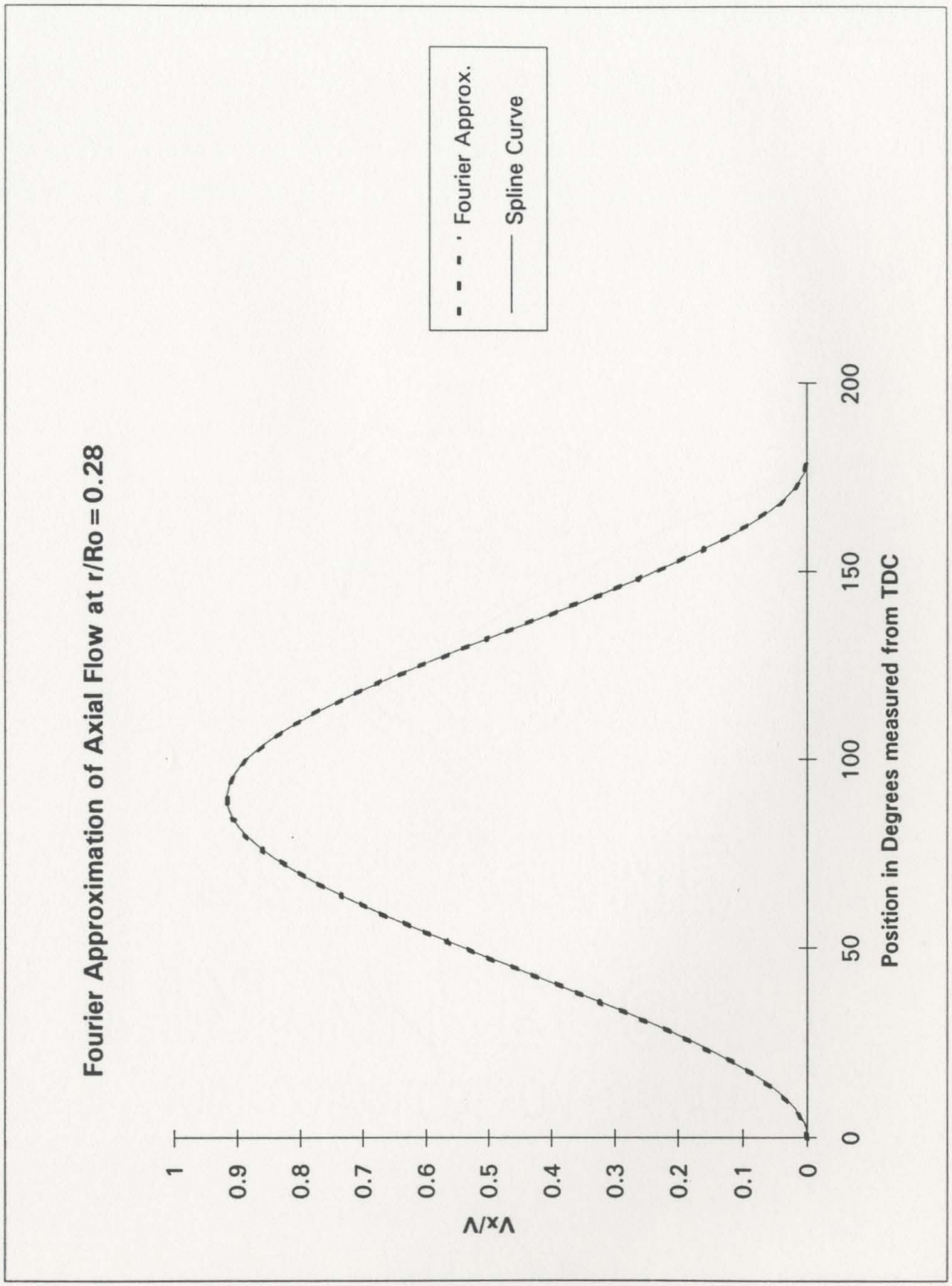

Figure 52 - Fourier Series Approximation of Flow Component - 0.28R.

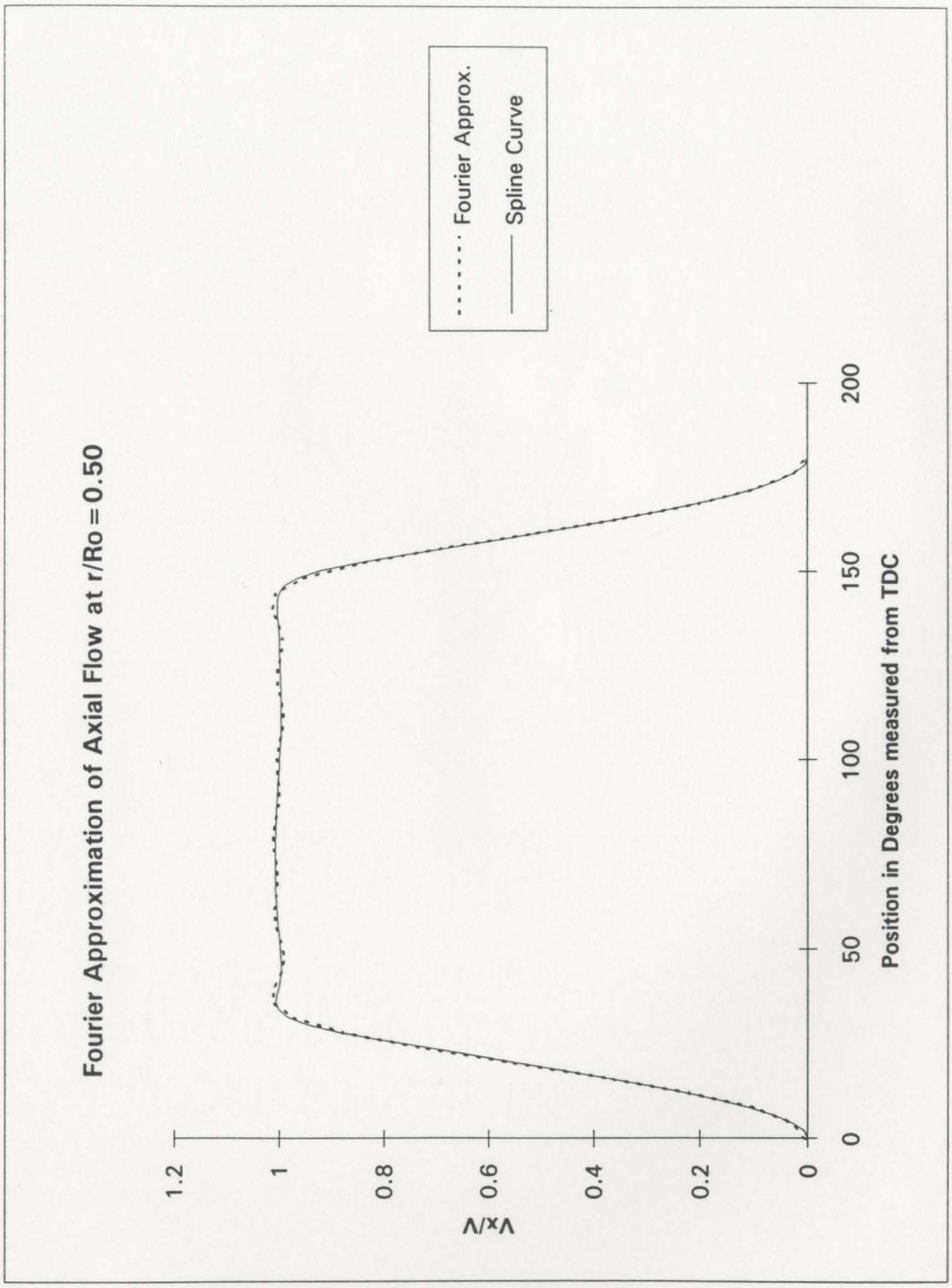

Figure 53 - Fourier Series Approximation of Flow Component - 0.5R.

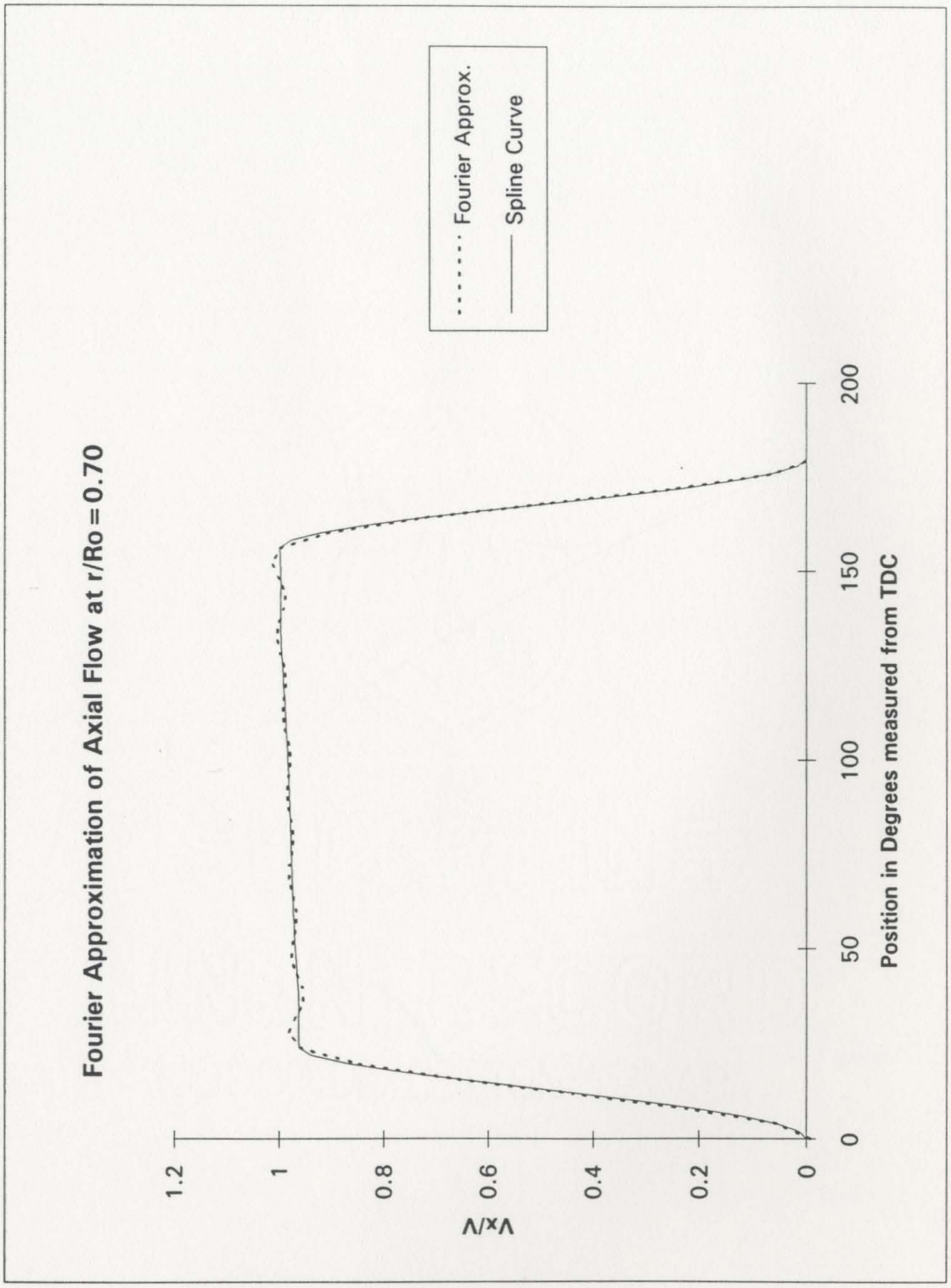

Figure 54 - Fourier Series Approximation of Flow Component - 0.7R.

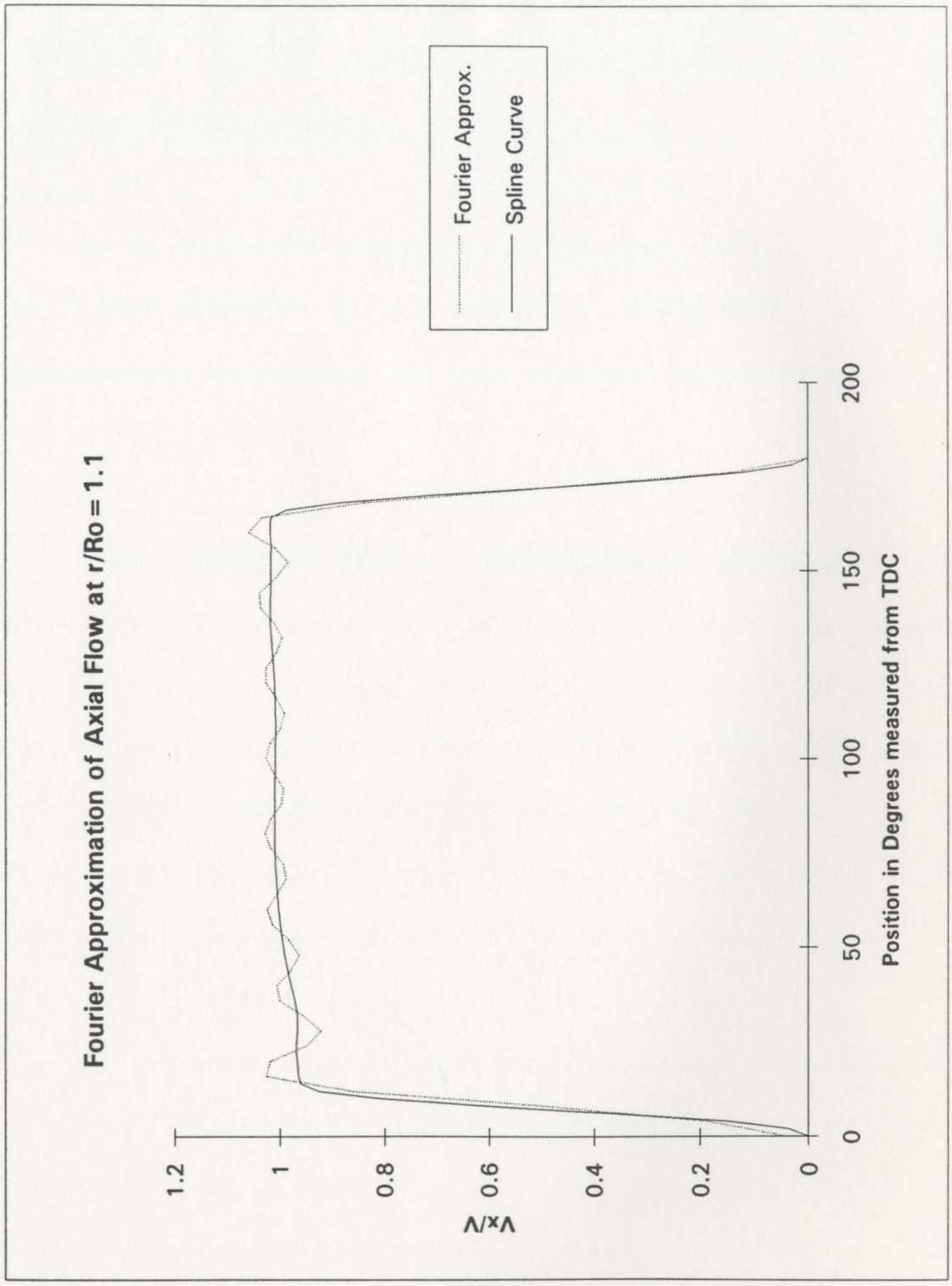

Figure 55 - Fourier Series Approximation of Flow Component - 1.1R.

A Fourier series description of circumferential velocity variations in the wake is a required input to PUF2. Propeller geometry and wake description data files developed for the work reported here are given in Appendix K.

For the purposes of this study the default blade section geometry supplied with the program was used. This geometry is based on a NACA(a=0.8) meanline. The remaining geometrical parameters (e.g. pitch, rake, skew and blade thickness) were computed and input for a B4.40 propeller.

Figure 56 shows the PUF2 performance predictions for the input geometry, but operating in a uniform wake, compared with the Oosterveld polynomial predictions for the same propeller in open water. At J=0.9 the lifting surface algorithm underpredicts thrust(KT) and torque(KQ) by 9% and 15% respectively. At the same value of J the efficiency (ETAO) is overpredicted by 7%. The discrepancy between the PUF2 results and the Oosterveld polynomial predictions was attributed to the difference between the section geometry of the B-series blades and the program default sections.

Figures 57 and 58 show the values of nondimensional thrust(KT) and torque(KQ) coefficient, as computed by PUF2, for a single propeller blade for one complete revolution and for two different values of J. The program calculates the thrust, torque and efficiency for the blade at 6° intervals. The coefficients are plotted against the

angular position (θ) of the blade relative to the skeg. The blade is advancing in the positive (θ) direction with bottom dead center at $\theta=180°$.

Figure 59 is a comparison of the lifting surface predictions for both the uniform flow and simulated wake conditions. Values of KT, KQ and ETAO, in the case of the simulated wake, were computed by taking the arithmetic mean of the values computed for each blade at the 6° intervals and by multiplying the result by the number of blades (4). For the propeller operating in the calculated wake and at J=0.9, the theory predicts decreases in thrust(KT) and torque(KQ) of 7% and 9% respectively. Open water efficiency (ETAO) is predicted to increase by about 2% at the same value of advance coefficient (J).

Lifting surface predictions for performance in the calculated wake are compared in Figure 60 with the experimental data for the propeller tested in the tunnel with the skeg. The theory underpredicts both thrust and torque over the entire range of J values. At J=0.9 the theoretical thrust and torque differs from the experimental values by 37% and 29% respectively.

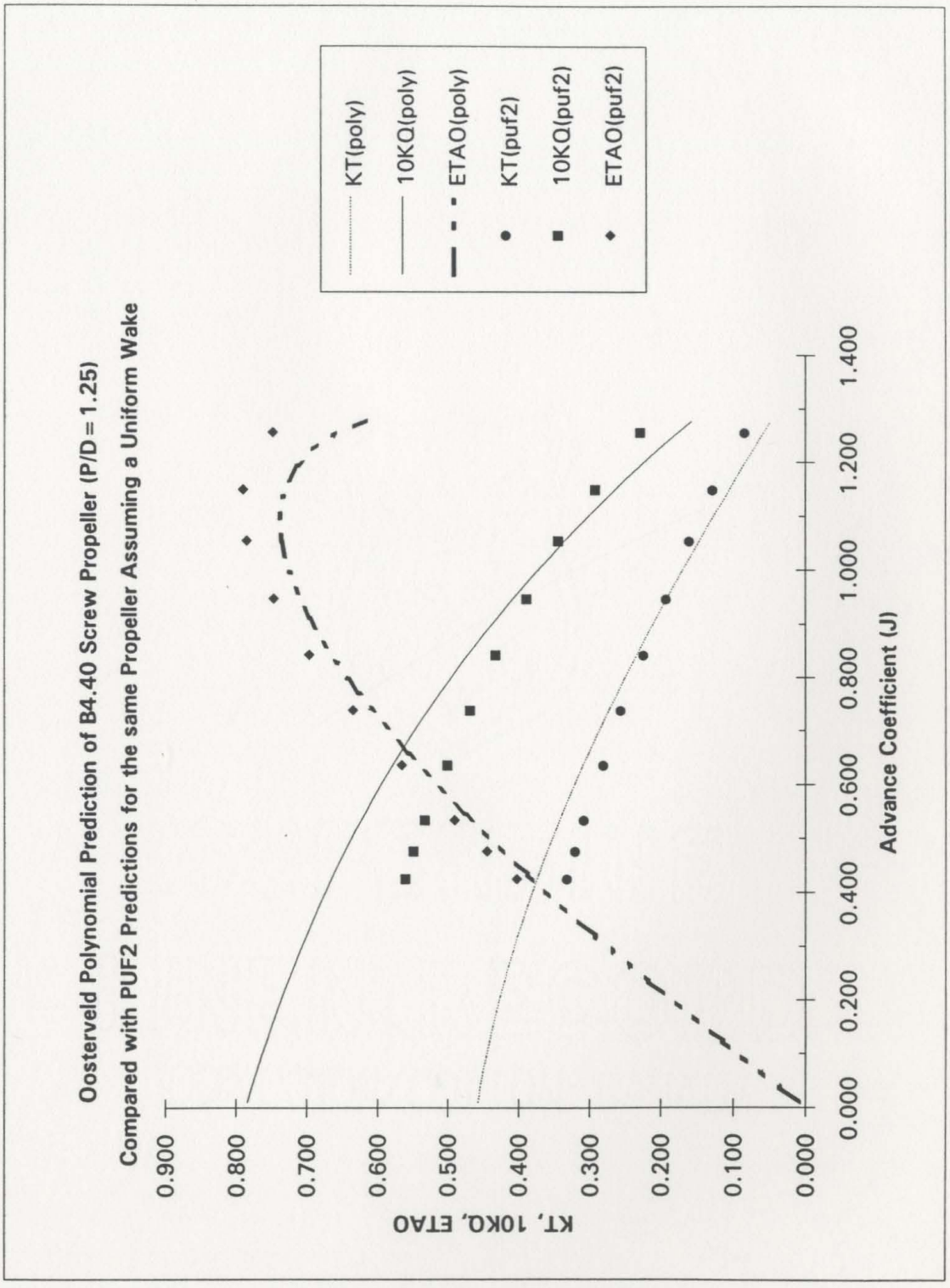

Figure 56 - PUF2 Predictions of Propeller Performance in Unifrom Flow

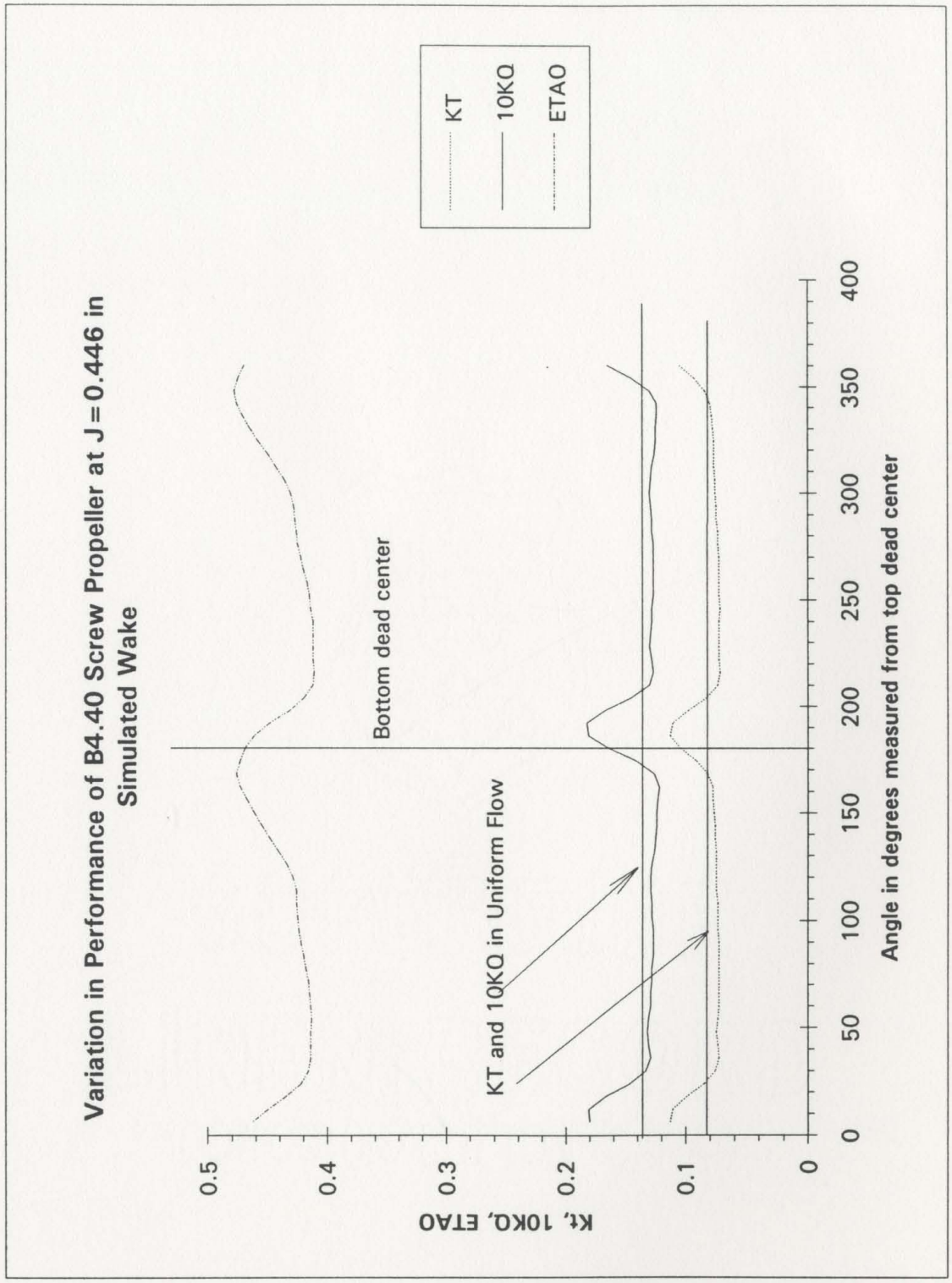

Figure 57 - PUF2 Predictions for Variation of Propeller Thrust and Torque in Simulated Wake (J=0.446).

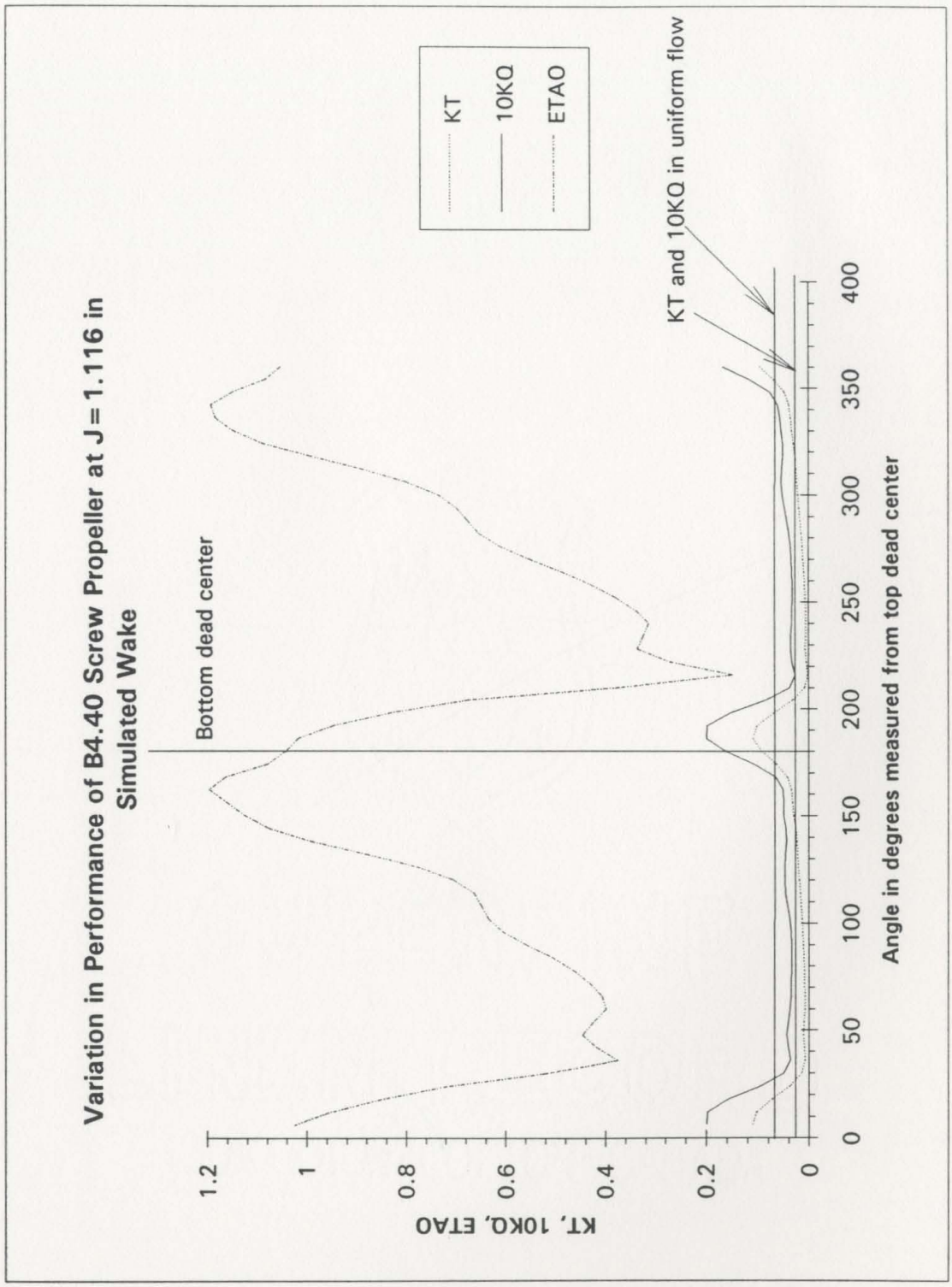

Figure 58 - PUF2 Predictions for Variation of Propeller Thrust and Torque in Simulated Wake (J=1.116).

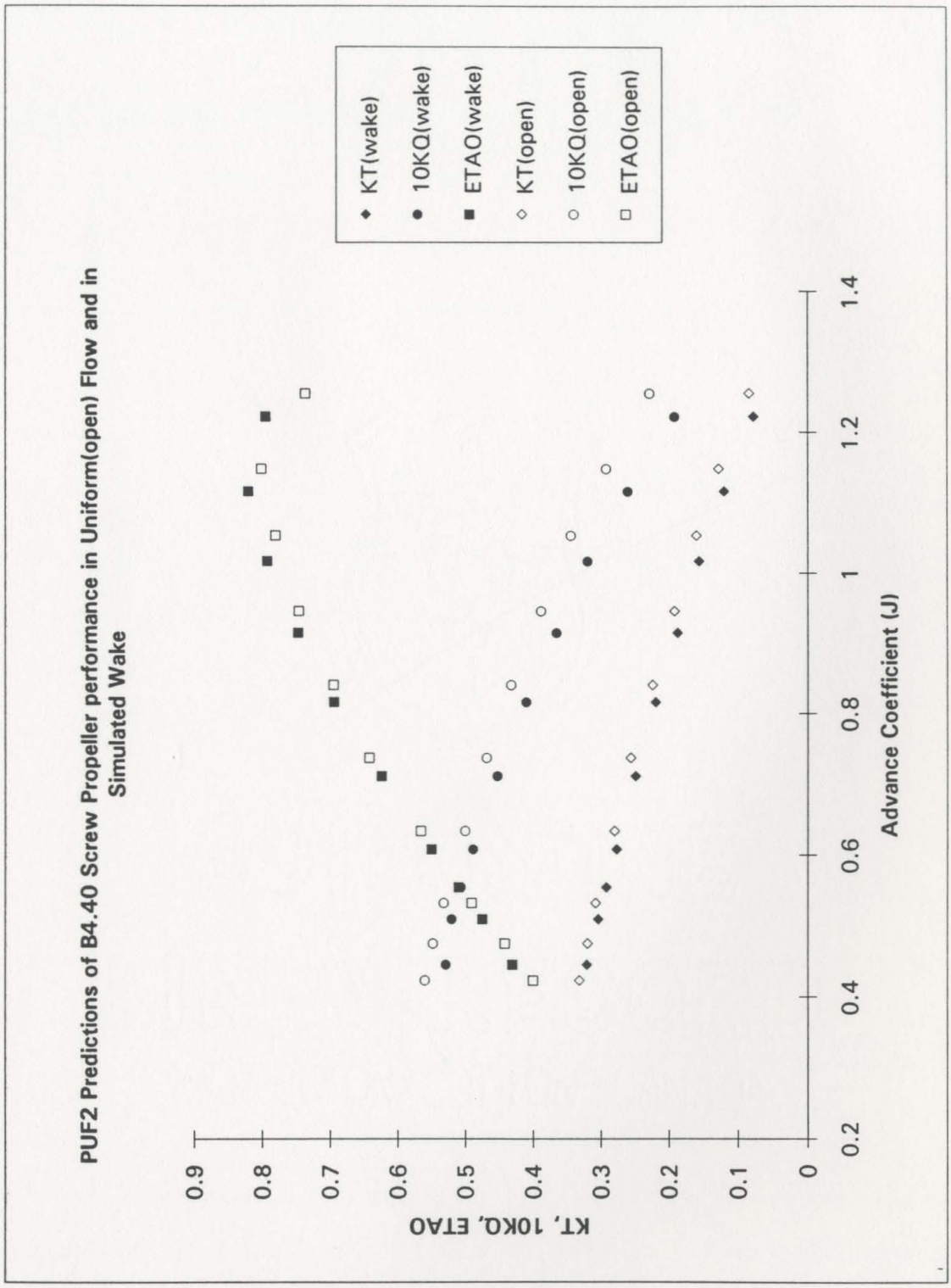

Figure 59 - Comparison of PUF2 Predictions in Uniorm Flow and in Simulated Wake.

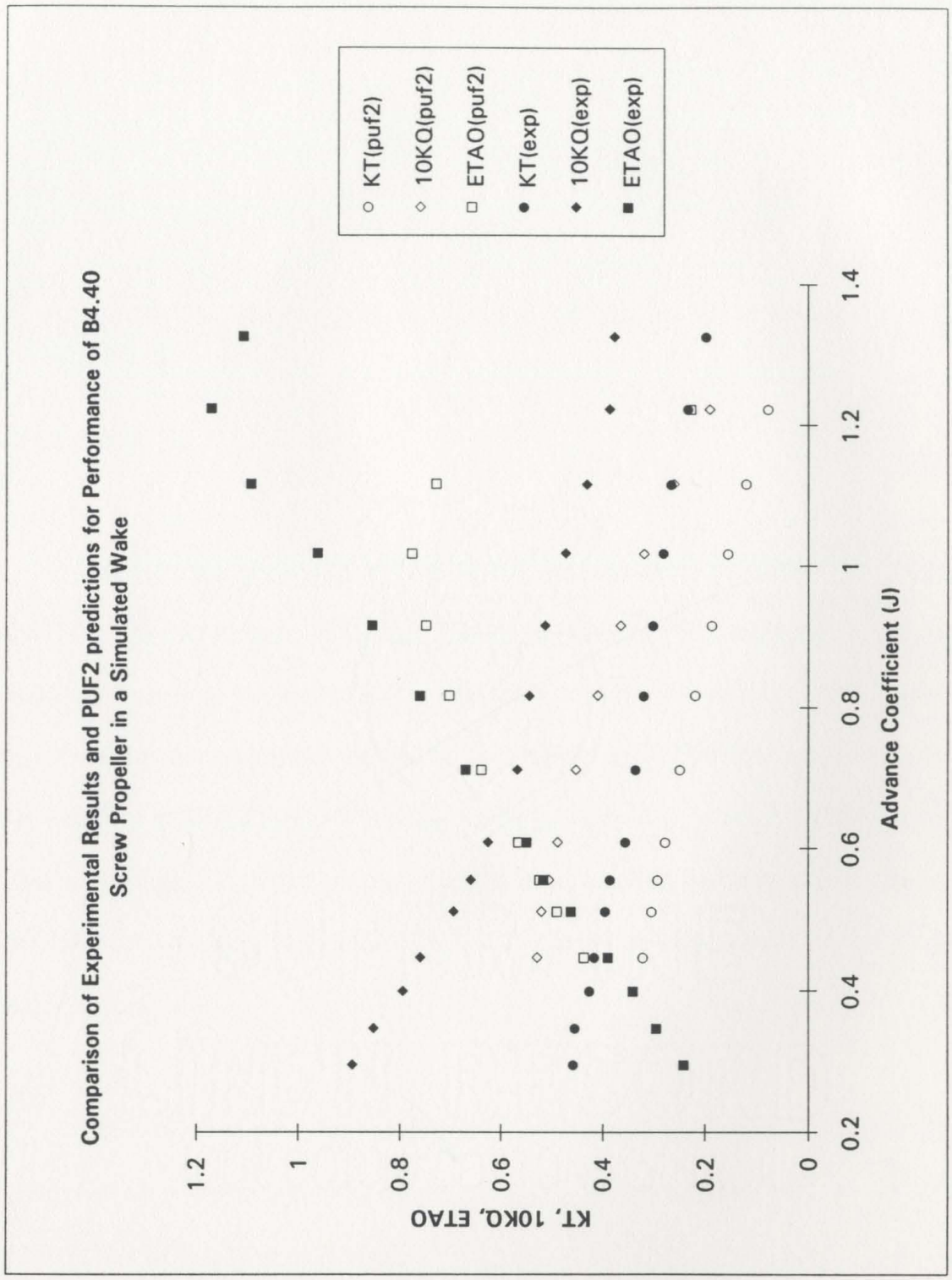

Figure 60 - Comparison of PUF2 Predictions in Simulated Wake With Experimental Results Obtained Behind Skeg.

Chapter 5

Discussion

The discussion presented in this chapter is divided into three parts. The first part deals with the performance of the Digital Particle Tracking Velocimetry(DPTV) system developed as part of this thesis. Following this is an evaluation of the DPTV system as a potential tool for wake measurements in a cavitation tunnel. The final portion discusses the suitability of the MIT-PUF-2 unsteady lifting surface code, using the DPTV measured wake as an input, to predict the performance of a propeller operating in the simulated wake flow field representing the blunt skeg of a typical 10 metre Newfoundland inshore fishing vessel.

The validity of the basic assumptions made in the design of the DPTV system: using a scanning mirror to provide the necessary illumination and then treating individual video fields as instantaneous 'snapshots' delimited by the electronic shutter speed of the video camera, is supported by the experimental results. For the case of uniform flow, Section 4.1, 91% of the measurements were within a grouping determined by the spatial

resolution of the image (0.072 m/s). The remaining 9% of the results differed from the low end of the main data grouping by an amount corresponding to a single pixel, see Figure 29. No experimental values occurred in a similar position above the sample mean, and the discrepancy was attributed to incomplete illumination resulting from a lack of synchronization between the camera 'shutter' and the scanning mirror, see Section 3.3. The low specific gravity of the seed particles did not have any measurable effect on the results in uniform flow.

For the case of 2-D flow around a cylinder the experimental results, for both velocity magnitude and direction, were generally in agreement with the predictions of potential theory. Upstream of the cylinder the level of agreement, as for the case of uniform flow, was limited by the image resolution of 0.072 m/s. The effect of incomplete illumination, as discussed above for uniform flow, could not be quantified for this case. Experimental results and theoretical predictions exhibit poor agreement downstream of the boundary layer separation point. This can be attributed more to the limitations of the theory than the accuracy of the DPTV system. Potential theory does not predict boundary layer separation and the formation of a wake. The acceleration of the fluid in the tunnel test section due to blockage effects was not considered in the potential model, Appendix G. The use of a more complex algorithm, to model the boundary layer and tunnel blockage effects, was considered unlikely to produce improved agreement with the experimental results. The major source of experimental error, incomplete tracks due to

the lack of camera/scanner synchronization, must be addressed before comparisons with a more comprehensive theoretical model is warranted.

With the camera/lens combination used for these experiments the field of view was fixed for each interrogation plane. Image resolution, expressed as millimetres per pixel, was thus different for each set of experiments conducted at different transverse locations within the tunnel. A minimum resolution of 0.29 mm/pixel was obtained at a distance of 288 mm from the camera lens, corresponding to the tunnel centreline position. A maximum resolution of 0.22 mm/pixel was obtained at a distance of 178 mm from the camera lens. This distance corresponds to the interrogation plane at 1.1R as described in Section 4.3.

It is apparent from the above that the accuracy of results from the DPTV system is primarily a function of resolution. The spatial resolution of a digitized image is inversely proportional to the field of view(FOV) of the camera. Reducing the dimensions of the FOV by one half corresponds to increasing spatial resolution by a factor of two. The FOV for these experiments was the minimum possible with the camera available. In principle achieving increased resolution implies simply changing the lens on the camera. However image resolution cannot be arbitrarily increased in this manner without considering the impact on other components of the DPTV system. In order to obtain complete tracks within a smaller FOV the exposure time for the camera must be decreased (increased shutter speed). However, while for a fixed flow velocity higher

shutter speeds produce shorter tracks, the decreased exposure time requires a corresponding increase in illumination intensity. Hence increasing resolution, by decreasing the FOV, may require a more powerful laser. The need for more intense illumination can also arise at a set image resolution for increased flow speed. For a given shutter speed the track length is a function of velocity. At some value of flow speed the length of the particle tracks will approach the same order of magnitude as the dimensions of the illuminated area. In such a situation the probability of having images which contain complete tracks is decreased. In order to maintain the level of resolution the shutter speed would have to be increased to produce a shorter track, again necessitating a more powerful laser. The system as described in Chapter 3 was capable of measuring flow speeds from 1 m/s up to about 2.5 m/s while maintaining a resolution of 0.29 mm/pixel with a FOV of 140 mm x 110 mm.

The results of experiments, using the DPTV system, to measure the wake behind a model of a ship's skeg in the cavitation tunnel agreed qualitatively with similar data measured behind a full model in a towing tank using constant temperature anemometry, Wu and Bose (1992c). The reduction in axial velocity near the underside of the suppressor plate was 2% to 5%. Close to the sidewall of the skeg the reduction was approximately 10%. Measurements at similar locations for the towing tank model showed reductions of about 30% and 18% respectively. The lower reductions observed in the cavitation tunnel were attributed to the much thinner boundary layer on the skeg model as compared with that of the full hull in the towing tank. The Reynolds number for the

towing tank experiments was 2.6×10^6 (calculated using the waterline length of the model hull). For the cavitation tunnel experiments the Reynolds number was 8.3×10^5 (calculated using the length of the vertical portion of the skeg model).

The main limitation of the DPTV system in this application was the restriction to planar flow measurements. From incomplete illumination coding it was possible to identify the presence of out of plane particle motion at the various interrogation planes, but not to positively identify direction or magnitude. This latter problem was exacerbated by inconsistencies in the illumination coding of the particle tracks. With a consistent pattern the magnitude of the out of plane motion could have been estimated by noting the percentage of the complete code visible in the image. The accuracy of measurements in different interrogation planes was dependant on the image resolution as described above. The data sampling rate, defined to be the average number of complete particle tracks per video frame, varied from 1 (at 0.28R) to slightly more than 2 (at 1.1R), see Table 1. This was acceptable for the initial investigation. However, if the system is to be developed further, this rate would be too low to be practical from the point of view of the analysis time required to produce a sufficient spatial density of measurements. Approximately three to five minutes were required to retrieve a stored image, apply contrast enhancement if required, and measure the length and attitude of a particle track. More than half this time was required for file selection and manipulation. The results of on-screen measurements were written directly to an output file by the analysis software, and the processing time was not increased significantly for images with multiple tracks.

For an efficient use of (analysis) time a sampling rate of about 10 to 15 would have been ideal. The particle concentration was not increased to provide such a rate as it was uncertain if such an amount in the tunnel water would adversely affect routine cavitation tests by other researchers using the cavitation tunnel facility. The time required to manually process an image containing 15 tracks is estimated at less than ten minutes.

The accuracy and repeatability of the manual cursor routines, used to make on-screen measurements, could not be quantified. However the consistency of the velocity measurements in uniform flow indicates that the level of this error is less than that introduced by image resolution.

The experimental results of the test propeller, without the skeg, showed higher levels of both thrust and torque over the entire range of advance coefficient (J) as compared with the polynomial predictions of Oosterveld and van Oossanen (1972). These polynomials are based on towing tank results from a systematic series of propellers. Some portion of the discrepancy seen in Figure 45 may have been due to the fact that a pitch/diameter ratio of 1.25 was not included as part of the B4.40 series, and the predictions given by the polynomials represent an interpolation based on the results of similar propellers with pitch-diameter ratios of 1.2 and 1.4. The remainder was attributed to problems associated with correcting cavitation tunnel results to correlate with results obtained in a towing tank. In a towing tank the propeller is operating in an essentially unbounded flow and in the presence of a free surface, whereas in a cavitation tunnel the

free surface is absent and in the present case the tunnel walls were only about 0.75 propeller diameters away from the blade tips. The correction given by Lindgren (1963) only address the wall effects on the velocity measurements made by the water manometers.

The quality of the test propeller was considered poor. The blades were slightly out of plane and their lengths differed by one to two millimetres. Observations using a strobe light also indicated poor agreement on blade profile. However the effect of model quality on measured performance cannot be quantified based on the results of these experiments.

The observed effects of the skeg on propeller performance were increased levels of vibration and propeller cavitation. The vibration was caused by cyclic loading on the propeller shaft as pairs of (propeller) blades moved into the vertical shadow of the skeg. The level of vibration was not measured directly, but could be detected by placing a hand on the tunnel casing. Visualization of cavitation was aided by the use of strobe lights. At low values of J (high propeller RPM) the cavitation on the back of the blades moved rapidly towards the propeller hub as the blade passed behind the skeg. For values of J up to about 0.6, the blade tip vortex, interacting with the shear vortex shed by the vertical trailing edge of the skeg, moved to the suppressor plate representing the underside of the hull. The hydro-acoustic noise generated by the propeller operating in the wake of the skeg was clearly audible within the tunnel enclosure. The unsteady lifting surface code PUF2 was developed for non-cavitating flows and any discussion on the

agreement between experiment and this lifting surface theory must be considered in light of this fact.

The predictions made using PUF2 were based on the geometry of a Wageningen B4.40 propeller but using a NACA(a=0.8) blade section meanline. Figure 56 shows the lifting surface predictions of performance, in a uniform flow, compared to the polynomial predictions. At J=0.9 the two predictions differ by 15% on torque and 9% on thrust, the PUF2 predictions being lower in both cases. Despite such differences the calculations could be used to assess the effectiveness of the predictions resulting from using this code on a propeller in these conditions of severe wake. The wake geometry details required in order to run PUF2 were taken to be those recommended in the user manual, and are given in Appendix K in the form of computer input files.

The measured effect of the presence of the skeg on propeller performance was a net increase in static thrust and torque for values of advance coefficient(J) above 0.6. At J=0.9 the presence of the skeg results in an increase of mean thrust and torque of 20% and 9% respectively. The increase, for both thrust and torque, was attributed to the propeller blades encountering the stalled flow behind the skeg. For values of J below about 0.6 the propeller was operating closer to the bollard pull condition and the difference in blade loading in the stalled flow behind the skeg was not as great. This was confirmed, qualitatively, by the 'time-series' data seen in Figures 57 and 58 which was generated by PUF2 using as input the wake measured by the particle tracking system.

The trend for propeller thrust and torque to increase with increasing J, in the simulated wake, was not predicted by the lifting surface theory. While the thrust and torque are both shown to increase for the blade directly behind the skeg, the values outside of the skeg area are lower than those predicted for the propeller at the same value of J but in a uniform flow. The arithmetic mean of the values predicted for one blade at 6° intervals for a single propeller revolution in the simulated wake, when multiplied by the number of blades was thus lower than what was predicted for the propeller in uniform flow at the same value of J. The reason for the lower predicted values in the essentially uniform, flow away from the skeg is uncertain.

The large discrepancy between the predicted and measured torque at low J values can be attributed primarily to difficulties in obtaining such conditions in a cavitation tunnel. At low values of J the rotation of the propeller will produce a non-uniform flow in the tunnel test section and tend to 'push' the water, thus increasing flow speed. Aside from this fundamental limitation of the propeller experiments, problems with making reliable torque measurements at high shaft RPM using the mechanical dynamometer at the cavitation tunnel have been noted previously by Veitch (1990). These problems may have been aggravated by the propeller shaft vibrations discussed above.

For the wake description file input to PUF2, the number of Fourier coefficients allowed by the program, fifteen(15), was not sufficient to describe such abrupt variations as were measured behind the skeg in the cavitation tunnel. The oscillation in the Fourier

description of non-dimensional axial velocity at 0.7R and 1.1R will have contributed to errors in predicted values of thrust and torque. The magnitude of such errors cannot be quantified without examining the effects of increasing the number of coefficients allowed by the program, but they are not expected to be large.

Chapter 6

Conclusions

The objectives of the study were: to develop a low cost optical technique for making quantitative measurements of two dimensional steady flow; and to investigate applicability of that technique to ship propulsion research.

With respect to the former objective a Digital Particle Tracking Velocimetry (DPTV) system was designed and tested. Capital outlay for a complete system, including the computer, camera and laser, would be approximately $25,000.00 (CDN).

The system used a 30 mW Argon-ion laser and a scanning mirror for illumination. Compared with other published works, this level of laser power was very low. Of those articles reviewed the laser power ranged from about 500 milliwatts to 5 watts or more. This reduction in required laser power represents a large equipment cost reduction.

A pulse-coded illumination was produced by the sweeping motion of the laser beam, avoiding the requirement for a separate light modulation unit. This further reduced the cost.

The commercially available micro-balloons, used as seed particles, were satisfactory for use in steady flow at the (flow) speed examined in this thesis. Alternatives may be required in a study of turbulent flow to ensure that the particles faithfully follow the motion of the fluid under study.

The digitization, processing and analysis system was adequate for this investigation. An automated analysis procedure would reduce the time required to process images, and could remove any errors introduced by the manual cursor routine used to make on-screen measurements.

For the system as tested, the video camera was not synchronized with the scanning mirror, thus the motion of some particles was not completely illuminated within the exposure time of the CCD array. The result of this was an error in track length measurements of approximately the same order of magnitude as the image resolution. The lack of a consistent illumination coding pattern also prevented positive identification of the principal direction of out of plane motion and estimates of the magnitude of the angle (of a particle's motion) relative to the light sheet. This situation can be avoided in

the future by including an external control loop to provide the necessary synchronizing pulse from the scanning mirror to the video camera.

The system was used to make velocity measurements in the test section of a cavitation tunnel. For a uniform flow of 1.6 m/s and a camera field of view of 140 mm x 110 mm, the image resolution was 0.29 mm/pixel. This corresponds to 0.075 m/s with a relative error on individual measurements of 4.3% for that combination of shutter speed, flow speed and field of view. Multiple particle illuminations within a single video field, and the choice of the cameras' electronic shutter speed as a time base, allowed the system to easily make measurements in flow speeds up to about 2.5 m/s with an effective (i.e. illuminated) field of view of only about 75 mm. This is well beyond what would be possible from a system with the same (illuminated) field of view but using an analysis scheme involving sequential video frames. Techniques using sequential frames from commercial video cameras for motion analysis are limited by the framing rate of 30 Hz. Single-frame techniques, which are not limited by the video framing rate, have typically used pulsed lasers or CW lasers with external modulation for flow illumination. In both applications, single-frame or multi-frame, the use of optical lenses to generate a light sheet has dictated a need for high powered lasers. The current work demonstrates a procedure whereby the limitations imposed by the video framing rate can be exceeded while at the same time avoiding the cost of a high powered pulsed laser, and/or separate modulation control.

The magnitude and direction of velocity vectors were determined for streaming flow past a 50 mm diameter right circular cylinder at a Reynolds number of 72,700. The results were compared with potential theory assuming a 2-D cylinder in an infinite flow field. Agreement between theory and experiment was found to be good upstream of the flow separation point on the cylinder. There was qualitative agreement between the video images and the flow patterns recorded by other researchers using streak photography of hydrogen bubbles, Van Dyke (1982).

With respect to the second objective: application of the technique to ship propulsion research, a nominal wake survey was conducted behind a model of a ship's skeg placed in the test section of the cavitation tunnel. Results agreed qualitatively with measurements on a full model of a similar hull form in a towing tank using constant temperature anemometry, Wu and Bose (1992c). The main source of discrepancy between the current results and those made on the full model in the towing tank was attributed to a thin boundary layer on the abbreviated model in the cavitation tunnel. Transverse flow close to the sidewall of the skeg was indicated by the presence of incomplete pulse coding patterns in the digitized images.

The wake measured behind the skeg was used as input to a lifting surface algorithm (MIT-PUF-2) to predict the thrust and torque of a B4.40 marine screw propeller operating behind the skeg. An increase in static thrust and torque was measured on the propeller when operating behind the skeg at values of $J > 0.6$. This increase,

caused by the propeller blades encountering stalled flow behind the skeg, was predicted by the theory on the basis of the loading on a single blade. The predicted average value of total propeller thrust and torque in the simulated wake indicated an opposite trend to what was measured in the cavitation tunnel.

The usefulness of the system, as tested, as a stand-alone instrument for general wake survey measurements is currently limited by a restriction to 2-D steady flow situations. However, the ability to provide low cost real-time, qualitative, visualization of the geometry of planar flow structure is a useful investigative tool. The DPTV system could be adapted for use in a towing tank environment by placing the laser and scanning mirror inside a model and directing the light out through a window in the hull.

References

Adrian, R.J., (1989). ' Applications of Particle Image Velocimetry', *Flow Visualization 1989* , Presented at the Winter Annual Meeting of the American Society of Mechanical Engineers, San Francisco, California, December 1989, pp. 23-28.

Adrian, R.J., (1991). 'Particle Imaging Techniques for Experimental Fluid Mechanics', *Annual Review of Fluid Mechanics,* Vol 23: 261-304.

Adrian, R.J. and Yao, C-S., (1985). 'Pulsed Laser Technique Application to Liquid and Gaseous Flows and the Scattering Power of Seed Materials', *Applied Optics,* Optical Society of America, Vol. 24, No. 1, January.

Agui, J.C. and Jimenez, J., (1987), 'On The Performance of Particle Tracking', *Journal of Fluid Mechanics,* Vol. 185, pp 447-468.

AT&T (1977), American Telephone and Telegraph Co. (1977), *Telecommunications Transmission Engineering Volume 1*, Bell System Center for Technical Education, North Carolina, 665 pages.

ANSI (1986), *Safe Use of Lasers.* ANSI Z-136.1 1-1986, American National Standards Institute, ANSI, New York.

Bachalo, W.B., (1987), 'The Evaluation of Particle Size and Velocity Measurement Technologies', 2nd International Conference on Laser Anemometry - Advances and Applications, Strathclyde, U.K., Sept 1987.

Brophy, M.C., Treaster, A.L., Stinebring, D.R. and Welz, J.P., (1987), ' Optimization of a Five-Hole Probe Wake Measuring System', American Society of Mechanical Engineers, *Fluids Engineering,* Volume 58, pp 37-44.

Dantec Sales Brochure, Probe Catalog, publication no.: 9607E, Dantec Electronics Ltd., Tonsbakken 16-18, DK-2740 Skovlunde, Denmark.

Doucet, J.M., (1992a). *Cavitation Tunnel Instruction Manual,* Report No. OERC92-TR-HYD-92005, Ocean Engineering Research Centre, Memorial University of Newfoundland, April.

Doucet, J.M., (1992(b)). *Cavitation Tunnel Manometer Calibration,* Report No. OERC92-TR-HYD-92004, Ocean Engineering Research Centre, Memorial University of Newfoundland, April.

Durrani, T.S. and Greated, C.A., *Laser Systems in Flow Measurement*, Plenum Press, New York, 289 pages

Erf, R.K., (1978). *Speckle Metrology,* Academic Press, New York, 331 pages.

Gad-el-Hak, M., (1989). 'Advances in Fluid Mechanics Measurements', *Springer-Verlag Lecture Notes in Engineering*, ed. C.A. Brebbia and S.A. Orszag.

Gharib, M. and Willert, C., (1989). 'Particle Tracing: Revisited', *Springer-Verlag Lecture Notes in Engineering*, ed. C.A. Brebbia and S.A. Orszag, pp 109-126.

Gunton, G.P., (1978), 'A Comparison of the Wake Survey Procedures of the National Research Council, Canada, and the Vickers Shipbuilding Group Limited, U.K.', Internal Report of the Vickers Shipbuilding Group Limited Ship Model Experiment Tank, St. Albans and Dumbarton.

Hamilton, J., Fish, S. and Anthony, D., (1992), ' Flow Field Measurements at a Free Surface Using Digital Particle Image Velocimetry', 23rd American Towing Tank Conference, New Orleans, Louisiana, June 1992

Harvald, Sv. Aa., (1983), *Resistance and Propulsion of Ships*, John Wiley and Sons, Inc., New York, 353 pages

Hesselink, L., (1988), 'Digital Image Processing in Flow Visualization', *Annual Review of Fluid Mechanics,* Vol. 20, pp. 421-85.

Hyun, B.S. and Patel, V.C., (1990), ' On Hot-Wire Measurements in the Wake of an Axisymmetric Body Driven by a Marine Propeller', Written Discussion to the Report of the 19th ITTC Propulsor Committee, 19th International Towing Tank Conference, Madrid, Spain

ITTC (1990), Report of the Resistance and Flow Committee to the 19th ITTC , 19th International Towing Tank Conference, Madrid, Spain

Jandel (1990), *JAVA Video Analysis Software - Users Manual*, Jandel Scientific, Corte Madera, California.

Jandel (1991), *JAVA, FGAR and X-Y Measurement Corrections,* Jandel Product Technical Note, Jandel Scientific, Corte Madera, California.

Kato, H. and Ukon, Y., (1990), ' Full Scale Measurement of Propeller Blade Pressure and Inflow Velocity Distributions', 19th International Towing Tank Conference, Madrid, Spain

Katz, J. and Huang, T.T., (1990), 'Quantitative Visualization of External and Internal Flows by Implementing the "Particle Displacement Velocimetry" Method', Invited paper to the Group Discussion on New Facilities and New Testing and Analysis Techniques, *19th International Towing Tank Conference,* Madrid, Spain, September 1990, Vol. 2

Kerwin, J.E. and Lee, C-S., (1978). 'Prediction of Steady and Unsteady Marine Propeller Performance by Numerical Lifting-Surface Theory', Society of Naval Architects and Marine Engineers, Transactions Volume 86, pp 218-253

Kerwin, J.E., (1985), *Propeller Unsteady Performance Analysis Progam MIT-PUF-2 Documentation*, Revised Version January 1985, Massachusetts Institute of Technology, Cambridge, Massachusetts.

Khalighi, B., (1989), 'Study of the Intake Swirl Process in an Engine Using Flow Visualization and Particle Tracking Velocimetry', *Flow Visualization 1989* , Presented at the Winter Annual Meeting of the American Society of Mechanical Engineers, San Francisco, California, December 1989, pp. 37-48.

Komura, T., Kato, H., Yamaguchi, H., (1991), 'A New Velocity Measurement Method for Field Use by Tracer/Multi TV Camera System', Fluid Measurement and Instrumentation Forum, American Society of Mechanical Engineers, Vol 108, pp 105-110

Kux, J., (1990), 'Full Scale LDV Measurements of Ship-Stern Flow Field', 19th International Towing Tank Conference, Madrid, Spain.

Lindgren, H., (1963), 'Propeller Cavitation Experiments in Uniform Flow - A Note on Test Procedure, Corrections and Presentation', 10th International Towing Tank Conference, Teddington, U.K.

Lourenco, L.M., Krothapalli, A. and Smith, C.A., (1989), 'Particle Image Velocimetry', *Springer-Verlag Lecture Notes in Engineering*, ed. C.A. Brebbia and S.A. Orszag, pp 127-200.

Marko, K.A. and Rimai, L., (1985), 'Video Recording and Quantitative Analysis of Seed Particle Track Images in Unsteady Flow', *Applied Optics*, American Institute of Physics, Vol. 24, No. 21, pp 3666-3672

Miles, M.D., (1978), 'Calibration and Analysis Procedures for Three Component Wake Surveys', National Research Council Canada, Division of Mechanical Engineering, Marine Dynamics and Ship Laboratory, Report LTR-SH-236, July 1978.

Miles, M.D., (1982), 'Practical Interactive Graphics Curve Fitting Procedures for Model Test Data', Bulgarian Ship Hydrodynamics Institute Jubilee Meeting, Varna, Bulgaria, November 1982.

Okuno, T., (1990), 'Velocity Field Measurements by Digital Flow Images', Paper presented to the Group Discussion on New Facilities and New Testing and Analysis Techniques, *19th International Towing Tank Conference,* Madrid, Spain, September 1990, Vol. 2

O'Neil, M.E. and Chorlton, F., (1986), *Ideal and Incompressible Fluid Dynamics*, John Wiley and Sons, New York,

Oosterveld, M.W.C., van Oossanen, P., (1972), 'Recent Developments in Marine Propeller Hydrodynamics', International Jubilee Meeting on the Occasion of the 40th Anniversary of the Netherlands Ship Model Basin, Wageningen, the Netherlands, August 1972.

Perry, A.E., (1982), *Hot-wire Anemometry*, Clarendon Press, Oxford, 184 pages

Pirrone, M. and Lindenmuth, W.T., (1992), 'Comparison of Flow Measurements Between 5-Hole Pitot Probes and Laser Doppler Velocimetry in the Ship Propeller Plane', 23rd American Towing Tank Conference, New Orleans, Louisiana, June 1992

Rawson, K.J. and Tupper, E.C., (1984), *Basic Ship Theory Volume 2*, Longman Inc., New York, 326 pages

Rimai, L., Li, P., Adamczyk, A.A., Klick, D.I., Marko, K.A., Ma, T., and Davies, M. (1986), 'Flow Velocity Field Mapping by Video Recording of Coded Seed Track Images', *Flow Visualization IV,* Proceedings of the Fourth International Symposium on Flow Visualization, Paris, France, August 1986, pp. 717-722.

Simpson, R.L., (1989), 'Scanning Laser Anemometry and Other Measurement Techniques for Separated Flows', *Springer-Verlag Lecture Notes in Engineering*, ed. C.A. Brebbia and S.A. Orszag, pp 357-400.

Suzuki, T., (1990), ' A Technique to Measure the Flow Velocity by an Analysis of Tracer Pathline Images', 19th International Towing Tank Conference, Madrid, Spain.

Tanibayashi, H., (1990), 'Full-Scale LDV Measurements of Ship Stern Flow', 19th International Towing Tank Conference, Madrid, Spain.

Tritton, D.J., (1988), *Physical Fluid Dynamics,* Oxford Science Publications, Oxford, 519 pages.

van Dyke, M., (1982), *An Album of Fluid Motion*, The Parabolic Press, Stanford, California, 176 pages.

van Lammeran, W.P.A., Troost, L. and Koning, J.G.,(1948). *Resistance, Propulsion and Steering of Ships*, The Technical Publishing Company, Staam, Haarlem, Holland.,366 p.

van Manen, J.D. and van Oossanen, P., (1988), "Chapter 6 - Propulsion", *Principles of Naval Architecture, Volume II - Resistance, Propulsion and Vibration*, (E.V. Lewis, ed.), Society of Naval Architects and Marine Engineers, Jersey City, New Jersey, pp 127-254.

Wickens, R.H. and Williams, C.D., (1985), 'Calibration and Use of Five-Hole Flow Direction Probes for Low Speed Wind Tunnel Application', Aeronautical Note NAE-AN-29, NRC No. 24468, National Research Council Canada.

Willert, C.E. and Gharib, M., (1991), 'Digital Particle Image Velocimetry', Experiments in Fluids Volume 10, pp 181-193, Springer-Verlag, Berlin 1991.

Wilson, M.B., (1989), 'Simulation of Ship Wakes in Water Tunnel Cavitation Testing of Models', 22rd American Towing Tank Conference, St. John's, Newfoundland, August 1989.

Winburn, D.C., (1987), *What Every Engineer Should Know About Lasers*, Winburn, New York, 203 pages.

Wu, S. and Bose, N., (1992a), 'Experience with Hot-Film Anemometry for Ship Model Nominal Wake Survey in a Towing Tank', 23rd American Towing Tank Conference, New Orleans, Louisiana, June 1992

Wu, S. and Bose, N., (1992b), 'Calibration of a Wedge-Shaped Vee Hot-Film Probe in a Towing Tank', *Measurement Science and Technology* , Institute of Physics, U.K., in press.

Wu, S. and Bose, N., (1992c), 'Axial Wake Survey behind a Fishing Vessel Model by Using a Wedge-Shaped Hot-Film Probe', Kansai Society of Naval Architects, Japan, May, 1992, pp 147-155

Wu, Z., Zhu, J., Chen, S., Yang, L., Xu, H. and Yang, J., (1991), 'An Image Processing System for Quantitatively Analyzing the 2-D Fluid Velocity-Field Image', Computers in Fluids, Vol. 20, No. 4, pp 359-371

Appendix A

Safety Precautions for use of Class IIIb Laser

Proposed Control Measures For The Use of a Class 3b Laser
at The Institute for Marine Dynamics' Cavitation Tunnel

(adapted from Table 10 of ANSI Z136.1-1986)

Engineering Controls

REQUIREMENT	RESPONSE
Protective Housing	Supplied with laser from Canpolar. Will NOT be removed during use
Service access panel	N/A
Key Switch Master	Supplied with laser
Viewing portals	N/A
Collecting optics	N/A
Limited open beam path	NHZ limited to Cav. Tunnel area. Area enclosed by heavy draping and physical barriers
Remote interlock connector	Limited to keyed master switch and circuit breakers for 120V Cav. Tunnel supply
Beam stop	None on laser - optical path ends at 0.75" brass plate inside tunnel
Activation warning system	Audible 2-tone siren prior to emission. Flashing hazard light during operation
Controlled area	Operation area fully enclosed by draping. Access to platform restricted by chains across entrance.
Labels	Affixed to laser.
Area posting	Tunnel platform carries four(4) 'DANGER - LASER IN USE' placards; two(2) signs hung on chains barring entrance to platform.

Administrative and Procedural

REQUIREMENT	RESPONSE
Admin. and Proc. controls	As proposed in the attached statements regarding operating procedures and description of usage.
Standard operating procedure	As proposed in the attached SOP.
Output emission limitation	N/A
Education and training	C. Harris has received instructions from Canpolar in the safe operation of equipment.
Authorized personnel	No formal authorization available. Suggest restriction to essential personnel
Alignment procedure	Will be performed in consultation with Canpolar
Eye protection	Suitable protective lenses supplied by Canpolar with laser equipment.
Spectator control	The Tunnel platform will be off-limits to spectators during laser operation.
Service personnel	N/A
Laser demonstration	Will NOT be available to the general public.
Laser fibre optics	N/A

Procedural Controls and Operating Procedures For Use of Class 3B Laser at the IMD Cavitation Tunnel

1. The laser shall be activated ONLY within the confines of the Cavitation Tunnel Platform area, with the area cleared of non-essential persons and completely enclosed by draping.

2. Prior to operation a siren will sound for a period of approximately five seconds. During operation a flashing hazard light will operate on top of the tunnel enclosure. The siren will sound twice, (in short bursts) when laser operation has ceased.

3. Protective eye-wear will be worn when practical during operation of the laser. Only eye-wear approved by the operator will be acceptable.

4. All persons working in the vicinity of the Tunnel shall observe the warning signs, both audible and visible, and avoid the Tunnel platform during laser operation.

5. To minimize the chance of accidental exposure to laser radiation persons should not enter the Tunnel platform area without verbal consent from the operator.

6. The commissionaires shall be notified by the operator on any day when there is the possibility of laser operation at the Tunnel

7. Tour groups and any other non-IMD residents shall be restricted from entering the general Tunnel area without the express consent of the Tunnel operator.

Appendix B

Material Safety Data Sheet for West System® 409 Microspheres

MATERIAL SAFETY DATA SHEET

Product Trade Name:
WEST SYSTEM® 409 Microspheres

HMIS Hazard Rating Index
-- Health
0 Flammability
0 Reactivity
-- Personal Protection

Manufacturer:
Gougeon Brothers, Inc
100 Patterson Ave.
Bay City, MI 48706 USA
(517) 684-7286

Emergency Telephone:
Chemtrec **(800) 424-9300**
Poison Hotline **(313) 745-5711**

Date Prepared: September 25, 1989
Replaces: June 2, 1989

Section 1 - Product Information

Chemical Tradename/Synonyms: . . . . . Inorganic microspheres
Chemical Family . . . . . Alumino silicate
DOT Hazard Classification: . . . . . Non-hazardous
Formula/Molecular Weight: . . . . . No information

Section 2 - Hazardous Ingredients

Material or component:	CAS Number	Contents %	ACGIH (TLV)	OSHA (PEL)	STEL
Listed in OSHA Federal Register Vol. 36 as an inert nuisance dust			15 mg/m^3		

Section 3 - Physical Data

Boiling Point:	+ 2500°F	Melting point:	n/a	Solubility in Water:	insoluble
% Volatile (vol):	0	Specific Gravity (water = 1):	0.18	Vapor pressure (mmHg):	n/a
Evaporation rate:	0	Vapor Density:	n/a	pH:	n/a
Freezing point:	n/a	Viscosity:	n/a	Critical temperature:	n/a

Appearance and odor: . . . White granules, no odor.

Other: . . . None

Section 4 - Fire & Explosion Hazard Data

Flash point (method): n/a
Autoignition temperature: No information
Flammable limits in air (%): Lower: n/a Upper: n/a

Extinguishing media: . . . . . Non-applicable

Special fire fighting procedures: . . . . Non-applicable

Unusual fire and explosion hazards: . .None known

Section 5 - Reactivity Data

Product corrosive: No
Stability: Stable

Hazardous polymerization: . . . . . Will not occur.

Conditions to avoid: . . . . . None known

Materials to avoid: . . . . . .None known

Hazardous decomposition products: . . None

Section 6 - Health Hazard Data

Ingestion: . . . . . .No information.

Inhalation: . . . . . Considered to be an inert nuisance dust.

Eye contact: . . . . Non-irritating.

Skin contact: . . . . Non-irritating.

Skin absorption: . . No information.

Chronic effects of overexposure: . . No information.

Section 7 - Emergency & First Aid Procedures

Ingestion: . . . . . .No harmful effects expected.

Inhalation: . . . . . Remove to fresh air.

Eye contact: . . . . Flush with water.

Skin contact: . . . . Wash with soap and water after use.

Section 8 - Spills, Leaks, Handling & Storage Procedures

Spill & leak procedures: . . . . . Sweep or vacuum.

Waste disposal method: . . . . . (Disposer must comply with federal, state or local waste disposal laws.) Dispose of in landfill.

Handling & storage methods: . . . . No special precautions are necessary.

Section

Ventilation requirements: . . . . . Use with adequate ventilation.

Respiratory protection: . . . . . (Use NIOSH/MSHA approved respirators.) Respirator should be worn for inert nuisance dust.

Protective clothing: . . . . . None required.

Eye protection: . . . . . Wear goggles.

Additional protective measures: . . . None required.

Section 10 - Special Precautions

None

Section 11 - Additional Information

None

Appendix C

American Laser Corporation Model 60B Argon-Ion Laser

Specifications

MODEL 60B
OEM AIR-COOLED ARGON ION LASER SYSTEMS

american laser corporation

FEATURES

- 3 - 100 MILLIWATTS
- COMPACT DESIGN
- OEM PRICING
- LIGHT CONTROLLED
- STANDBY (IDLE)/RUN MODE
- SWITCHING POWER SUPPLY

LASER HEAD

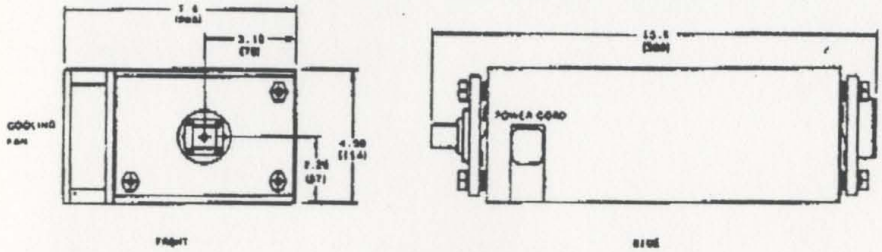

POWER SUPPLY

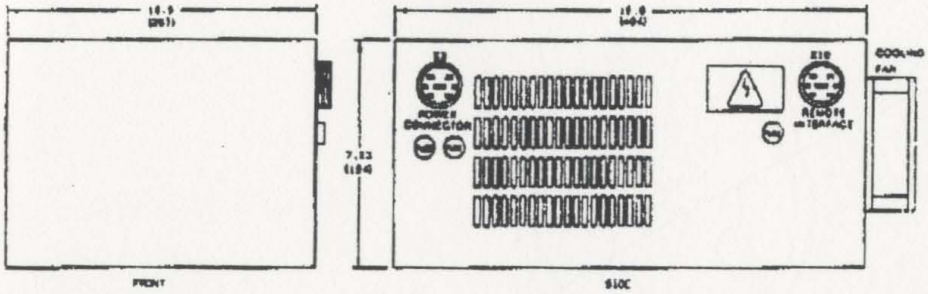

Dimensions in inches
Dimensions in parentheses in millimeters

SPECIFICATIONS

OUTPUT POWER (Argon All-Lines)	100 mW
CW Operation (TEM 00)	0.6 mm
Beam Diameter (TEM 00)	0.7 mrad
Beam Divergence (TEM 00)	> 100:1 E-Vector vertical ± 5°
Beam Polarization Ratio	Solid Invar Rod
Optical Resonator	In light control < ± 2%
Amplitude Power Stability	In current control < ± 3%
	In light control < 2% pp (1DHz to 1 MHz)
Optical Noise	In current control < 5% pp
Operating Environment	10° - 40°C (50° - 104°F)
Temperature	0-95% non-condensing
Humidity	0-10,000 FL
Altitude	Beryllium Oxide (BeO) Ceramic
Plasma Tube Bore Material	
Electrical Service	115 V (+10%/-5%), single phase
Voltage	20 amp
Current	50/60 Hz
Frequency	7.9 x 4.5 x 15.0 in. (200 x 114 x 380 mm)
Laser Head Size	2 - Dayton pole blowers model 4C443A or equivalent,
Head Cooling Requirements	plus integral fans (120 CFM)
	10.5 x 7.6 x 15.9 in. (267 x 194 x 404 mm)
Power Supply Size	Air - 2 Fan (Integral), 120 CFM
Power Supply Cooling	

american laser corporation
1832 South 3850 West
Salt Lake City, UT 84104
Telephone: (801) 972-1311
Telex: 389 464
Fax: 801-972-5251

american laser gmbh
Hans Pinsel Strasse 9B-10B
8013 Haar, West Germany
Telephone: 89-464070
Telex: 5214063
Fax: 89-4603644

OPTIONS & ACCESSORIES

Multimode operation
Single line or wavelength tunable
Remote control module

Specifications represent the general performance of standard models. American Laser reserves the right to change any information provided, at any time, and without notification, and declines responsibility for errors that may occur.

LASER SAFETY
CDRH warning logotypes, similar to that shown on the right appear on the lasers to indicate the CDRH classification and to verify that the output power of the laser will not exceed the power level printed on the logotype.

Appendix D

IDS Series Optical Scanners

GENERAL SCANNING INC.
500 Arsenal Street, P.O. Box 307, Watertown, MA 02272
(617) 924-1010 Telex: 443-0105 FAX (617) 926-0708

IDS SERIES OPTICAL SCANNERS

Outline Drawing: IDS Series

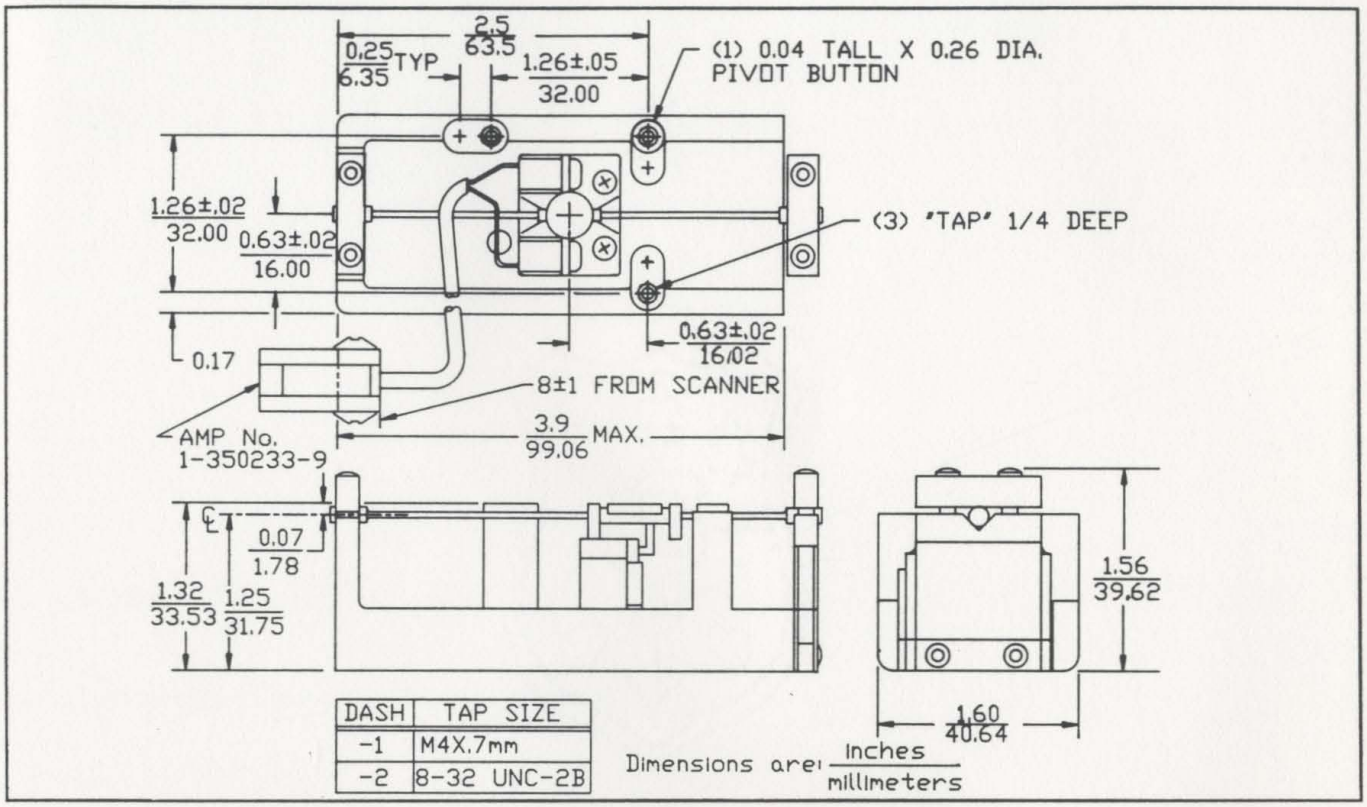

SPECIFICATIONS (nominal values)

IDS Model[5]:	2512	3006	3008
Frequency [1]	1200 Hz	600 Hz	800 Hz
Excursion [3] (peak-to-peak)	50°	60°	60°
Mirror Dimension [2]	9 mm ca.	9 mm ca.	9 mm ca.
Drive Power	0.05 watt	0.07 watt	0.10 watt
Sagittal Wobble [3] (same direction)	25 µradian	25 µradian	25 µradian
Sagittal Wobble [3] (retrace)	175 µradian	175 µradian	175 µradian
Synchronization Signal	0.05 mvolt-s/deg	0.05 mvolt-s/deg	0.05 mvolt-s/deg
Temperature Stability			
Frequency	-200 ppm/°C	-200 ppm/°C	-200 ppm/°C
Sensor Output	200 ppm/°C	300 ppm/°C	----------

Notes: (1) Standard Frequency ±2%.
(2) All standard mirrors are flat to 1/4 wave @ 632 nm.
(3) Angles are in optical degrees.
(4) Environmental: storage -10 to 70°C; operating +10° to 50°C.
(5) Larger mirrors and lower frequencies available on special order.

Appendix E

Panasonic Omni-Movie PVS350-K CCD Camera

Service Manual

S-VHS-MOVIE

Panasonic Omnivision S-VHS

PV-S350

Consists of PV-S350D/PV-A22MB

PV-S350-K

Consists of PV-S350D-K/PV-A22MB-K

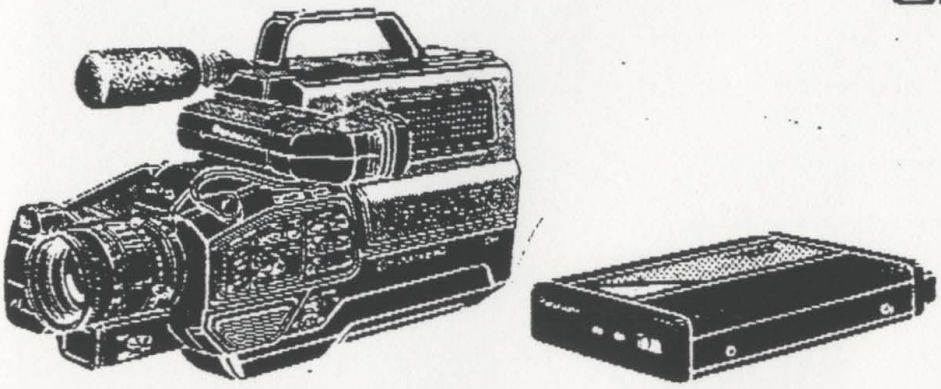

Model PV-S350D
PV-S350D-K

Model PV-A22MB
PV-A22MB-K

ITEM	SPECIFICATIONS	MODEL 1	MODEL 2
Power	Source: S-VHS Movie: DC12V	○	–
	AC Adaptor: 110/120/220/240 V AC 50/60 Hz	–	○
	Consumption: S-VHS Movie: 12 V DC 15W	○	–
	AC Adaptor: 40 W	–	○
Video	Heads: 4 rotary heads, helical scanning system	○	–
	Input/Output Level :		
	(Composite) : VIDEO IN/OUTPUT Jack (Phono type)	–	○
	: 1.0 Vp-p 75Ω unbalanced		
	(Component) : S-VIDEO CONNECTOR (DIN Type 4 pin)	○	–
	: Luminance 1.0 Vp-p 75Ω unbalanced		
	: Chrominance 0.63 Vp-p 75Ω unbalanced		
	Cyanogen (Standard NTSC Color Bar)		
	: Burst 0.286 Vp-p 75Ω unbalanced		
	Signal-to-Noise Ratio: VHS Mode : SP : more than 43dB	○	–
	: : SLP : more than 41dB		
	: S-VHS Mode: SP : more than 44dB		
	: SLP : more than 42dB		
	Horizontal Resolution: Color/Monochrome:	○	–
	: VHS Mode : more than 230 lines		
	: S VHS Mode: more than 400 lines		
Audio	Head: Normal Mono: 1 stationary head	○	–
	Input Level: AUDIO IN Jack (Phono type) −10 dB 50 kΩ unbalanced	–	○
	MIC IN Jack (M3 type) −70 dB 4.7 kΩ unbalanced	○	–
	Output Level: AUDIO OUT Jack (Phono type) −8 dB 500Ω unbalanced	–	○
	Frequency Response: Normal Mono: SP: 100 Hz−8 kHz SLP: 100Hz−5kHz	○	–
	Signal-to-Noise Ratio: SP : more than 42 dB	○	–
	SLP: more than 40 dB	○	–

1. PV-S350D, PV-S350D-K (S-VHS Movie)
2. PV-A22MB, PV-A22MB-K (AC Adaptor)

Specifications are subject to change without notice.

(Please see reverse side)

Panasonic

Matsushita Services Company
50 Meadowland Parkway.
Secaucus, New Jersey 07094

Panasonic Hawaii Inc.
91-238 Kauhi St. Ewa Beach
P.O. Box 774
Honolulu, Hawaii 96808-0774

Matsushita Electric
of Canada Limited
5770 Ambler Drive, Mississauga,
Ontario, L4W 2T3

Panasonic Sales Company,
Division of Matsushita Electric
of Puerto Rico, Inc.
Ave. 65 De Infanteria, KM 9.7
Victoria Industrial Park
Carolina, Puerto Rico 00630

(Continued from cover page)

ITEM	SPECIFICATIONS	MODEL 1	MODEL 2
RF Out	Ch 3/Ch 4 switchable, 72 dBμ (Open Voltage) 75Ω unbalanced	–	○
Television System	EIA Standard (525 lines, 60 fields) NTSC Color Signal	○	–
Tape Speed	SP: 1-5/6 i.p.s (33.35mm/sec) SLP: 7/16 i.p.s (11.12mm/sec) Record/Playback Time: 160 min. with 160 min. type tape FF/REW Time: Less than 8 min. (E-60 min. type tape)	○	–
Tape Format	Tape width 1/2" (12.7mm) high density tape	○	–
Operating Condition	32°F (0°C) –104°F (40°C) (Temperature) 10%–75% (Humidity)	○	○
Pick-up System	Sequential color difference, field reverse system	○	–
Pick-up Device	One integral color filter Charge Coupled Device (CCD)	○	–
Lens	8:1 Zoom Lens Auto Iris: closed with power off Auto Zoom Lens and Macro construction Auto Focus System F: 1.2 f: 8.5mm ~ 68mm Lens filter diameter: 49mm	○	–
Electronic View Finder	Monochrome 2/3 inch B/W CRT, built in	○	–
Optimum Light Intensity on optical image	1500 Lux 150 footcandles	○	–
Dimension	16-1/4" (413mm) (W) × 9" (228mm) (H) × 4-5/8" (117mm) (D) 7-7/8" (200mm) (W) × 1-7/16" (36mm) (H) × 4-1/8" (105mm) (D)	○ –	– ○
Weight	6.6 lbs (3.0kg) 1.9 lbs (0.86kg)	○ –	– ○

1. PV-S350D, PV-S350D K (S-VHS Movie)
2. PV-A22MB, PV-A22MB-K (AC Adaptor)

Weight and dimensions shown are approximate.
Specifications are subject to change without notice.

CONTENTS

Appendix F

Imaging System - Hardware and Software Calibrations

JAVA® and TARGA+® Imaging System - Hardware and Software Calibrations

There are two distinct calibrations required prior to using the image analysis system described in this thesis.

The first is to establish the degree of geometric distortion inherent to the imaging and digitizing equipment. This is a hardware dependant effect and such a calibration is required to be repeated only once for each unique collection of imaging hardware.

The second calibration is required to relate the image attributes of position, area, distance and intensity to 'real world' values. Although a certain degree of hardware dependency is implied in this procedure it is primarily a function of experimental setup. This calibration is required for each experiment that involves a change to either the lens magnification or the distance from the camera to the object focal plane.

The calibration process, as carried out for the work described in this thesis, is described in this appendix. The procedures described in the JAVA® user manuals are incorrect and this fact was acknowledged by Jandel in a technical note dated December 1991. However, the procedure described in that technical note is incomplete, and rigorous adhesion to the new procedure will lead to errors in digital image measurement.

Hardware Calibration (Frame Grabber Aspect Ratio-FGAR) and Geometric Corrections

The pixels displayed on a video monitor are not square; in fact they are rectangular in the ratio of approximately Y:X=4:3. In addition to this simple relationship there are also interactions between system components which can further distort the image. However for each combination of imaging hardware the Frame Grabber Aspect Ratio (FGAR) is a unique constant. Relating pixels within an image to real-world geometry requires a mapping process, and hence an image of an object with precisely known geometry (graph paper was used for these experiments). Utilizing the hardware, and physical set-up, to be used for subsequent experiments the following procedure should be followed.

1. Capture (digitize) an image of known geometry (e.g. graph paper)
2. Set FGAR=1.0
3. Load and Run Java®
4. Use the CALIB feature within JAVA to calibrate the software for X-Y measurements.
5. Measure and record the maximum (equal) distance in the horizontal(X) and vertical(Y) directions. Be sure that you have measured the same 'physical' distance in both instances.
6. Exit JAVA and set FGAR equal to the ratio of Y/X as measured in step 4.
7. Restart JAVA® and use the CALIB feature to properly calibrate the system for ALL geometric measurement functions using the (known) image geometry. Pay special attention to ANGLE calibration, if FGAR has not been properly set then large errors can result in the measurement of small angles.

Appendix G

Qbasic Program to Calculate the Potential Flow of a Uniform Stream around a 2-D Cyinder

```
'************************************************************
'                        PROGRAM - flocomp
'************************************************************
' Programmed by C. J. Harris (MUN # 8012114)  22-June-1992
'************************************************************
' Program FLOCOMP calculates the velocity vectors corresponding to the flow
' of an (ideal) fluid stream around an semi-infinite 2-D  cylinder.
' The algorithim is based on the superposition of the velocity potentials
' for two elementary planar flows, ie the velocity potential  representing a
' a uniform stream and the velocity potential representing a  doublet.
'
' A graphics screen output is currently supported and hardcopy is only by
' SHIFT+PRINT SCREEN.
'          ********** WARNING **********
' THIS PROGRAM WAS DEVELOPED FOR A PARTICULAR SET OF
' EXPERIMENTS - VERY FEW  IF ANY USER INPUT VALUES ARE
' ALLOWED. PERSONS USING THIS PROGRAM DO SO AT
' THEIR OWN RISK AND THE AUTHOR TAKES NO RESPONSIBILITY FOR
' INCORRECT ANSWERS.
'
'************************************************************
REM: INITIALIZE VALUES FOR
REM:    DIPOLE STRENGTH (DSTRENGTH) [M^2/S]
REM:    FREE STREAM VELOCITY (STREAM) [M/S]
REM:    RELATIVE ANGLE (THETA) [DEG]
REM:    RADIUS (RAD) [M]
REM: DIMENSION ARRAYS FOR VELOCITY COMPONENTS
DIM radius(100, 2)
DIM angled(100, 2)
DIM angler(100, 2)
DIM vrad(100, 2)
DIM vtheta(100, 2)
DIM velmag(100)
DIM veldir(100)
DIM axe1(10)
DIM aye1(10)
DIM vmag(100)
DIM vdir(100)
DIM INARRAY(100, 4)
' accept filename
INPUT "ENTER input FILENAME.....", file$
filename$ = file$
' open file for input on LUN 2
OPEN file$ FOR INPUT AS #2
```

```
INPUT "enter number of datasets in file ", numpnts
FOR i = 1 TO numpnts
        FOR j = 1 TO 4
        INPUT #2, num
        INARRAY(i, j) = num
        NEXT j
NEXT i
' accept output file name
INPUT "ENTER output FILENAME.....", file$
OPEN file$ FOR OUTPUT AS #1
DSTRENGTH = .001035  'corresponds to a cylinder of d=50 mm
stream = 1.656
' initialize counter values
i = 1
j = 1
CONST pi = 3.141592654#
' calculate Pot. Theory values at experimental locations
SCREEN 12
FOR i = 1 TO numpnts
        axe = (91! - INARRAY(i, 1)) / 1000'' .....(i) / 10000
        aye = (91! - INARRAY(i, 2)) / 1000'' aye1(i) / 10000
        radius(i, j) = SQR(axe ^ 2 + aye ^ 2)
        RAD = radius(i, j)
        THETAR = ATN(aye / axe) + pi
'        angler(I, j) = THETAR
'calculate radial and tangential velocities
        vrad(i, j) = ((-1 * DSTRENGTH * COS(THETAR)) / RAD ^ 2) + (stream *
COS(THETAR))
        vtheta(i, j) = ((-1 * DSTRENGTH * SIN(THETAR)) / RAD ^ 2) - (stream *
SIN(THETAR))
'calculate magnitude and direction of resultant velocity
        velmag(i) = SQR(((vrad(i, j)) ^ 2) + ((vtheta(i, j)) ^ 2))
        veldir(i) = ((THETAR + (ATN(vtheta(i, j) / vrad(i, j)))))
NEXT i
'plot pot theory vectors
i = 1
j = 1
FOR i = 1 TO numpnts
        x1 = 4 * INARRAY(i, 1)
        y1 = 479 - 4 * INARRAY(i, 2)
        x2 = x1 - 15 * velmag(i) * COS(veldir(i))
        y2 = y1 + 15 * velmag(i) * SIN(veldir(i))
        vd = 180 - veldir(i) * 180 / pi'convert radians to degrees
       LINE (x1, y1)-(x2, y2), , , &H8888
```

```
NEXT i
'plot experimental vectors
FOR i = 1 TO numpnts
      x1 = 4 * INARRAY(i, 1)'      68.418
      y1 = 479 - (4 * INARRAY(i, 2))'   49.728)
      vmag(i) = INARRAY(i, 3) * .24588
      vdir(i) = 360 - INARRAY(i, 4)'       13.633
      x2 = x1 + 15 * vmag(i) * COS(vdir(i) * pi / 180)
      y2 = y1 + 15 * vmag(i) * SIN(vdir(i) * pi / 180)
      LINE (x1, y1)-(x2, y2), , , &HF0F0
NEXT i
' set graphics screen, clear screen and draw reference lines
SCREEN 12
'cls
CIRCLE (364, 116), 100, 12
LINE (0, 116)-(640, 116), 12
x1 = 0
y1 = 0
x2 = 400
y2 = 200
LINE (364, 0)-(364, 400), 12
'
''draw reference line representing 1.656 m/s
x1 = 25
y1 = 55
x2 = 49.84
y2 = 55
LINE (x1, y1)-(x2, y2), 12
LOCATE 4, 8
PRINT "Uo=1.656 m/s"

'print plot title
LOCATE 28, 18
PRINT "Flow around a cylinder - Potential theory vs. PIV data"
'
'print legend.....
'for PIV results
LINE (475, 55)-(490, 55), , , &HF0F0
'for Potential theory
LINE (475, 25)-(490, 25), , , &H8888
LOCATE 2, 63
PRINT "potential theory"
LOCATE 4, 63
PRINT "PIV results"
```

```
'
'output data to file
PRINT #1, "   X1        Y1          Velocity          %          Direction          %"
PRINT #1, "                    Theory   Experiment   diff   Theory   Experiment
diff"
PRINT #1, " "
FOR i = 1 TO numpnts
x1 = 4 * INARRAY(i, 1)'      68.418
y1 = 479 - (4 * INARRAY(i, 2))'   49.728)
veldird = 180 - (veldir(i) * 180 / pi)
diffvel = ((velmag(i) - vmag(i)) / velmag(i)) * 100
diffdir = ((veldird - vdir(i)) / veldird) * 100
PRINT #1, USING "###.##    ###.##     #.##      #.##       ##.#    ##.##     ##.##
  ##.#"; x1; y1; velmag(i); vmag(i); diffvel; veldird; vdir(i); diffdir

PRINT #1, " "
NEXT i
'
'plot axes
LINE (0, 420)-(640, 420)
LINE (20, 5)-(20, 480)
' plot ticks on y axes
x1 = 15
x2 = 25
strt = 420
FOR i = 1 TO 20
y1 = strt - (i * 20)
y2 = y1
LINE (x1, y1)-(x2, y2)
NEXT i
'plot ticks on x axes
y1 = 415
y2 = 425
strt = 20
FOR i = 1 TO 30
x1 = strt + (i * 20)
x2 = x1
LINE (x1, y1)-(x2, y2)
NEXT i
```

Appendix H

Tabulated Results for Flow Measurements Around a Cylinder

		Velocity [m/s]			Angle [deg]		
X1	Y1	Theory	Exper.	% diff	Theory	Exper.	% diff
141.26	256.74	1.57	1.56	0.90	7.88	6.80	13.60
154.10	280.94	1.62	1.62	-0.30	7.99	4.26	46.70
175.63	80.04	1.25	1.35	-8.10	-7.47	-10.52	-40.90
149.32	280.90	1.61	1.55	4.00	7.75	4.47	42.40
155.31	281.88	1.62	1.55	4.40	8.02	4.47	44.30
132.94	251.10	1.56	1.26	19.30	7.43	5.61	24.50
167.36	69.76	1.30	1.13	13.20	-7.84	-12.55	-60.00
110.00	272.22	1.58	1.48	6.30	6.03	7.15	-18.60
91.33	234.08	1.54	1.49	2.90	5.13	9.49	-85.10
164.80	187.43	1.39	1.48	-6.30	9.78	7.15	26.90
153.90	198.45	1.44	1.42	1.30	8.90	9.97	-12.10
321.69	261.93	2.29	1.87	18.10	9.48	11.35	-19.70
241.76	248.30	1.77	1.59	10.40	16.53	13.42	18.80
153.01	70.57	1.34	1.33	0.70	-6.16	-5.31	13.90
185.57	147.77	1.20	0.96	19.60	8.58	7.32	14.60
132.81	162.14	1.39	1.18	15.20	4.82	0.00	100.00
288.14	269.07	2.05	1.83	10.50	12.55	15.57	-24.00
135.15	166.80	1.39	1.18	15.30	5.34	5.96	-11.60
153.17	260.52	1.58	1.49	5.90	8.57	9.49	-10.80
239.12	269.59	1.79	1.86	-3.50	13.23	7.61	42.40
190.28	257.15	1.62	1.20	26.00	11.45	11.70	-2.20
165.94	294.00	1.65	1.49	9.60	8.06	9.49	-17.70
82.44	276.63	1.58	1.41	10.90	4.92	7.51	-52.70
246.74	334.52	1.82	1.71	6.10	7.02	8.28	-17.90
273.50	191.13	1.86	1.64	12.00	38.75	31.05	19.90
227.38	250.96	1.71	1.59	7.30	15.08	13.42	11.00
247.18	193.69	1.55	1.33	14.40	29.95	27.50	8.20
223.73	258.36	1.72	1.49	13.10	13.88	9.41	32.20
264.98	205.88	1.82	1.59	12.60	30.07	22.68	24.60
241.02	211.24	1.63	1.73	-6.00	23.82	20.73	13.00
248.89	354.92	1.81	1.70	6.20	5.78	6.23	-7.70
315.00	221.11	2.61	1.80	31.00	20.70	9.88	52.30
140.83	190.02	1.43	1.40	1.80	7.25	5.02	30.70
147.63	221.56	1.50	1.71	-14.00	8.66	8.27	4.50
293.89	286.72	2.03	1.71	15.70	9.56	10.29	-7.60
179.00	299.68	1.67	1.56	6.50	8.33	9.04	-8.50
268.98	372.68	1.83	1.55	15.30	4.47	4.55	-1.70
257.51	231.76	1.84	1.66	9.80	21.04	22.64	-7.60
280.15	316.36	1.95	1.79	8.00	6.81	10.49	-54.00
291.15	316.36	1.95	1.79	8.00	6.81	10.49	-54.00

NOTE: X1 and Y1 are screen coordinates with (0,0) at the top left corner. The cylinder center is at (364,116) with a diameter of 100 screen units. Velocity units are [m/s], and angles are in [deg] with 0.0 degrees being horizontal pointing right and increasing clockwise.

Appendix I

Fabrication Details for Skeg Model

DRG NO 11 302-1112-4

DO NOT SCALE FROM DRAWING

FORWARD

AFT

SEE DRG 302-1112-401 FOR DETAILS OF SHAFT CONSTRUCTION

NOTES
1) 4 FULL SPACERS REQ'D (P1 – P4)
2) 1 PARTIAL SPACER REQD (P5)
3) INSIDE FACE OF P2 & P3 25mm EITHER SIDE OF SHAFT ℄
4) BORE SHAFT CLEARANCE HOLE Ø48mm

250

P1

CLEARANCE HOLE P2

Ø=42mm

CLEARANCE 3mm ALL AROUND = TOTAL DIAMETER = 48mm

SHAFT ℄

P3

P4

P5

FILLER PIECE CUT TO FIT UNDER FIRST SPACER

SKEG FASTENED VIA CLEANOUT FROM THIS SIDE

50

12mm AL SPACERS

292 (AT TRAILING EDGE)

Ø=48mm CLEARANCE FOR SHAFT ± 3mm ALL AROUND

250

DRAWING 302-1992-04

SCALE 1:1

SEE TABLE 302-1992-T1
FOR OFFSETS

LAYOUT FOR ALUMINUM SPACERS AND CONSTRUCTION DETAILS

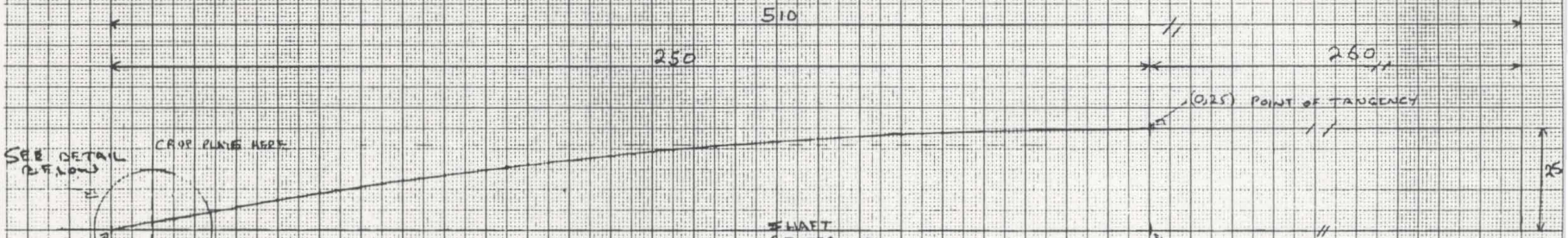

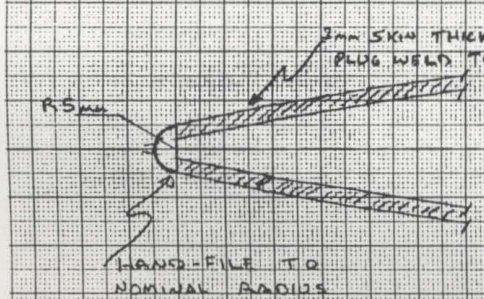

LEADING EDGE CONSTRUCTION DETAIL

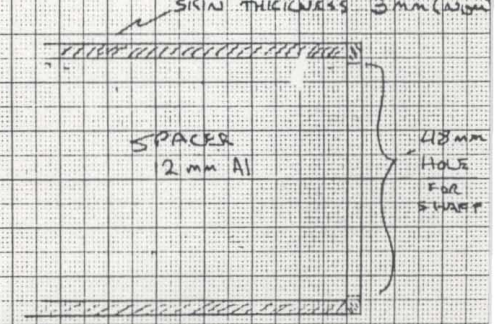

TRAILING EDGE CONSTRUCTION DETAIL

Appendix J

Particulars for Wageningen B4.40 Screw Propeller

B-SERIES PROPELLER DATA

DATA FILE NAME := B8_40_P125

Propeller Diameter:= 8.0000
Expanded Blade Area Ratio, Ae/Ao:= 0.4000
Number of blades:= 4
Pitch is 1.2500 with NO Hub reduction
Rake angle is 15.000 degrees
Maximum Section Thickness at Hub:= 0.3600
Required Hud Diameter:= 1.3334
Maximum Section Width is 1.7494 at Radius 2.4000

DEFINTION OF TERMS

MT - Blade maximum thickness for section
BW - Overall Blade width for section
DTE - Distance from generator line to Trailing edge
TRD - Trailing edge rounding diameter
DLE - Distance from generator line to leading edge
LRD - Leading edge rounding diameter
DMTE - Distance from maximum thickness to Trailing edge
DMLE - Distance from maximum thickness to leading edge
DGMT - Distance from generator line to maximum thickness

*** NOTE *** Value of -88.8888 in data for LRD or TRD indicates that the section has infinite slope at that edge.

RADIUS AT SECTION := 0.8000

MT	BW
0.2928	1.3310

DTE	TRD	DLE	LRD
0.5105	0.0187	0.8205	-88.8888

DMTE	DMLE	DGMT
0.8651	0.4658	0.3546

Ordinates at given distance from point of maximum thickness

Back of Blade

	TE	100%	90%	80%	70%	60%	50%	40%
ABS=		-0.8651	-0.7786	-0.6921	-0.6056	-0.5191	-0.4326	-0.3461
ORD=		0.0878	0.1265	0.1555	0.1836	0.2099	0.2335	0.2538

	30%	20%	10%	MT	20%	40%	60%
ABS=	-0.2595	-0.1730	-0.0865	0.0000	0.0932	0.1863	0.2795
ORD=	0.2703	0.2825	0.2902	0.2928	0.2889	0.2767	0.2547

	80%	90%	95%	97.5%	99.5%	99.9%	100%	LE
ABS=	0.3727	0.4193	0.4425	0.4542	0.4635	0.4654	0.4658	
ORD=	0.2178	0.1884	0.1667	0.1520	0.1325	0.1239	0.1171	

Face of Blade

	TE	100%	90%	80%	70%	60%	50%	40%
ABS=		-0.8651	-0.7786	-0.6921	-0.6056	-0.5191	-0.4326	-0.3461
ORD=		0.0878	0.0658	0.0536	0.0423	0.0321	0.0230	0.0152

	30%	20%	10%	MT	20%	40%	60%
ABS=	-0.2595	-0.1730	-0.0865	0.0000	0.0932	0.1863	0.2795
ORD=	0.0089	0.0041	0.0010	0.0000	0.0014	0.0064	0.0173

	80%	90%	95%	97.5%	99.5%	99.9%	100%	LE
ABS=	0.3727	0.4193	0.4425	0.4542	0.4635	0.4654	0.4658	
ORD=	0.0394	0.0595	0.0764	0.0884	0.1048	0.1116	0.1171	

RADIUS AT SECTION := 1.2000

MT	BW
0.2592	1.5038

DTE	TRD	DLE	LRD
0.5829	0.0168	0.9209	-88.8888

DMTE	DMLE	DGMT
0.9775	0.5263	0.3946

Ordinates at given distance from point of maximum thickness

Back of Blade

	TE	100%	90%	80%	70%	60%	50%	40%
ABS=		-0.9775	-0.8797	-0.7820	-0.6842	-0.5865	-0.4887	-0.3910
ORD=		0.0657	0.1029	0.1310	0.1579	0.1830	0.2055	0.2247

	30%	20%	10%	MT	20%	40%	60%
ABS=	-0.2932	-0.1955	-0.0977	0.0000	0.1053	0.2105	0.3158
ORD=	0.2400	0.2509	0.2572	0.2592	0.2551	0.2435	0.2221

	80%	90%	95%	97.5%	99.5%	99.9%	100%	LE
ABS=	0.4211	0.4737	0.5000	0.5132	0.5237	0.5258	0.5263	
ORD=	0.1879	0.1624	0.1423	0.1286	0.1119	0.1043	0.0973	

Face of Blade

	TE	100%	90%	80%	70%	60%	50%	40%
ABS=		-0.9775	-0.8797	-0.7820	-0.6842	-0.5865	-0.4887	-0.3910
ORD=		0.0657	0.0442	0.0328	0.0230	0.0150	0.0087	0.0042

	30%	20%	10%	MT	20%	40%	60%
ABS=	-0.2932	-0.1955	-0.0977	0.0000	0.1053	0.2105	0.3158
ORD=	0.0013	0.0000	0.0000	0.0000	0.0001	0.0034	0.0119

	80%	90%	95%	97.5%	99.5%	99.9%	100%	LE
ABS=	0.4211	0.4737	0.5000	0.5132	0.5237	0.5258	0.5263	
ORD=	0.0281	0.0429	0.0575	0.0687	0.0836	0.0912	0.0973	

RADIUS AT SECTION := 1.6000

MT	BW
0.2256	1.6378

DTE	TRD	DLE	LRD
0.6525	0.0149	0.9853	-88.8888

DMTE	DMLE	DGMT
1.0646	0.5732	0.4120

Ordinates at given distance from point of maximum thickness

Back of Blade

	TE	100%	90%	80%	70%	60%	50%	40%
ABS=	-1.0646	-0.9581	-0.8517	-0.7452	-0.6388	-0.5323	-0.4258	
ORD=	0.0403	0.0782	0.1076	0.1346	0.1587	0.1795	0.1966	

	30%	20%	10%	MT	20%	40%	60%
ABS=	-0.3194	-0.2129	-0.1065	0.0000	0.1146	0.2293	0.3439
ORD=	0.2097	0.2189	0.2240	0.2256	0.2217	0.2104	0.1903

	80%	90%	95%	97.5%	99.5%	99.9%	100%	LE
ABS=	0.4586	0.5159	0.5446	0.5589	0.5704	0.5727	0.5732	
ORD=	0.1589	0.1357	0.1180	0.1059	0.0906	0.0835	0.0778	

Face of Blade

	TE	100%	90%	80%	70%	60%	50%	40%
ABS=	-1.0646	-0.9581	-0.8517	-0.7452	-0.6388	-0.5323	-0.4258	
ORD=	0.0403	0.0228	0.0140	0.0075	0.0032	0.0008	0.0000	

	30%	20%	10%	MT	20%	40%	60%
ABS=	-0.3194	-0.2129	-0.1065	0.0000	0.1146	0.2293	0.3439
ORD=	0.0000	0.0000	0.0000	0.0000	0.0000	0.0009	0.0059

	80%	90%	95%	97.5%	99.5%	99.9%	100%	LE
ABS=	0.4586	0.5159	0.5446	0.5589	0.5704	0.5727	0.5732	
ORD=	0.0173	0.0283	0.0403	0.0504	0.0649	0.0720	0.0778	

RADIUS AT SECTION := 2.0000

MT	BW
0.1920	1.7211

DTE	TRD	DLE	LRD
0.7134	0.0129	1.0077	-88.8888

DMTE	DMLE	DGMT
1.1101	0.6110	0.3967

Ordinates at given distance from point of maximum thickness

Back of Blade

	TE	100%	90%	80%	70%	60%	50%	40%
ABS=	-1.1101	-0.9991	-0.8881	-0.7771	-0.6661	-0.5551	-0.4440	
ORD=	0.0186	0.0547	0.0830	0.1086	0.1310	0.1500	0.1656	

	30%	20%	10%	MT	20%	40%	60%
ABS=	-0.3330	-0.2220	-0.1110	0.0000	0.1222	0.2444	0.3666
ORD=	0.1775	0.1858	0.1905	0.1920	0.1884	0.1773	0.1583

	80%	90%	95%	97.5%	99.5%	99.9%	100%	LE
ABS=	0.4888	0.5499	0.5804	0.5957	0.6079	0.6104	0.6110	
ORD=	0.1299	0.1090	0.0934	0.0830	0.0697	0.0634	0.0584	

Face of Blade

	TE	100%	90%	80%	70%	60%	50%	40%
ABS=	-1.1101	-0.9991	-0.8881	-0.7771	-0.6661	-0.5551	-0.4440	
ORD=	0.0186	0.0075	0.0036	0.0009	0.0000	0.0000	0.0000	

	30%	20%	10%	MT	20%	40%	60%
ABS=	-0.3330	-0.2220	-0.1110	0.0000	0.1222	0.2444	0.3666
ORD=	0.0000	0.0000	0.0000	0.0000	0.0000	0.0000	0.0014

	80%	90%	95%	97.5%	99.5%	99.9%	100%	LE
ABS=	0.4888	0.5499	0.5804	0.5957	0.6079	0.6104	0.6110	
ORD=	0.0079	0.0162	0.0254	0.0330	0.0461	0.0528	0.0584	

RADIUS AT SECTION := 2.4000

MT	BW
0.1520	1.7494

DTE	TRD	DLE	LRD
0.7684	0.0103	0.9811	-88.8888

DMTE	DMLE	DGMT
1.0689	0.6805	0.3006

Ordinates at given distance from point of maximum thickness

Back of Blade

	TE	100%	90%	80%	70%	60%	50%	40%
ABS=	-1.0689	-0.9620	-0.8551	-0.7482	-0.6413	-0.5345	-0.4276	
ORD=	0.0078	0.0372	0.0606	0.0821	0.1010	0.1170	0.1298	

	30%	20%	10%	MT	20%	40%	60%
ABS=	-0.3207	-0.2138	-0.1069	0.0000	0.1361	0.2722	0.4083
ORD=	0.1397	0.1466	0.1507	0.1520	0.1483	0.1379	0.1210

	80%	90%	95%	97.5%	99.5%	99.9%	100%	LE
ABS=	0.5444	0.6125	0.6465	0.6635	0.6771	0.6799	0.6805	
ORD=	0.0968	0.0790	0.0661	0.0576	0.0467	0.0415	0.0372	

Face of Blade

	TE	100%	90%	80%	70%	60%	50%	40%
ABS=	-1.0689	-0.9620	-0.8551	-0.7482	-0.6413	-0.5345	-0.4276	
ORD=	0.0078	0.0008	0.0000	0.0000	0.0000	0.0000	0.0000	

	30%	20%	10%	MT	20%	40%	60%
ABS=	-0.3207	-0.2138	-0.1069	0.0000	0.1361	0.2722	0.4083
ORD=	0.0000	0.0000	0.0000	0.0000	0.0000	0.0000	0.0000

	80%	90%	95%	97.5%	99.5%	99.9%	100%	LE
ABS=	0.5444	0.6125	0.6465	0.6635	0.6771	0.6799	0.6805	
ORD=	0.0017	0.0067	0.0127	0.0184	0.0279	0.0330	0.0372	

RADIUS AT SECTION := 2.8000

MT	BW
0.1248	1.7159

DTE	TRD	DLE	LRD
0.8166	0.0086	0.8992	-88.8888

DMTE	DMLE	DGMT
0.9557	0.7601	0.1391

Ordinates at given distance from point of maximum thickness

Back of Blade

	TE	100%	90%	80%	70%	60%	50%	40%
ABS=		-0.9557	-0.8602	-0.7646	-0.6690	-0.5734	-0.4779	-0.3823
ORD=		0.0000	0.0271	0.0481	0.0666	0.0824	0.0956	0.1063

	30%	20%	10%	MT	20%	40%	60%
ABS=	-0.2867	-0.1911	-0.0956	0.0000	0.1520	0.3040	0.4561
ORD=	0.1145	0.1202	0.1237	0.1248	0.1214	0.1113	0.0947

	80%	90%	95%	97.5%	99.5%	99.9%	100%	LE
ABS=	0.6081	0.6841	0.7221	0.7411	0.7563	0.7594	0.7601	
ORD=	0.0713	0.0551	0.0437	0.0362	0.0275	0.0237	0.0200	

Face of Blade

	TE	100%	90%	80%	70%	60%	50%	40%
ABS=		-0.9557	-0.8602	-0.7646	-0.6690	-0.5734	-0.4779	-0.3823
ORD=		0.0000	0.0000	0.0000	0.0000	0.0000	0.0000	0.0000

	30%	20%	10%	MT	20%	40%	60%
ABS=	-0.2867	-0.1911	-0.0956	0.0000	0.1520	0.3040	0.4561
ORD=	0.0000	0.0000	0.0000	0.0000	0.0000	0.0000	0.0000

	80%	90%	95%	97.5%	99.5%	99.9%	100%	LE
ABS=	0.6081	0.6841	0.7221	0.7411	0.7563	0.7594	0.7601	
ORD=	0.0000	0.0008	0.0031	0.0060	0.0126	0.0167	0.0200	

RADIUS AT SECTION := 3.2000

MT	BW
0.0916	1.5745

DTE	TRD	DLE	LRD
0.8459	0.0064	0.7286	-88.8888

DMTE	DMLE	DGMT
0.8203	0.7542	-0.0255

Ordinates at given distance from point of maximum thickness

Back of Blade

	TE	100%	90%	80%	70%	60%	50%	40%
ABS=		-0.8203	-0.7383	-0.6562	-0.5742	-0.4922	-0.4102	-0.3281
ORD=		0.0000	0.0204	0.0359	0.0494	0.0610	0.0706	0.0783

	30%	20%	10%	MT	20%	40%	60%
ABS=	-0.2461	-0.1641	-0.0820	0.0000	0.1508	0.3017	0.4525
ORD=	0.0842	0.0883	0.0908	0.0916	0.0874	0.0778	0.0636

	80%	90%	95%	97.5%	99.5%	99.9%	100%	LE
ABS=	0.6033	0.6788	0.7165	0.7353	0.7504	0.7534	0.7542	
ORD=	0.0442	0.0316	0.0233	0.0175	0.0115	0.0092	0.0068	

Face of Blade

	TE	100%	90%	80%	70%	60%	50%	40%
ABS=		-0.8203	-0.7383	-0.6562	-0.5742	-0.4922	-0.4102	-0.3281
ORD=		0.0000	0.0000	0.0000	0.0000	0.0000	0.0000	0.0000

	30%	20%	10%	MT	20%	40%	60%
ABS=	-0.2461	-0.1641	-0.0820	0.0000	0.1508	0.3017	0.4525
ORD=	0.0000	0.0000	0.0000	0.0000	0.0000	0.0000	0.0000

	80%	90%	95%	97.5%	99.5%	99.9%	100%	LE
ABS=	0.6033	0.6788	0.7165	0.7353	0.7504	0.7534	0.7542	
ORD=	0.0000	0.0000	0.0000	0.0001	0.0022	0.0043	0.0068	

RADIUS AT SECTION := 3.6000

MT	BW
0.0576	1.2657

DTE	TRD	DLE	LRD
0.8222	0.0064	0.4435	0.0064

DMTE	DMLE	DGMT
0.6329	0.6329	-0.1894

Ordinates at given distance from point of maximum thickness

Back of Blade

	TE	100%	90%	80%	70%	60%	50%	40%
ABS=		-0.6329	-0.5696	-0.5063	-0.4430	-0.3797	-0.3164	-0.2531
ORD=		0.0000	0.0141	0.0237	0.0320	0.0390	0.0448	0.0495

	30%	20%	10%	MT	20%	40%	60%
ABS=	-0.1899	-0.1266	-0.0633	0.0000	0.1266	0.2531	0.3797
ORD=	0.0531	0.0556	0.0571	0.0576	0.0556	0.0495	0.0390

	80%	90%	95%	97.5%	99.5%	99.9%	100%	LE
ABS=	0.5063	0.5696	0.6012	0.6170	0.6297	0.6322	0.6329	
ORD=	0.0237	0.0143	0.0089	0.0061	0.0038	0.0033	0.0000	

Face of Blade

	TE	100%	90%	80%	70%	60%	50%	40%
ABS=		-0.6329	-0.5696	-0.5063	-0.4430	-0.3797	-0.3164	-0.2531
ORD=		0.0000	0.0000	0.0000	0.0000	0.0000	0.0000	0.0000

	30%	20%	10%	MT	20%	40%	60%
ABS=	-0.1899	-0.1266	-0.0633	0.0000	0.1266	0.2531	0.3797
ORD=	0.0000	0.0000	0.0000	0.0000	0.0000	0.0000	0.0000

	80%	90%	95%	97.5%	99.5%	99.9%	100%	LE
ABS=	0.5063	0.5696	0.6012	0.6170	0.6297	0.6322	0.6329	
ORD=	0.0000	0.0000	0.0000	0.0000	0.0000	0.0000	0.0000	

RADIUS AT SECTION := 3.8000

MT	BW
0.0408	0.9521

DTE	TRD	DLE	LRD
0.7468	0.0064	0.2052	0.0064

DMTE	DMLE	DGMT
0.4760	0.4760	-0.2708

Ordinates at given distance from point of maximum thickness

Back of Blade

	TE	100%	90%	80%	70%	60%	50%	40%
ABS=		-0.4760	-0.4284	-0.3808	-0.3332	-0.2856	-0.2380	-0.1904
ORD=		0.0000	0.0095	0.0159	0.0221	0.0273	0.0315	0.0349

	30%	20%	10%	MT	20%	40%	60%
ABS=	-0.1428	-0.0952	-0.0476	0.0000	0.0952	0.1904	0.2856
ORD=	0.0375	0.0393	0.0404	0.0408	0.0393	0.0349	0.0273

	80%	90%	95%	97.5%	99.5%	99.9%	100%	LE
ABS=	0.3808	0.4284	0.4522	0.4641	0.4736	0.4756	0.4760	
ORD=	0.0159	0.0086	0.0057	0.0043	0.0005	0.0001	0.0000	

Face of Blade

	TE	100%	90%	80%	70%	60%	50%	40%
ABS=		-0.4760	-0.4284	-0.3808	-0.3332	-0.2856	-0.2380	-0.1904
ORD=		0.0000	0.0000	0.0000	0.0000	0.0000	0.0000	0.0000

	30%	20%	10%	MT	20%	40%	60%
ABS=	-0.1428	-0.0952	-0.0476	0.0000	0.0952	0.1904	0.2856
ORD=	0.0000	0.0000	0.0000	0.0000	0.0000	0.0000	0.0000

	80%	90%	95%	97.5%	99.5%	99.9%	100%	LE
ABS=	0.3808	0.4284	0.4522	0.4641	0.4736	0.4756	0.4760	
ORD=	0.0000	0.0000	0.0000	0.0000	0.0000	0.0000	0.0000	

RADIUS AT SECTION := 3.9000

MT	BW
0.0324	0.6875

DTE	TRD	DLE	LRD
0.6551	0.0062	0.0324	0.0062

DMTE	DMLE	DGMT
0.3438	0.3438	-0.3114

Ordinates at given distance from point of maximum thickness

Back of Blade

	TE	100%	90%	80%	70%	60%	50%	40%
ABS=	-0.3438	-0.3094	-0.2750	-0.2406	-0.2063	-0.1719	-0.1375	
ORD=	0.0000	0.0081	0.0133	0.0182	0.0222	0.0255	0.0280	

	30%	20%	10%	MT	20%	40%	60%
ABS=	-0.1031	-0.0688	-0.0344	0.0000	0.0688	0.1375	0.2063
ORD=	0.0300	0.0313	0.0321	0.0324	0.0313	0.0280	0.0222

	80%	90%	95%	97.5%	99.5%	99.9%	100%	LE
ABS=	0.2750	0.3094	0.3266	0.3352	0.3420	0.3434	0.3438	
ORD=	0.0133	0.0074	0.0049	0.0040	0.0004	0.0001	0.0000	

Face of Blade

	TE	100%	90%	80%	70%	60%	50%	40%
ABS=	-0.3438	-0.3094	-0.2750	-0.2406	-0.2063	-0.1719	-0.1375	
ORD=	0.0000	0.0000	0.0000	0.0000	0.0000	0.0000	0.0000	

	30%	20%	10%	MT	20%	40%	60%
ABS=	-0.1031	-0.0688	-0.0344	0.0000	0.0688	0.1375	0.2063
ORD=	0.0000	0.0000	0.0000	0.0000	0.0000	0.0000	0.0000

	80%	90%	95%	97.5%	99.5%	99.9%	100%	LE
ABS=	0.2750	0.3094	0.3266	0.3352	0.3420	0.3434	0.3438	
ORD=	0.0000	0.0000	0.0000	0.0000	0.0000	0.0000	0.0000	

RADIUS AT TIP:= 4.0000

MT	DGMT	LRD
0.0240	-0.3523	0.0064

Ordinates at given distance from generator line

Back of Blade, % of overall propeller radius

	97.75%	98%	98.25%	98.50%	98.75%	99%	99.25%
ABS=	-0.3155	-0.3195	-0.3236	-0.3277	-0.3318	-0.3359	-0.3400
ORD=	0.0315	0.0305	0.0292	0.0275	0.0252	0.0222	0.0185

	99.50%	99.75%	99.875%	99.969%	99.986%	99.996%
ABS=	-0.3441	-0.3482	-0.3503	-0.3518	-0.3521	-0.3523
ORD=	0.0141	0.0086	0.0053	0.0025	0.0018	0.0010

Appendix K

Computer Input Files for MIT-PUF-2

B-440 Propeller Geometry Input File for MIT-PUF-2

```
4    1    1    0
11    15    9   10   15    4   60
8.0    1.125    739.   0.000  0.0070
B4.40 RH with p/d=1.25
0.2000 0.3000 0.4000 0.5000 0.6000 0.7000 0.8000 0.9000 0.9500 0.9750 1.0000
8.2200 8.8700 9.5000 9.9200 10.000 10.000 10.000 10.000 10.000 10.000 10.000
0.4288 0.6431 0.8574 1.0718 1.2862 1.5005 1.7149 1.9292 2.0364 2.0900 2.1436
25.396 18.841 14.753 11.365 7.1763 2.8463 -0.457 -3.014 -4.083 -4.575 -5.047
1.3310 1.5038 1.6378 1.7211 1.7494 1.7159 1.5745 1.2657 0.9521 0.6875 0.0000
0.1464 0.1296 0.1128 0.0960 0.0760 0.0624 0.0458 0.0288 0.0204 0.0162 0.0000
0.2928 0.2592 0.2256 0.1921 0.1520 0.1248 0.0916 0.0576 0.0408 0.0324 0.0240
1
0.0036 0.0062 0.0104 0.0176 0.0296 0.0372 0.0400 0.0397 0.0358 0.0289 0.0199 0.0100 0.0049 0.0026 0.0010
0.0019 0.0046 0.0092 0.0178 0.0315 0.0404 0.0442 0.0425 0.0372 0.0288 0.0188 0.0092 0.0045 0.0032 0.0009
0.0009 0.0035 0.0087 0.0183 0.0343 0.0448 0.0494 0.0490 0.0431 0.0350 0.0241 0.0120 0.0060 0.0031 0.0012
0.0001 0.0033 0.0089 0.0190 0.0367 0.0481 0.0530 0.0534 0.0495 0.0412 0.0293 0.0153 0.0077 0.0039 0.0016
0.0011 0.0039 0.0090 0.0182 0.0340 0.0450 0.0505 0.0512 0.0480 0.0412 0.0300 0.0155 0.0077 0.0039 0.0016
0.0012 0.0045 0.0070 0.0192 0.0335 0.0436 0.0496 0.0518 0.0498 0.0439 0.0340 0.0207 0.0112 0.0056 0.0023
0.0017 0.0053 0.0096 0.0165 0.0270 0.0348 0.0400 0.0423 0.0408 0.0362 0.0282 0.0167 0.0095 0.0047 0.0019
0.0028 0.0045 0.0072 0.0119 0.0195 0.0248 0.0278 0.0288 0.0278 0.0248 0.0195 0.0119 0.0071 0.0036 0.0014
0.0017 0.0029 0.0043 0.0080 0.0137 0.0175 0.0197 0.0204 0.0197 0.0175 0.0137 0.0080 0.0048 0.0024 0.0010
0.0016 0.0025 0.0037 0.0067 0.0111 0.0140 0.0157 0.0162 0.0157 0.0140 0.0111 0.0067 0.0041 0.0021 0.0008
0.0000 0.0000 0.0000 0.0000 0.0000 0.0000 0.0000 0.0000 0.0000 0.0000 0.0000 0.0000 0.0000 0.0000 0.0000



0.800   0.830   0.830   90.00   360.0   18.00  20.00
```

Wake Geometry Input File for MIT-PUF-2 (Uniform flow)

```
 4
0.25000  0.35000  0.45000  0.55000  0.65000  0.75000  0.85000  1.00000

1.00000  0.00000  0.00000  0.00000  0.00000  0.00000  0.00000  0.00000
0.00000  0.00000  0.00000  0.00000  0.00000  0.00000  0.00000  0.00000
```

0.00000 0.00000 0.00000 0.00000 0.00000 0.00000 0.00000 0.00000

0.00000	0.00000	0.00000	0.00000	0.00000	0.00000	0.00000	0.00000
0.00000	0.00000	0.00000	0.00000	0.00000	0.00000	0.00000	0.00000
0.00000	0.00000	0.00000	0.00000	0.00000	0.00000	0.00000	0.00000
0.00000	0.00000	0.00000	0.00000	0.00000	0.00000	0.00000	0.00000
0.00000	0.00000	0.00000	0.00000	0.00000	0.00000	0.00000	0.00000
0.00000	0.00000	0.00000	0.00000	0.00000	0.00000	0.00000	0.00000
0.00000	0.00000	0.00000	0.00000	0.00000	0.00000	0.00000	0.00000
0.00000	0.00000	0.00000	0.00000	0.00000	0.00000	0.00000	0.00000
0.00000	0.00000	0.00000	0.00000	0.00000	0.00000	0.00000	0.00000
0.00000	0.00000	0.00000	0.00000	0.00000	0.00000	0.00000	0.00000
0.00000	0.00000	0.00000	0.00000	0.00000	0.00000	0.00000	0.00000

Wake Geometry Input File for MIT-PUF-2 (Behind Skeg Model)

```
 4
 0.28000  0.50000  0.70000  1.10000
 0.45851  0.00142 -0.45244 -0.00154 -0.00001  0.00020 -0.00506 -0.00010
 0.00000  0.00004 -0.00069 -0.00002  0.00000  0.00001 -0.00018 -0.00001
 0.81070  0.00168 -0.34841  0.00284 -0.25899  0.00043 -0.14845 -0.00337
-0.05738 -0.00184 -0.00684 -0.00017  0.00886  0.00017  0.00534  0.00033
 0.84471 -0.01918 -0.25929  0.00107 -0.22375  0.00308 -0.17090  0.00275
-0.11546  0.00358 -0.06479  0.00396 -0.02558  0.00342 -0.00152  0.00223
 0.91731 -0.01989 -0.17250  0.00154 -0.15344  0.00514 -0.14024  0.00399
-0.12434  0.00262 -0.10537  0.00198 -0.08489  0.00181 -0.06469  0.00164
 0.00000  0.00000  0.00000  0.00000  0.00000  0.00000  0.00000  0.00000
 0.00000  0.00000  0.00000  0.00000  0.00000  0.00000  0.00000  0.00000
 0.00000  0.00000  0.00000  0.00000  0.00000  0.00000  0.00000  0.00000
 0.00000  0.00000  0.00000  0.00000  0.00000  0.00000  0.00000  0.00000
 0.00000  0.00000  0.00000  0.00000  0.00000  0.00000  0.00000  0.00000
 0.00000  0.00000  0.00000  0.00000  0.00000  0.00000  0.00000  0.00000
 0.00000  0.00000  0.00000  0.00000  0.00000  0.00000  0.00000  0.00000
 0.00000  0.00000  0.00000  0.00000  0.00000  0.00000  0.00000  0.00000
 0.00000  0.00000  0.00000  0.00000  0.00000  0.00000  0.00000  0.00000
 0.00000  0.00000  0.00000  0.00000  0.00000  0.00000  0.00000  0.00000
 0.00000  0.00000  0.00000  0.00000  0.00000  0.00000  0.00000  0.00000
 0.00000  0.00000  0.00000  0.00000  0.00000  0.00000  0.00000  0.00000
 0.00000  0.00000  0.00000  0.00000  0.00000  0.00000  0.00000  0.00000
 0.00000  0.00000  0.00000  0.00000  0.00000  0.00000  0.00000  0.00000
 0.00000  0.00000  0.00000  0.00000  0.00000  0.00000  0.00000  0.00000
 0.00000  0.00000  0.00000  0.00000  0.00000  0.00000  0.00000  0.00000
 0.00000  0.00000  0.00000  0.00000  0.00000  0.00000  0.00000  0.00000
 0.00000  0.00000  0.00000  0.00000  0.00000  0.00000  0.00000  0.00000
 0.00000  0.00000  0.00000  0.00000  0.00000  0.00000  0.00000  0.00000
 0.00000  0.00000  0.00000  0.00000  0.00000  0.00000  0.00000  0.00000
 0.00000  0.00000  0.00000  0.00000  0.00000  0.00000  0.00000  0.00000
 0.00000  0.00000  0.00000  0.00000  0.00000  0.00000  0.00000  0.00000
 0.00000  0.00000  0.00000  0.00000  0.00000  0.00000  0.00000  0.00000
 0.00000  0.00000  0.00000  0.00000  0.00000  0.00000  0.00000  0.00000
 0.00000  0.00000  0.00000  0.00000  0.00000  0.00000  0.00000  0.00000
 0.00000  0.00000  0.00000  0.00000  0.00000  0.00000  0.00000  0.00000
 0.00000  0.00000  0.00000  0.00000  0.00000  0.00000  0.00000  0.00000
 0.00000  0.00000  0.00000  0.00000  0.00000  0.00000  0.00000  0.00000
 0.00000  0.00000  0.00000  0.00000  0.00000  0.00000  0.00000  0.00000
 0.00000  0.00000  0.00000  0.00000  0.00000  0.00000  0.00000  0.00000
 0.00000  0.00000  0.00000  0.00000  0.00000  0.00000  0.00000  0.00000
 0.00000  0.00000  0.00000  0.00000  0.00000  0.00000  0.00000  0.00000
```

0.00000 0.00000 0.00000 0.00000 0.00000 0.00000 0.00000 0.00000

```
0.00000 0.00000 0.00000 0.00000 0.00000 0.00000 0.00000 0.00000
0.00000 0.00000 0.00000 0.00000 0.00000 0.00000 0.00000 0.00000
0.00000 0.00000 0.00000 0.00000 0.00000 0.00000 0.00000 0.00000
0.00000 0.00000 0.00000 0.00000 0.00000 0.00000 0.00000 0.00000
0.00000 0.00000 0.00000 0.00000 0.00000 0.00000 0.00000 0.00000
0.00000 0.00000 0.00000 0.00000 0.00000 0.00000 0.00000 0.00000
0.00000 0.00000 0.00000 0.00000 0.00000 0.00000 0.00000 0.00000
0.00000 0.00000 0.00000 0.00000 0.00000 0.00000 0.00000 0.00000
0.00000 0.00000 0.00000 0.00000 0.00000 0.00000 0.00000 0.00000
0.00000 0.00000 0.00000 0.00000 0.00000 0.00000 0.00000 0.00000
```